

REVIEWS OF TOPICAL PROBLEMS

PACS numbers: **05.45.–a**, **47.27.–i**, 52.35.Ra

Investigation of intermittency and generalized self-similarity of turbulent boundary layers in laboratory and magnetospheric plasmas: towards a quantitative definition of plasma transport features

V P Budaev, S P Savin, L M Zelenyi

DOI: 10.3367/UFNe.0181.201109a.0905

Contents

Abstract. **A comparative analysis of the fundamental properties of fluctuations in the vicinity of boundaries in fusion plasmas and in plasmas of magnetospheric turbulent boundary layers (TBLs) shows the similarity of their basic statistical characteristics, including the scaling of the structure functions and mutifractal parameters. Important features observed include intermittent fluctuations and anomalous mass and momentum transport, due to sporadic plasma flow injections with large flow amplitudes occuring with a much higher probability than predicted for classical Gaussian diffusion. Turbulence in edge fusion plasmas and in TBLs exhibits general self-similarity in a wide range of scales extending to the dissipation scale. Experimental scalings obtained for plasma TBLs are compared with neutral fluid results, revealing the universal properties of developed turbulence. TBL scalings are described within the log-Poisson model, which takes quasi-one-dimensional dissipative structures into account. The time (τ) dependence of the mean-square displacement $\langle \delta x^2 \rangle$ obtained from the experimental parameters of the log-Poisson distribution takes the form $\langle \delta x^2 \rangle \propto \tau^{\alpha}$ with $\alpha \approx 1.2-1.8$ and indicates the presence of superdiffusion in the TBLs studied. Determining the nature of the generalized diffusion process from available regular data is a necessary step toward the quantitative description of TBL transport.**

V P Budaev Russian Research Center "Kurchatov Institute,"
pl. Kurchatova 1, 123182 Moscow, Russian Federation,
Space Research Institute, Russian Academy of Sciences,
ul. Profsoyuznaya 84/32, 117997 Moscow, Russian Federation
Tel. (7-495) 333 11 00. Fax (7-495) 333 12 48
E-mail: budaev@mail.ru
S P Savin, L M Zelenyi Space Research Institute,
Russian Academy of Sciences,
ul. Profsoyuznaya 84/32, 117997 Moscow, Russian Federation
Tel. (7-495) 333 11 00. Fax (7-495) 333 12 48
E-mail: ssavin@iki.rssi.ru, lzelenyi@iki.rssi.ru

Received 2 July 2010, revised 22 February 2011
Uspekhi Fizicheskikh Nauk **181** (9) 905 – 952 (2011)
DOI: 10.3367/UFNr.0181.201109a.0905
Translated by K A Postnov; edited by A M Semikhatov

1. Introduction

1.1 Turbulent boundary layers in Nature and the laboratory

Turbulence is a natural state of both space and laboratory plasmas. Plasma turbulence studies, along with studies of neutral fluid turbulence, are very important in understanding the fundamental properties of Nature. Significant progress in the understanding of the basic properties of turbulence was made due to the classic work by Kolmogorov [1, 2] (the K41 model), in which a hierarchical cascade process of energy transfer in a homogeneous and isotropic developed turbulence was studied. Kolmogorov laid the groundwork for turbulence cascade studies by assuming the statistical quasi-equilibrium of turbulent fluctuations in the inertial range and by formulating the main hypotheses on the statistical distribution of physical quantities in a turbulent flow. The independence or weak dependence of properties of the central regions of a turbulent flow on boundary conditions at large Reynolds numbers allowed Kolmogorov to construct the K41 model of isotropic developed turbulence.

Turbulence usually emerges in a flow due to boundary effects. In hydrodynamic flows, the velocity shear near the flow boundary strongly affects the development of turbulence. For a viscous fluid (even with an arbitrarily low viscosity coefficient), the velocity must vanish at the flow boundary. In turbulent plasma flows near the boundary (for example, a material wall in laboratory installations), this condition is not always satisfied. The possible reason can be the recombination of ions and electrons near the surface, due to which the velocity of plasma flow at the boundary can be nonzero.

In the hydrodynamic problem of the formation of the near-wall boundary layer, frictional forces are comparable to inertial ones, which allows estimating the thickness δ of the boundary layer as $\delta = L/\mathrm{Re}^{1/2}$, where Re is the Reynolds number and L is the characteristic scale of the flow. In the simplest case, the boundary layer is described by the system of equations derived by Prandtl et al. (see [3]). Solutions of these equations and the corresponding estimates have been in reasonable agreement with many experiments in a broad range of Reynolds numbers, but drastically deviate from observations at very large Reynolds numbers (exceeding $\sim 10^6$; see [3]).

Despite great progress in describing developed turbulence, the character of influence of the flow boundary and its geometry on the overall properties of the flow at very large Reynolds numbers is still an open issue. Recently, reliable experimental data on turbulent boundary layers (TBLs) have been obtained that call for a revision of the classical theory of TBLs. Experiments discovered the formation of TBLs that strongly change the characteristics of the entire flow. In hydrodynamic turbulence, this effect was demonstrated, for example, by elegant experiments with a turbulent flow between two counter-rotating smooth cylinders [4], in which the emerging TBLs do not allow the angular momentum to reach the $\mathrm{Re}^{1/2}$ dependence on the Reynolds number as predicted by the K41 turbulence model at high Reynolds numbers $\mathrm{Re} \sim 10^6$. When the TBL is destroyed by small paddles on the cylinders, this law is actually observed [5].

The well-known phenomenological theory [3, 6, 7] describes a turbulent flow near the surface and is applied for near-surface atmospheric layers. It leads to a logarithmic dependence of the mean velocity $U(z)$ and the Reynolds number $\mathrm{Re} = U(z)\,z/\nu$ on the height z in the near-surface layer with viscosity ν. Many experimental observations in a broad range of Reynolds numbers are described by a logarithmic law. Recently, a more detailed description of the boundary layers by a power-law dependence of parameters in TBLs on the Reynolds number has been proposed (see [8–11]). Such an approach corresponds to the general paradigm of considering the scale invariance of turbulence, which assumes the existence of power-law dependences of measured parameters on time and space scales.

In magetohydrodynamics (MHD), theoretical considerations become even more complicated. Here, not only material boundaries of the flow but also the scales of structures (waves, eddies, etc.) formed by the magnetic (**B**) and electric (**E**) fields must be taken into account. In plasma flows, turbulence can be formed by many classes of instabilities: drift-dissipating, kinetic, MHD, and so on [12, 13]. In plasma experiments, the important role of boundary effects is always taken into account whenever the best conditions of plasma confinement in a trap and plasma heating are to be obtained. This is especially important in experiments with fusion devices (FDs) with magnetic plasma confinement, including tokamaks, stellarators, and linear devices. Many experiments with such machines (see, e.g., [14, 15]) show evidence of a strong, developed plasma turbulence in the central and peripheral parts of the confinement volume. The turbulence leads to an enhanced transport of plasma across the confining magnetic field, which decreases the confinement efficiency and increases thermal load on the elements of the vacuum chamber in contact with the hot plasma. In the last few decades, detailed experimental studies of plasma turbulence in FDs have been carried out, revealing a very complex dependence of the turbulence properties on the plasma parameters and the conditions of its heating and confinement. Different regimes of plasma confinement are observed, depending on the energy content. Spontaneous transitions from one regime to another are possible (so-called L–H transitions), which are considered to be the result of restructuring all the plasma properties, including turbulence and plasma flows. Plasmas in FDs demonstrate properties of complex systems with self-organization [16]. A mutual dependence of the confinement regimes and the properties of plasma turbulence is observed. The level of turbulence (the ratio of the fluctuation amplitude to the mean level) and turbulent flows across the magnetic field increase in the near-wall region. This behavior is observed in installations of various sizes, with various magnetic topologies and mechanisms of plasma heating. Several reasons for such turbulent level enhancement have been considered, but the boundary effects strengthening turbulent processes appear to be universal and raise no doubts.

The magnetic structure of FDs provides the confinement of high-temperature plasma in a strong magnetic field, which attains 5 T in modern installations. The structure of the magnetic field is formed by toroidal coils and plasma currents. One distinguishes the central confinement region and the edge zone, the region with $r/a > 0.9$ (Fig. 1). The transition between these zones is not sharp; it can contain magnetic surfaces both closed and destroyed (with a large number of magnetic islands), as well as the 'pedestal' zone where the transport barrier responsible for the transition to the high-confinement regime is formed.

In the edge plasma zone (in the limiter shadow and divertor zones), the magnetic field lines are typically open (this zone is called the scrape-off layer, SOL); see Fig. 1a. The field lines terminate at conducting metal diaphragms (limiters) or at divertor plates and penetrate into the region with variable curvature of the magnetic field (in a tokamak or stellarator). The edge plasma region is characterized by significant spatial variations of the plasma parameters: the pressure across the magnetic field, density, temperature, and plasma potential, as well as by the poloidal dependence of these parameters. In spite of significant progress in achieving record plasma parameters in large-scale fusion devices (in the largest JET tokamak, the plasma size is 2.5 m, the plasma ion temperature at the center reaches 40 keV, and the plasma

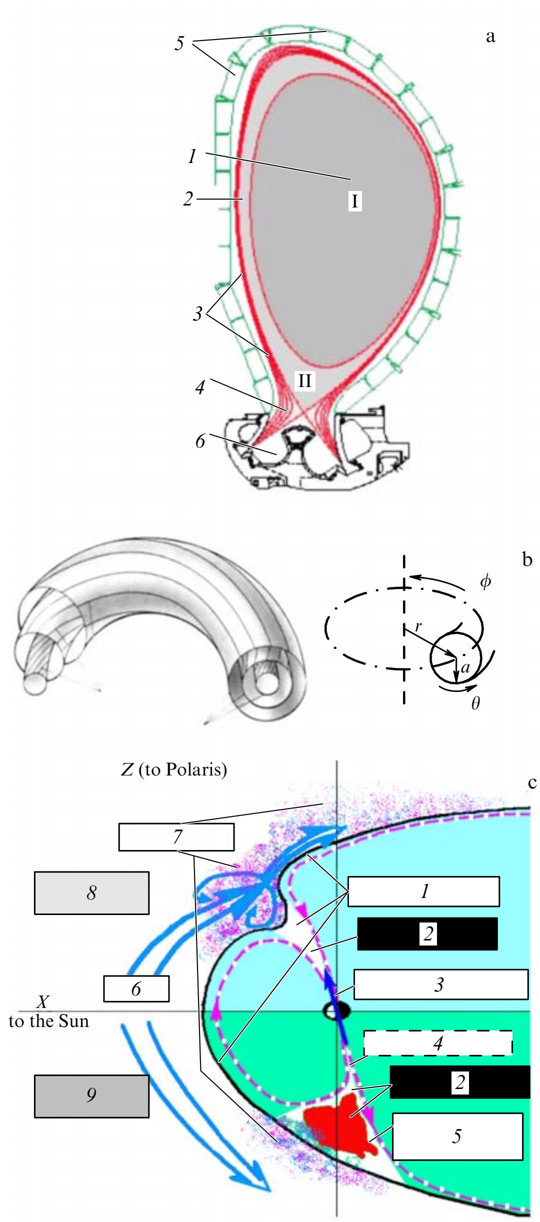

Figure 1. Turbulent boundary layers in laboratory and magnetospheric plasma: (a) the plasma discharge cross section in a tokamak with a poloidal divertor: 1 — central zone, 2 — periphery zone, the pedestal region, 3 — SOL, 4 — divertor plasma, 5 — camera wall, 6 — divertor camera; (b) the structure of enclosed magnetic surfaces in a tokamak and the coordinate system in a tokamak: the radial (r), poloidal (θ), and toroidal (ϕ) coordinates; (c) a schematic of the solar wind streaming around the magnetopause and the formation of a turbulent boundary layer near polar cusps of Earth's magnetosphere in the noon meridian plane; the z axis is directed toward Polaris, the x axis is directed toward the Sun; *1* — magnetopause, *2* — polar cusp, *3* — dipole moment, *4* — magnetic field, *5* — plasma cloud, *6* — plasma flow, *7* — TBL, *8* — summer (the upper half of the figure), *9* — winter (the bottom half of the figure).

density is $n = 2 \times 10^{20}$ m^{-3}), the properties of the wall plasma and the near-wall turbulence remain similar in machines with different sizes: the electron plasma temperature is $T_e \sim 10-100$ eV and the density is $n \sim 10^{12}-10^{13}$ cm^{-3}, with a high level of plasma density variation $\delta n/n \sim 5-100\%$. Fluctuations of the potential and temperature due to the density fluctuations are of the same order of magnitude. The fluctuation amplitude increases toward the wall bounding the plasma discharge.

The features of the periphery turbulence in FDs are related to the pressure gradient across the magnetic field. The strong plasma turbulence in the near-wall zone shows up as plasma density, temperature, and potential fluctuations in the frequency range from ~ 0.1 kHz to ~ 1 MHz and is determined by plasma instabilities. That is why this turbulence is sometimes referred to as low-frequency turbulence (i.e., the one not connected with Langmuir oscillations), microturbulence (the one that develops on characteristic scales much smaller than the large-scale MHD oscillations), or electrostatic turbulence. The characteristic time of the quasi-equilibrium state of the near-wall turbulence is much longer than the time of energy confinement in a magnetic trap. This turbulence is classified as a state with nonlinear saturation of drift-wave or flute (interchange) instabilities. It leads to an enhanced plasma transport across the confining magnetic field (anomalous diffusion). Experimental data show that the properties of the edge plasma, as well as of the low-frequency turbulence, significantly affect the pedestal zone (see review [14]), which is related to the transport barrier at the discharge periphery and the formation of H-regimes of high confinement.

The near-wall turbulence demonstrates the property of intermittency, which appears in the form of large-scale coherent structures with an increased density and a cross-field size as high as ~ 10 cm (i.e., around 10^2-10^3 gyroradii). These large-scale structures, called 'bursts' or 'blobs', have a size up to several dozen meters along the magnetic field, and move across the field, thus leading to an anomalously high plasma leakage from the magnetic trap exceeding the level predicted by classical diffusion.

Space explorations of cosmic plasmas provide experimental data on the properties of turbulence on spatial and temporal scales that are unavailable in ground-based laboratory experiments. Studies of the nature of the low-frequency MHD turbulence in the solar wind and Earth's magnetosphere in the frequency range $10^{-7} \leqslant f \leqslant 1$ Hz are especially important because such measurements are complementary to laboratory experiments. The difference in the frequency ranges is due to different values of the magnetic field (the magnetic field near the magnetosphere boundary is 10–100 nT), whence follow different values of gyrofrequencies and gyroradii of ions that respectively restrict the MHD approximation applicability range in the time and space region from above and from below. At the boundary of Earth's magnetosphere (Fig. 1a), a complex structure of turbulence with intermittency is also observed [17–20].

At the boundary of the geomagnetic trap [18–22], an external boundary layer is formed due to the interaction of the collisionless plasma with plasma at rest and/or with the magnetic field. In this layer, the super-Alfvenic subsonic laminar flow enters the dynamic regime in which accelerated magnetosonic streams and decelerated Alfvenic flows with the characteristic relaxation time 10–20 min are formed. The interaction of fluctuations in the original flow (the solar wind thermalized after crossing the external bow shock, the magnetosheath) with waves reflected from an obstacle qualitatively explains the observed chaotization of the flow in the boundary layer [21]. Cherenkov resonance with the beating of oscillations in the boundary layer and the incoming flow is suggested as the plausible formation mechanism of the accelerated magnetosonic streams. The inertial drift of the influx ions in the transverse electric field increasing toward the boundary quantitatively explains their observed acceleration [19]. The plasma jets can carry up to 40% of the unperturbed flow momentum along the flow; their dynamic pressure often exceeds the magnetic field pressure at the obstacle boundary. A pulsed drop in the kinetic energy by the bypassing flow due to such jets provides an alternative to laminar streaming [17, 19]. A comparison with a model turbulent current sheet in [22] confirms that nonlinear fluctuations in TBLs are an effective (partially transparent) obstacle for the ion thermal pressure dominated collisionless plasma flow bypassing the boundary layer.

In the magnetosheath (MSH) – magnetosphere interaction, the main processes are mutually connected and globally synchronized by low-frequency magnetosonic oscillations of the diurnal MSH as a whole [19–22]. On medium scales in the TBL, such self-organization is observed due to inverse cascades caused by waves reflected from the boundary and focused by a locally concave obstacle, the cusp throat. We are therefore dealing not with response to additive perturbations in the solar wind and MSH but with a complex multiscale nonlinear system. Here, a 'catastrophic' rearrangement of the flow and the magnetic topology occurs (e.g., the appearance of accelerated and decelerated streams and the transition from the laminar stagnation region to the irregular structure of the boundary layer). There is a dependence on the prehistory (at the characteristic relaxation time scale of Alfvenic flows), the appearance of long-range and large-scale anomalously strong correlations of coherent structures in the form of streams that provide anomalous plasma transport.

Analytic models of MHD flows fail to describe complex turbulent processes observed in Earth's magnetosphere and in laboratory fusion devices. To treat the properties of turbulence on large time and space scales, methods of statistical physics and cascade models developed in hydrodynamic theories are needed.

The properties of turbulence of (space and laboratory) plasmas are scale dependent. One of the most important issues is to what extent the anisotropy due to the magnetic field is preserved on intermediate and small scales. Despite many theoretical studies, the problem of plasma turbulence isotropy on small scales remains open and continues to be actively discussed. To solve this problem, the corresponding experimental data are required, especially those related to the influence of boundary effects on turbulence properties. The most productive methods of the description of turbulence invoke symmetries of the scale invariance, which is the main feature of turbulence. Apparently, one of the features of TBLs in any turbulent flow (hydrodynamic and magnetohydrodynamic) is the anisotropy emerging due to the effect of the flow boundary or the dissipation scale. This anisotropy locally violates symmetries that are allowed in the flow as a whole and preserves only those that are responsible for the turbulent cascade; it preserves the scale invariance not in the infinite band but only in a restricted range of scales. Therefore, the TBL properties are related not only and not so much to physical mechanisms of the dominating instability growth, but rather to symmetries responsible for the scale invariance in the significantly restricted range of scales in the TBL. Such an approach to the treatment of TBL properties suggests a description of experimental data in various turbulent media in the framework of a single paradigm, including the description of the most prominent feature of TBLs, intermittency.

1.2 Specific properties of plasma turbulence with intermittency

Both laboratory and magnetospheric plasmas are a dynamical system with a large number of degrees of freedom, in which various instabilities can develop. In the boundary zones near the wall (in laboratory plasmas) or the magnetopause (in the MSH), there can be several types of instabilities, including drift dissipating, magnetohydrodynamic, and kinetic. MHD instabilities lead to magnetic field fluctuations; drift-dissipating and kinetic instabilities induce fluctuations of the electric fields, density, and temperature of the plasma. Several instabilities, often nonlinearly coupled, can simultaneously be responsible for the development of plasma turbulence.

Plasma turbulence is characterized not only by the Reynolds number Re, which is determined by the kinematic viscosity, but also by the magnetic Reynolds number $\mathrm{Re_m}$, which is related to the magnetic viscosity. For relatively small values $\mathrm{Re_m} < 10^3 - 10^4$ and under the influence of the plasma boundary, intermittency can emerge in a turbulent flow. In this case, the plasma parameters (Fig. 2) are observed as random variables with a non-Gaussian distribution, i.e., turbulent pulsations with large amplitudes appear with a much higher probability than the Gaussian law (the normal distribution) predicts.

Intermittency was the phenomenon first considered by Novikov and Stewart [23]; it represents a break of the homogeneity of turbulence, in which active regions coexist with passive (quasilaminar) ones. Intermittency is observed in hydrodynamic turbulent flows of neutral liquids [24] and in turbulent magnetized plasma (see, e.g., [25] and the references therein) at both high and moderate Reynolds numbers (< 1000). The presence of magnetic and electric fields introducing an additional anisotropy is a specific feature of intermittency in plasma boundary layers. In the central regions of a plasma object, where the boundary layer effects are insignificant, the properties of plasma turbulence can be significantly different in different objects.

In turbulent plasma of laboratory FDs and in the magnetosphere, intermittency is observed as large-amplitude

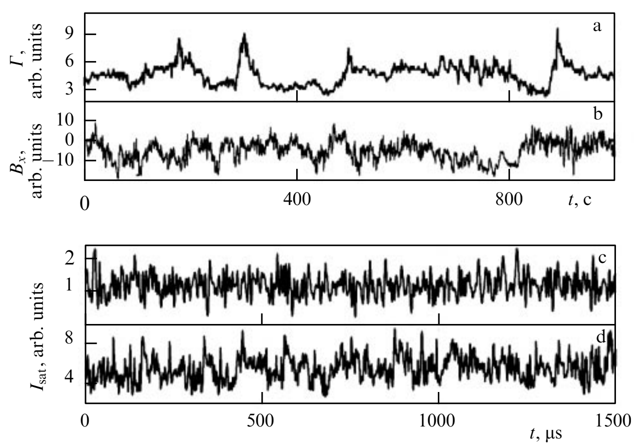

Figure 2. Intermittency of plasma turbulence. (a) Signal recorded by Interball-1 spacecraft in the TBL near Earth's magnetopause: the ion flux Γ, 29.03.1996; (b) the magnetic field component B_x along the axis directed to the Sun, 19.06.1998. The saturation current on the probe (the plasma density) I_{sat} in the edge plasma of fusion devices: (c) in the linear plasma device NAGDIS-II; (d) in the tokamak T-10.

pulsations. The laws of scale similarity (scaling law) in such turbulence are described by parameters depending on the scale (multiscaling). It follows from theoretical considerations [31] that the turbulence intermittency is due to hidden statistical symmetries (symmetries of scale invariance) of the dynamic equations describing the motion and the scale invariance being established in a bounded near-wall space. Random pulsations of the velocity and other parameters of a turbulent intermittent flow demonstrate a non-Gaussian statistics, i.e., cannot be described by the classical (normal) dispersion law. Very general theoretical considerations suggest that the dynamics of this process can be described by power-law distributions with multiple scales, i.e., by a spectrum of characteristic scales. Long-range correlations due to the multiscale invariance and non-Gaussian statistics lead to an enhanced turbulent transport — the anomalous diffusion. Presently, it is impossible to solve the 3D problem of the dynamics of turbulent plasma analytically or numerically or to determine the turbulent scaling laws with the required accuracy on large time scales (for example, during the running time of a tokamak). Therefore, the statistical properties of turbulence related to scale invariance should be determined from experiments. It is also necessary to estimate the scaling law (the exponents in the assumed power-law dependences of the plasma parameters; see below), which would then allow improving the physical models of plasma turbulence and would provide both a quantitative and a qualitative description of the plasma transport process in turbulent boundary layers in the MSH and laboratory plasma in greater detail than is currently possible.

The specific conditions in plasma (electric and magnetic fields interacting with plasma particles, currents, anisotropy determined by the fields and dissipation of propagating waves and their dispersion, and so on) lead to differences in some properties of turbulence in plasmas and neutral fluids. In the boundary turbulence of a laboratory FD, the effect of the $[\mathbf{E} \times \mathbf{B}]$ drift and interchange instabilities is considered (see, e.g., [26, 27]). To describe plasma properties in the magnetosphere, different models are used [28, 29] taking the destruction of magnetic surfaces due to the growth of low-frequency electromagnetic perturbations into account. The observed strong turbulence in boundary layers of plasma objects is essentially three-dimensional, and hence two-dimensional models and the weak turbulence approach fail to describe all properties of the intermittency.

Yet experimental results suggest that the turbulence of plasmas in a magnetic field demonstrates many properties making it similar to the turbulence of neutral fluids (see [24, 25, 30–32]), including multiple scales, cascades, intermittency, and nonlinear scaling laws. The statistical properties of hydrodynamic turbulence have been studied well, both theoretically and experimentally. Studies of statistical properties of turbulence emerging in the edge plasma of laboratory machines and the TBL of the magnetosphere started only relatively recently.

In plasma boundary layers near the wall of a laboratory device or the magnetopause, a universal scaling law of turbulence should be expected. The idea of universal scaling laws plays a crucial role in the physics of condensed matter and critical phenomena. Universal scaling laws (mainly for low-order moments) are also considered in turbulence, but significant progress has so far been achieved only in the description of isotropic fully developed turbulence, under the assumption of a Gaussian statistics for the velocity field. In boundary layers, the process is described by non-Gaussian statistics, and due to the complexity of processes in different media, universal turbulence laws in boundary layers have not been established so far.

1.3 Models of turbulence

1.3.1 Analytic models. Turbulent flows represent a nonlinear system with an enormous number of degrees of freedom. The exact mathematical determination of the time dependence of the velocity field, temperature, pressure, and so on appears to be impossible. An analytic description of such a system is only possible using statistical methods that consider statistical properties of an ensemble of flows. The statistical description of turbulent flows does not fully coincide with the gas kinetic theory, where statistical ensembles of a large number of molecules are also considered. Turbulence appears in a continuous medium, which is described by systems of partial differential equations, while discrete ensembles of molecules are described by systems of ordinary differential equations. The most significant difference from the gas kinetic theory, where the energy of the ensemble is conserved, is the energy dissipation due to viscosity; a turbulent medium is an open system. Therefore, the mathematical apparatus of kinetic theory is inadequate for describing turbulence, and methods of statistical hydromechanics [3] must be invoked together with other methods that consider systems of nonlinearly interacting fields with infinitely many degrees of freedom, for example, quantum field theory and theories studying open dissipative systems [33, 34].

Turbulence occur in the same continuous media where laminar flows can exist. To describe laminar flows in continuous media, appropriate methods of mathematical physics were elaborated, and significant progress was achieved in this field. To describe turbulent flows, much more complicated methods are required, and the construction of the mathematical apparatus to describe turbulence is far from being completed.

Analytic theories of turbulence are usually confined to the linear approximation. The straightforward numerical solution of the equations in such theories meets the fundamental problem: the number of the degrees of freedom increases algebraically when passing to smaller scales due to the cascade nature of the process. In describing turbulence with intermittency, due to the restrictive inertia region and the significant influence of the dissipative zone, the scaling of dissipative structures and boundary conditions of the cascade must be accurately taken into account. In analytic models, the spectrum is frequently cut-off, ignoring the possible effect of noises from the dissipative zone, which limits the applicability of such models.

The cascade turbulence models seem to be more appropriate for describing the turbulence with intermittency. Although phenomenological cascade models for turbulence with intermittency are not directly derived from equations of motion, the cascade properties are related to the structure and symmetries of dynamic equations. Hypotheses used in different cascade models relate to scaling properties of structures with different intensities. Such an approach is an effective tool for the analysis of the turbulence structure on different scales. The use of a stochastic cascade allows describing many properties of turbulence with intermittency, including multiple scales and multifractality [24, 35], i.e., taking the dependence of the self-similarity on the local scale into account.

Progress in the analytic description of turbulence was achieved due to the treatment of turbulence in two-dimensional, instead of three-dimensional, space. By two-dimensional turbulence, we mean studies of solutions of the equations of motion (MHD equations for plasma or the Navier–Stokes equations in hydrodynamics) that depend on two coordinates only. The velocity along the third coordinate here satisfies the simple advection–diffusion equation and does not depend on the two-dimensional flow along the first two coordinates. It is therefore assumed to depend on two coordinates only and is described by a flux function. The vorticity equation contains no term responsible for the deformation (stretching) of vortices, and thus one of the main properties of the tree-dimensional turbulence disappears. Within the two-dimensional approach, some characteristic phenomena, such as a tornado in geophysics, can be analyzed easier than in the tree-dimensional case. In magnetized plasma, the two-dimensional approach is widely used in the 'leading center' approximation (i.e., when the average over the rotation of particles in the magnetic field is calculated). In two-dimensional turbulence, one more conservation law appears, related to the conservation of enstrophy, the quantity $\langle \omega^2 \rangle$, where ω is the vorticity. The two-dimensional turbulence has a very important feature — the inverse cascade of the energy transfer from small to large scales with a $k^{-3/2}$ spectrum (more precise studies suggested a logarithmic correction to this law). This is an analog of the Kolmogorov (direct) cascade with the $k^{-5/3}$ spectrum. The study of the applicability of the two-dimensional turbulence is important for constructing a statistical model of the turbulent flow with the dominant role of coherent structures that can be identified and parameterized. The statistical mechanics developed by Boltzmann and other physicists assumes equilibrium distributions for conservative Hamiltonian dynamics. Three-dimensional turbulence is a dissipative system in which the energy dissipation is finite, even for an arbitrarily small viscosity. The two-dimensional Navier–Stokes equation with zero viscosity reduces to the Euler equation, which can be written in the Hamiltonian form. However, an open fundamental problem is where the applicability bounds of the conservative approach to the two-dimensional turbulence are and how the enstrophy dissipation can be correctly taken into account (such a dissipation always appears in numerical experiments; see [24]). In two-dimensional turbulence, vortices are mainly observed, while in the tree-dimensional case, the topology of emerging structures can be much richer, including one-dimensional filaments, two-dimensional sheets, infinitely thin vortex lines, Rankin vortices, Batchelor vortices, and other compact and open structures (see [8, 24]). All questions of the applicability of two-dimensional turbulence are also related to plasma turbulence. If the plasma in a strong magnetic field is considered in the MHD framework, a strong anisotropy due to the turbulent cascade in the direction across the mean magnetic field must be taken into account, which is especially important in laboratory fusion devices. An approach often used in the literature is to study the dynamics in the plane across the magnetic field in the framework of the two-dimensional MHD model. For example, such an approach was used in numerical experiments by Müller and Biskamp [31]. In this approach, the important properties of plasma (contributions from Alfven frequencies, dispersion relations, and so on; see [36]) are preserved. But the applicability conditions of the two-dimensional approach should be carefully checked each time, especially for the edge plasma. The validity of the two-dimensional approach depends on the required level of details and characteristics.

Although powerful analytic methods (for example, the quasilinear approximation [37], the weakly nonlinear coupling (direct coupling) approximation [38, 39], and renormalization group methods; see review [40]) have been developed in the theory of turbulence, modern analytic models are still far from being so detailed and precise as semi-empirical cascade models based on statistical methods. In particular, this applies to a description of turbulence with intermittency. In analytic models, the renormalization group methods in fact reduce to a renormalization of the viscosity and force in order to take the effect of other scales on a given scale into account. The evolutionary equation for the Fourier components of velocity $\hat{u}(k, t)$ (where k is the wave vector) then takes the form [3, 4]

$$\left[\frac{\partial}{\partial t} + v_{\mathrm{R}}(k, t)\, k^2\right] \hat{u}(k, t) = \hat{f}_{\mathrm{R}}(k, t)\,, \tag{1}$$

where v_{R} and $\hat{f}_{\mathrm{R}}$ are the renormalized viscosity and force, and the hat denotes the Fourier component. The amplitude distribution is assumed to be quasi-Gaussian. Such a description in the mean field approximation cannot fully describe the intermittency. The intermittency is not only a result of the turbulent 'activity,' but also a turbulent 'activity' itself with intermittency distributed nonhomogeneously. The distribution function is then described by power laws and not by exponentials. Nontrivial algebraic and other laws are currently considered in the literature to describe the turbulence in hydrodynamic and plasma flows in laboratory devices and in astrophysics.

1.3.2 Symmetry properties of the equations describing plasma turbulence. The most complete description of the plasma dynamics is given by kinetic theory, i.e., by the system of Maxwell–Boltzmann equations. A large number of numerical methods are based on the solution of MHD equations that describe the space–time evolution of moments of the Boltzmann equations. To describe plasma, the Braginsky equations [41] and different variants of reduced equations are used (see, e.g., [26, 27, 42–45] and the references therein). For example, the models include simplifications such as the vanishing of some parameters (which in many cases changes or breaks the symmetry of the problem). A turbulent process can have several types of symmetries, including scale invariance symmetries. When constructing a solution on a wide range of time and space scales, symmetry breaking can lead to physically incorrect solutions. As a result, the predictive strength of such models can be significantly reduced; this especially concerns the description of turbulence on long time scales. This problem must be tackled within group theory [46, 47] by analyzing the group properties of symmetries of the reduced system of equations.

Any system of partial differential equations has symmetries called Lie (group) symmetries (see [46, 47]). The knowledge of such symmetries allows predicting the scaling of solutions, constructing particular solutions, and sometimes decreasing the order of equations (see [46–50] and the references therein). The intermittency property of a turbulent flow is determined by scale invariance and the properties of the group responsible for the anisotropy of the problem. The symmetries of two-dimensional and three-dimensional reduced MHD equations (for example, the Kadomtsev–Pogutse equations) were studied in [48, 49]. The symmetries of MHD equations [48–50] are equivalent to those of Navier–Stokes equations [51, 52]. Among such symmetries is the scale invariance under the transformation of space–time coordinates t, $\mathbf{r}$, $\mathbf{u} \to \lambda^{1+h} t$, $\lambda \mathbf{r}$, $\lambda^{-h}\mathbf{u}$ with a scaling factor λ. This equivalence of symmetries (groups of transformations) allows considering the scaling law (i.e., the scale invariance) of the turbulent plasma using the results obtained for hydrodynamic turbulence. The knowledge of the symmetry allows estimating the leading contribution of the isotropy under specific conditions. A theoretical analysis of isotropy and anisotropy and their contribution to statistical moments of the distribution function can be done using the SO(3) symmetry (see review [53]). We consider the symmetry properties of equations describing a plasma. The standard MHD equations for an incompressible plasma are given by

$$\begin{aligned}
&\frac{\mathrm{D}\mathbf{u}}{\mathrm{D}t} = -\nabla p + \nu \Delta \mathbf{u} + (\nabla \times \mathbf{b}) \times \mathbf{b}\,, \\
&\frac{\mathrm{D}\mathbf{b}}{\mathrm{D}t} = (\mathbf{b}\nabla)\,\mathbf{u} + \eta \Delta \mathbf{b}\,, \qquad (2)\\
&\nabla \mathbf{u} = 0\,, \\
&\nabla \mathbf{b} = 0\,, \\
&\frac{\mathrm{D}}{\mathrm{D}t} \equiv \frac{\partial}{\partial t} + (\mathbf{u}\nabla)\,,
\end{aligned}$$

where ν is the kinematic viscosity, η is the magnetic viscosity, u is the velocity, p is the pressure, and the magnetic field induction b is expressed in units of the Alfven velocity.

The structure of the MHD equations is equivalent to that of the Navier–Stokes equation. When the magnetic field vanishes, the MHD equations become the Navier–Stokes equation for an incompressible hydrodynamic flow:

$$\begin{aligned}
&\frac{\mathrm{D}\mathbf{u}}{\mathrm{D}t} = -\nabla\left(p + \frac{1}{2}\,|\mathbf{u}|^2\right) + u_i \nabla u_i + \nu \Delta \mathbf{u}\,, \\
&\nabla \mathbf{u} = 0\,, \qquad (3)
\end{aligned}$$

where summation over repeated indices is assumed. This equation has shear and rotational symmetries; it as also symmetric under the Galilei transformations and has scale invariance.

The Navier–Stokes and MHD equations belong to the class of the Weber–Clebsch evolution equations [54]

$$\begin{aligned}
&\frac{\mathrm{D}\mathbf{Z}}{\mathrm{D}t} = -\nabla P + u_i \nabla Z_i + k \Delta \mathbf{Z}\,, \\
&\nabla \mathbf{Z} = 0\,. \qquad (4)
\end{aligned}$$

In the Navier–Stokes equations, $\mathbf{Z} = \mathbf{u}$, $P = p + |\mathbf{u}|^2/2$, and $k = \nu$. The MHD equations can also be written in form (4) [54]. For this, the vector potential A in the Coulomb gauge $\mathbf{b} = \nabla \times \mathbf{A}$, $\nabla \mathbf{A} = 0$, is introduced. Using the identity

$$\nabla \left[u_i \nabla A_i - (\mathbf{u}\nabla)\,\mathbf{A}\right] = (\mathbf{b}\nabla)\,\mathbf{u} - (\mathbf{u}\nabla)\,\mathbf{b} - (\nabla \mathbf{u})\,\mathbf{b}\,,$$

Eqn (2) can be written as

$$\frac{\mathrm{D}\mathbf{A}}{\mathrm{D}t} = -\nabla c + u_i \nabla A_i + \eta \Delta \mathbf{A}\,. \qquad (5)$$

This equation corresponds to the general form (4) with $\mathbf{A} = \mathbf{Z}$, $\eta = k$, and $c = P$. Hence, all the results obtained in the studies of scale invariance of the Navier–Stokes equation can be applied to objects described by the MHD equations [54].

The symmetry of an equation is a group transformation $\mathcal{G}$ that acts on the solution $u(\mathbf{r}, t)$ of the equation such that $\mathcal{G}\,u(\mathbf{r}, t)$ is also a solution (the invariance under the symmetry).

The types of symmetries of Navier–Stokes and MHD equations include

— spatial shifts $\mathcal{G}_R : t, \mathbf{r}, \mathbf{u} \to t, \mathbf{r} + \mathbf{R}, \mathbf{u}$, $R \in \Re^3$;

— temporal shifts $\mathcal{G}_t : t, \mathbf{r}, \mathbf{u} \to t + T, \mathbf{r}, \mathbf{u}$, $t \in \Re$;

— Galilei transformations $\mathcal{G}_G : t, \mathbf{r}, \mathbf{u} \to t, \mathbf{r} + \mathbf{U}t, \mathbf{u} + \mathbf{U}$, $U \in \Re^3$;

— parity reversal $t, \mathbf{r}, \mathbf{u} \to t, -\mathbf{r}, -\mathbf{u}$;

— rotations $\mathcal{G}_A : t, \mathbf{r}, \mathbf{u} \to \mathbf{t}, A\mathbf{r}, A\mathbf{u}$, $A \in \mathrm{SO}(\Re^3)$;

— scale invariance $\mathcal{G}_h : t, \mathbf{r}, \mathbf{u} \to \lambda^{1+h} t, \lambda \mathbf{r}, \lambda^{-h}\mathbf{u}, \lambda, h \in \Re$.

The pressure scales as $|\mathbf{u}|^2$. The Galilei transformation $\mathbf{u}(t, \mathbf{r} - \mathbf{U}t) + \mathbf{U}$ leads to the mutual concelation of the terms $\partial \mathbf{u}/\partial t$ and $(\mathbf{u}\nabla)\,\mathbf{u}$. The parity change $\mathbf{u} \to -\mathbf{u}$ is an invariance only if the nonlinear term is ignored. The rotation symmetry may not be preserved if the problem with periodic boundary conditions is considered. All symmetries (except the scale invariance) of the Navier–Stokes equation follow from the symmetries of the Newton equations describing the motion of molecules.

Symmetries responsible for scale invariance determine the properties of energy cascades in a turbulent flow. Under the scale transformations of variables (also called self-similarity transformations) t, $\mathbf{r}$, $\mathbf{u} \to \lambda^{1+h} t$, $\lambda \mathbf{r}$, $\lambda^{-h}\mathbf{u}$, the factors λ^{-2h-1} and λ^{-h-2} appear in the Navier–Stokes equation:

$$\lambda^{-2h-1}\,\frac{\partial \mathbf{u}}{\partial t} + \lambda^{-2h-1}\left[(\mathbf{u}\nabla)\,\mathbf{u} + \rho^{-1}\nabla p\right] = \nu \lambda^{-h-2} \Delta \mathbf{u}\,. \qquad (6)$$

For a finite viscosity, this is an invariance for only one value of the self-similarity index $h = 1$. As $\nu \to 0$, the invariance is possible for any index h. Therefore, it is then possible to consider many scale invariance symmetries. The K41 monofractal model of developed turbulence proposed by Kolmogorov is characterized by $h = 1/3$. In multifractal models, the continuous spectrum of indices $h \in [h_{\min}, h_{\max}]$ forms subsets with different self-similarity scaling laws (scale invariance). We note that the coexistence of regions with different scaling laws in a turbulent flow was already considered in the K62 model by Kolmogorov [55].

As noted above, the MHD equations have the same structure as the Navier–Stokes equation. MHD equations (2) or Navier–Stokes equations (3), as well as the related advection–diffusion equations for the scalar field θ,

$$\frac{\partial \theta}{\partial t} + (\mathbf{u}\nabla)\,\theta = \chi \nabla^2 \theta + f_0 \qquad (7)$$

(where f_0 is the force acting on the scalar field and χ is the diffusion coefficient), remain invariant under any affine transformation of spatial coordinates and time with a scale factor: $x \to \lambda x$, $t \to \lambda^{1+h} t\,\lambda$ (h is the self-similarity index). The dependent variables are also renormalized:

$$\mathbf{u} \to \frac{\mathbf{u}}{\lambda^h}\,, \quad \theta \to \frac{\theta}{\lambda^h}\,, \quad \rho \to \frac{\rho}{\lambda^h}\,, \quad f \to \frac{f}{\lambda^{2h+1}}\,. \qquad (8)$$

We note the same self-similarity law in Eqn (8) for the velocity $\mathbf{u}$ and density ρ. This shows that scale invariance laws are similar for the velocity and density fields. Such a similarity allows experimental studies of the scaling laws of plasma density fluctuations using methods developed for the analysis of the velocity field.

The classic group analysis studies properties of the invariance of systems of differential equations, irrespective of the initial and boundary conditions for these equations. The constructed invariant solutions can also be used in initial and boundary value problems [56].

In mechanics, symmetries are considered jointly with conservation laws. According to the Noether theorem, each symmetry corresponds to a conservation law in the global sense. This is true for conservative systems. The MHD and Navier–Stokes equations describe dissipative systems. Yet the symmetry laws are also studied there, since the existence of hidden statistical symmetries describing local conservation laws or the scale invariance is assumed.

In the case of a finite viscosity, the symmetry group of the equations describing a turbulent plasma is nontrivial, and not all the irreducible representations of this group have been fully studied yet. Therefore, experimental studies of scaling laws and indices that characterize scale invariance are important for the description of turbulence.

The modern approach to the anisotropy problem. Because the Navier–Stokes equations describing a neutral fluid and the MHD equations describing a plasma are invariant under rotations in three-dimensional space, the rotation invariance of all quantities is investigated. In the isotropic case, rotation invariance was used to derive the functional dependence of the second- and third-order correlation functions [6]. The key idea of this approach is that the statistical means of any function depending on the velocity components do not change in any coordinate system under rotations or reflections of the coordinates. Intermittency studies provide growing evidence that even in the limit of the infinitely large Reynolds number, the scaling law of structure functions in the inertial range can differ from that predicted by the K41 model. The anisotropy effect may be the possible reason. When passing to progressively smaller and smaller scales, the restoration of isotropy can occur more slowly than Kolmogorov's model predicts. In a turbulent flow, fluctuations with different degrees of anisotropy can be present, which have different anisotropy loss rates, for example, fluctuations of a passive scalar of vector quantities or fluxes in the magnetic field [53]. To study this phenomenon, group methods are used: the SO(3) group of rotations in three-dimensional space is considered. The vector and tensor quantities under study in the problem, such as the structure functions, statistical means, moments of force gradients, and Green's functions, are decomposed with respect to the basis of irreducible representations of the SO(3) group, which enables the isotropic and anisotropic components of the relevant quantities to be singled out and the quantitative anisotropy contribution to be estimated.

Renormalization group and self-similarity. The concept of a self-similarity is closely related to renormalization group transformations. When calculating transport phenomena to study the dynamics of strong turbulence, different authors use the renormalization group method. The term 'renormalization' refers to removing singularities in electrodynamics and quantum electrodynamics (Feynman, Schwinger, and Tomonaga [57]). In the Richardson cascade, there is a hierarchy of increasing scales, and the dynamics on a given scale modify the effective parameters describing the dynamics on the next scale. The renormalization group (RG) established the transformation rule, and, as a result, the scaling law (the scale invariance laws) is determined by the asymptotic behavior of the iteration rule (for an infinite number of iterations in the ideal case). Perturbative methods are applied either for a small amplitude of turbulent pulsations or for a rapid (almost instant) decay of correlations of turbulent quantities. In the real turbulent plasma in TBLs, such conditions are not satisfied.

The use of RG methods (see, e.g., [58]) in the theory of developed turbulence demonstrated the efficiency of the traditional RG technique to the description of the Kolmogorov turbulence spectrum. However, the modern RG technique does not yet allow solving the so-called infrared scaling problem in the deviation from the Kolmogorov scaling (in the RG terms, the appearance of additional powers in correlators, or an essentially nonlinear scaling of structure functions). The solution of this problem requires all dangerous operators to be taken into account and their contribution to correlators to be summed (the so-called infrared perturbation theory) [58]. This complicated problem is still to be solved, and its analysis can be performed only using experimental data about the scaling laws of moments (structure functions).

A very important observation follows from the consideration of the group properties. In numerical simulations of plasma turbulence using the MHD equations, scales are separated to facilitate the computation. As a rule, the resolution scale and other scales are artificially introduced for the parameterization. This procedure automatically breaks the symmetry of the original analytic equations. This means that the numerical solution obtained using such a parameterization does not have all the group symmetry properties of the original equations, the self-similarity in particular. This point is especially important in studying the behavior of the system on long time scales (the predictability problem). The growth of noise perturbations that enter the system from scales smaller than the discretization scale in numerical models becomes a fundamental problem. For example, if perturbations are taken in the form of a Gaussian noise $G(t)$ with intensity σ, then in the space of variables $\mathbf{X} = \{X_1, X_2, \ldots, X_N\}$, the system evolves in the N-dimensional space according to the equation

$$\frac{\mathrm{d}\mathbf{X}}{\mathrm{d}t} = F(\mathbf{X}, t) + G(t)\,. \tag{9}$$

Here, it is assumed that the system can be described by a finite number N of independent variables. The Liouville equation for the probability density $\rho(\mathbf{X}, t)$ (for the volume $\mathrm{d}X_1 \mathrm{d}X_2 \ldots \mathrm{d}X_N$ in the space of variables $\mathbf{X}$) is generalized to the Fokker–Planck equation

$$\frac{\partial \rho(\mathbf{X}, t)}{\partial t} + \sum_{i=1}^{N} \frac{\partial}{\partial X_i'} \left[X_i'(t)\, \rho(\mathbf{X}, t) \right] - \sigma \Delta_{\mathbf{X}} \rho(\mathbf{X}, t) = 0\,. \tag{10}$$

If the noise is correlated (for example, a non-Gaussian 'color' noise), the Fokker–Planck equation with noninteger derivatives should be considered [59–61]. Solutions of this equation are highly irregular, and hence the error (i.e., the unpredictability) in such a problem can significantly increase in a finite time interval. The exponential growth of errors in stochastic systems is predicted in classical papers by Lyapunov [62] and in ergodicity studies [63].

1.3.3 Semi-empiric cascade models. Strong turbulence is characterized by a large number of degrees of freedom, and nonlinearly interacting modes are characterized by a multi-scale structure and random pulsations of velocities and fields. Therefore, methods of statistical physics and probability theory are used to describe it. The nonlinear interaction of waves can be described in terms of the interaction of individual harmonics, which leads to wave phase chaotization (see [64]). This allows the statistical description of waves to be applied and the distribution function of some variables to be introduced. The statistical description is related to some procedure of information coarse-graining and leads to a reduction in the number of variables in the problem, and consequently, a significant part of the information on the state of individual particles (or quasiparticles, i.e., waves) is lost, but sufficient information on the macroscopic character of motion and the probability distribution over the system states is preserved.

To describe the turbulence in the framework of statistical mechanics and to fully use the achievements of the theory developed by Boltzmann, Gibbs, Planck, Einstein, and others [65], it is required to invoke additional laws describing the probability distribution function of turbulent fluctuations. The difficulty of the turbulence description in the framework of the thermodynamic approach is that motion as a whole is nonequilibrium, turbulent eddies of different scales are not equivalent, and their distribution function cannot be considered in the same way as the distribution function in a thermodynamically equilibrium system (see [3]). Therefore, special methods and approaches must be applied to describe the turbulence. For a full description of a turbulent process, the distribution function of amplitudes of fluctuations of all parameters (the probability density distribution function, PDF) must be known.

The probability distribution of fluctuations in the simplest case of a Gaussian random process follows the Gaussian (normal) law

$$P(x) = \frac{1}{\sigma\sqrt{2\pi}} \exp\left[-\frac{(x-\mu)^2}{2\sigma^2}\right],$$

where μ is the mean value and σ is the standard deviation. For example, classical Brownian motion is described by the Gaussian statistics (see [66]). There are other distributions in the probability theory [66], for example, the Lorentz distribution

$$P(x, \mu, b) = \frac{1}{\pi} \frac{b}{(x-\mu)^2 + b^2},$$

(where b is the scale parameter of the half-width at half-maximum), which can describe processes with long-range correlations. More complicated random processes with memory and long-range correlations are also considered in probability theory. The distribution functions of such processes cannot always be expressed in terms of known mathematical functions and series, and for many types of random processes, only the mean of their distribution function approximation is known.

To describe the strong turbulence in hydrodynamic flows [3] and in laboratory and space plasmas, nontrivial algebraic, fractional stable [67, 68], log-normal [55], log-Poisson [69, 70], log-Lévy [71], and other laws known in probability theory (see [66]) are used in the literature. The approximation of experimentally measured distribution functions by analytic functions is a very complicated task. In practice, to describe a distribution function, the scaling law of its moments, also known as the structure functions, are often used.

Any analytic theory of plasma turbulence remains in the framework of the linear approximation in treating non-Gaussian distribution functions. The direct numerical solution of the equations describing real plasmas encounters a fundamental problem: due to the cascade character of the process, the number of the degrees of freedom increases algebraically when passing to smaller scales. Therefore, the cascade models of turbulence are more suitable for describing turbulence with intermittency, including that in TBLs.

The turbulent cascade phenomenology in hydrodynamic turbulence has been considered starting from the work of Richardson. The redistribution of the energy flux between eddies of smaller scales at each consecutive step of the cascade process is the main assumption in phenomenological models of turbulence [1, 2, 24, 55, 69–71]. Here, the small eddies only modulate the energy that passes through them from larger scales. A hierarchy of turbulent eddies in a turbulent medium, which becomes more and more inhomogeneous on smaller scales, is considered. The stochastic cascade adequately describes many features of turbulence with intermittency.

The basic principles of the developed turbulence studies were founded by Kolmogorov [1, 2]. He proposed the strategy of investigation of developed turbulence, which led to the construction of theories of turbulence with different degrees of complexity; significant progress was achieved in describing various turbulent media.

In Kolmogorov's theory, the structure functions (moments) of order q for the velocity difference are considered on a space scale l: $\delta_l u = u(x+l) - u(x)$, $S_q(l) \equiv \langle |\delta_l u|^q \rangle$, or on a time scale τ: $\delta_\tau u = u(t+\tau) - u(t)$, $S_q(\tau) \equiv \langle |\delta_\tau u|^q \rangle$. For a turbulent field $X(t)$, the qth-order structure function is defined as the statistical mean over the ensemble of differences $\delta_\tau X = X(t+\tau) - X(t)$, $S_q(\tau) \equiv \langle |\delta_\tau X|^q \rangle$. The statistical averaging $\langle \ldots \rangle$ is performed with a weight function, the distribution function for $\delta_\tau X$. Studying structure functions is equivalent to studying the distribution function of turbulent fluctuations. From the practical standpoint, it is simpler to study the structure functions because some of them can be measured in experiment. The structure functions (see [3]) allow a detailed description of the inhomogeneity of the distribution on different scales of the process. For an isotropic developed turbulence, Kolmogorov considered the turbulent cascade and assumed that in the inertial range $\eta \ll l \ll L$ (where η is the dissipation scale and L is the global scale) at high Reynolds numbers, all statistically averaged moments $S_q(l)$ of the velocity field u on a scale l depend only on the mean dissipation rate ε_l and the scale l (the property of locality, the K41 model). In the inertial range, the K41 theory assumes a statistical quasi-equilibrium of fluctuations and the Gaussian statistics for the velocity pulsations. The dynamics in the inertial range are independent of the way the turbulence was excited and are determined by the invariant energy flux through this range: the mean energy flux is assumed to be conserved. Scaling laws (i.e., the scale invariance laws) for $S_q(l)$ and the energy dissipation rate ε_l are then given by [1–3]

$$S_q(l) \sim \langle |\delta_l u|^q \rangle \sim l^{\zeta(q)}, \quad \langle \varepsilon_l^q \rangle \sim l^{\tau(q)}, \tag{11}$$

with the mutually dependent exponents $\zeta(q) = q/3 + \tau(q/3)$. Based on dimensional analysis, Kolmogorov derived the famous scaling law $E_{\rm K}^{(k)} \sim k^{-5/3}$ for the energy flux spectrum (the 'five thirds' law) for developed turbulence in the inertial range. In the K41 model, the scaling of structure functions is linear, $\zeta(q) = q/3$, which reflects the fact of the simplest self-similarity.

The K41 model satisfactorily explained many experimental observations in turbulent hydrodynamic flows [3]. But in some hydrodynamic flows, an insignificant deviation of the index γ in the law $E_{(k)} \sim k^{-\gamma}$ from five thirds was found: $\gamma = 1.71 \pm 0.02$ (see, e.g., [3, 24]). This correction of the scaling law is of fundamental importance because it is related to special symmetries and describes the inhomogeneity structure of turbulence. This property leads to a significant deviation of higher-order structure function scaling laws (at large $q > 3$) from the linear Kolmogorov scaling law $\zeta(q) = q/3$. In the case of intermittent turbulence, the higher-order structure functions demonstrate a scaling law where $\zeta(q)$ is a nonlinear function of q. This fact reflects deviations of PDFs from the Gaussian law.

The K41 model is based on the assumption of the local character of turbulence. This means that in the inertial range, the change in energy on a given scale is determined only by the interaction of eddies with close wave numbers, and the interaction time is long (longer than the time of eddy's 'turnover'). The interaction of eddies with strongly different sizes is small. In the K41 model, turbulent eddies of each scale fill all the space homogeneously. From the standpoint of topology, the turbulent cascade can be described by a fractal: the energy is transferred via the fractal tree that consists of a hierarchical structure of eddies with different sizes. The use of fractal geometry for describing turbulence and the cascade process led to significant progress in describing scaling laws (see, e.g., [72]).

Fractal structures are scale invariant and are described by power laws, which corresponds to properties of turbulence. Power laws of the scale similarity (scaling laws) can have scale-dependent exponents (multiscaling). These laws can describe the intermittency observed in turbulent plasma and hydrodynamic flows. The scale similarity laws of the turbulent cascade determine symmetries that must be present in the equations describing turbulence: these symmetries underlie the relation between the semi-empirical cascade and hydrodynamic models.

Based on studies of self-similarity properties of turbulence (which is equivalent to the search for statistical symmetries and studies of fractal properties of turbulence [24]), several models of hydrodynamic turbulence were constructed, such as the log-normal K62 model [55], the α, β, and p-models (see [24]), the multifractal [24] and log-Poisson [69, 70] models.

In the K62 model, Kolmogorov proposed taking the local inhomogeneity of turbulence into account — the similarity hypothesis (power laws) for the energy dissipation moments and the normal law for the energy dissipation logarithm (the log-normal law). The log-normal hypothesis has not been confirmed, either experimentally or theoretically (see [3]). Nevertheless, starting from the K62 model, the statistical inhomogeneity has been considered in subsequent turbulent cascade models.

The subsequent α, β, and p-models treated the cascade process taking the inhomogeneous character of the process into account. These models studied the general features of turbulence with intermittency, while properties of the dissipative (viscous) range were not studied, which precluded a full description of intermittency by these models.

1.3.4 The two-dimensional Iroshnikov–Kraichnan MHD model. A magnetic field in interplanetary and laboratory fusion plasmas makes dynamical processes in the plasma strongly anisotropic. In the literature, the plasma dynamics in the plane across the magnetic field are therefore studied in the framework of the two-dimensional model. Two-dimensional turbulence models study solutions of the equations of motion (the MHD equations in plasma or the Navier–Stokes equations in hydrodynamics) that depend only on two coordinates.

Two-dimensional turbulence is not a pure simplification of the three-dimensional one (see [32]). In planar geometry, a turbulent motion acquires qualitatively different properties (see above). It has been found that purely two-dimensional turbulence can hardly be realized in nature. But the two-dimensional approach remains attractive because it is amenable to numerical simulation. The two-dimensional approach enables the treatment of some effects, such as extremely large eddies (the phenomenon of a tornado in the atmospheric turbulence). In this case, we are dealing with a quasi-two-dimensional approach. To describe turbulent processes in which a high degree of anisotropy on the global scale strongly affects small-scale fluctuations, the Kraichnan approach [73, 74] is used. Turbulence in a magnetized plasma is frequently described by the two-dimensional Iroshnikov–Kraichnan (IK) model [75, 76]. The energy spectrum in the IK model is

$$E_{\rm IK}(k) = \left\langle |\delta u(k)|^2 \right\rangle k^2 \propto k^{-3/2}\,. \qquad (12)$$

In comparison with the Kolmogorov spectrum $E_{\rm K}(k) \propto k^{-5/3}$, the rate of energy transfer on small scales in this model is significantly reduced and the energy transfer time increases. The structure function scaling law in the IK model is $S_q(l) \sim l^{q/4}$. The essential assumption of the IK model is the equal size of turbulent eddies in the direction along and across the field (Fig. 3) and the absence of correlations between different eddies. This assumption has not been justified in all possible cases.

The invalidity of the 'weak coupling approximation' used in the IK model to describe small-scale fluctuations of developed turbulence is clarified in Kadomtsev's paper [12]. The Kraichnan scheme overestimates the effect of large-scale

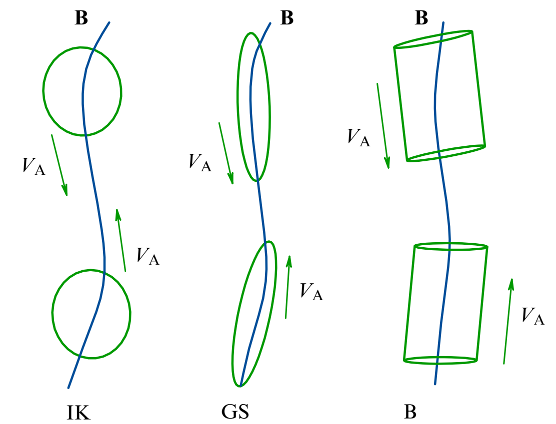

Figure 3. The form of turbulent perturbations moving with the Alfven velocities $V_{\rm A}$ in a strong magnetic field **B**, symmetric in the Iroshnikov–Kraichnan (IK) model, elliptical, stretched along the field in the Goldreich–Sridhar (GS) model, ribbon-like, stretched along the field in the Boldyrev (B) model.

fluctuations on the evolution of small-scale inhomogeneities: this effect reduces to the transfer of small-scale fluctuations with their small deformation (the adiabatic approximation). Despite the shortcomings, the IK model continues to be used in many papers (for example, to interpret the properties of interplanetary plasma turbulence or of tokamak plasmas).

The phenomenology of the IK model was used in the subsequent MHD turbulence models. The large-scale anisotropy and mixing in the turbulent magnetic field on microscales are considered in detail in the model of moderately strong MHD turbulence by Goldreich and Sridhar (GS95 [77]). This model of turbulence takes the balance of nonlinear terms in the MHD equation into account and was dubbed moderate or intermediate turbulence. It differs from the model of weak MHD turbulence and describes the Kolmogorov spectrum, observed in space plasma, of fluctuations in the direction perpendicular to the magnetic field. In the GS95 model, the motion of asymmetric cells (Fig. 3) mixes magnetic field lines in the direction locally normal to the field. The cascade spectrum across the field is close to the Kolmogorov one, and the turbulence becomes local, similar to hydrodynamic one. The GS95 model superseded the IK model in MHD turbulence because it explains experimental data in interplanetary plasma. The applicability of the GS95 model to edge plasma in laboratory devices remains an open issue that requires experimental verification.

The MHD turbulence model of Boldyrev [79] further develops the approach suggested in the GS95 model and considers the anisotropy of turbulent eddies not only along but also across the local magnetic field. Such anisotropy admits the introduction of sheet (ribbon-like) turbulent structures that occur in numerical simulations [80].

The GS95 and Boldyrev models use two-dimensional sheets and ribbon-like formations as dissipative structures based on the modern theoretical and experimental results on MHD turbulence.

We emphasize that determining the geometry of dissipative structures (their size and anisotropy) is one of the key questions in the treatment of strong turbulence. The anisotropy usually changes when passing to smaller scales, which is experimentally observed in many turbulent media. For example, in plasma, turbulent eddies can change their characteristic form on different scales (this is considered in the GS95 model [77]), and the small-scale isotropization probably plays a more important role than anisotropy effects on large scales.

1.3.5 The log-Poisson model of turbulence with intermittency. *The log-Poisson models* of turbulence appeared in the mid-1990s and represent a generalization of fractal models developed earlier, in particular, the β-model [24]. These models were elaborated after phenomenological observation of an extended self-similarity in hydrodynamic turbulence [81]. In the log-Poisson model, multiplicative random cascades and the coexistence of regions with different scaling laws in a turbulent flow are assumed. From the standpoint of fractal topology, this is a multifractal structure.

A multifractal random cascade can describe turbulence with intermittency (see review [82]). The multifractal model has a boundary scale (for example, the maximum scale). It is based on the assumption that consecutive cascades determine the flux distribution over smaller-scale cells and that the cascade between any scales l_1 and l_2 ($l_1 < l_2$, $l_1 = \lambda l_2$, $l_2 = \lambda' L$) is equivalent to that from the largest scale L to l_2 with the scale factor $\lambda\lambda'$. A random multiplicative process can be described by an equation expressing the interdependence of energy fluctuations ε_l on two different scales, l_1 and l_2: $\varepsilon_{l_2} = W(l_1, l_2)\,\varepsilon_{l_1}$, or of velocity fluctuations, $\delta u(l_2) = W(l_1, l_2)\,\delta u(l_1)$. Multifractality can be described by a multiplicative cascade,

$$\delta u(l) = W(l, L)\,\delta u(L), \quad \delta u(l) = u(x + l) - u(x), \quad l < L\,. \tag{13}$$

In the simplest case, it is assumed that the generator W is independent of ε_l. The distribution function for W can be nontrivial and have fitting parameters corresponding to physical quantities, which can be determined from experiment. The generator $W(l, L)$ is a random scalar value proportional to $(l/L)^h$. For $l_1 < l_2 < l_3$, we can then derive

$$W(l_2, l_3) = W(l_1, l_2) \bullet W(l_2, l_3)\,, \tag{14}$$

where $\bullet$ stands for logical multiplication. The generator W determines the scaling law $\zeta(q)$,

$$\zeta(q) = \frac{\lg \left\langle W^q(l_1, l_2) \right\rangle}{\lg(l_1/l_2)}\,, \tag{15}$$

as well as the statistics and self-similarity properties of the process. The scaling law $\zeta(q)$ is the characteristic function of the generator W (see [83, 84]).

The assumptions used in models of stochastic multiplicative cascades are based on intuitively clear arguments: statistical states of fluctuations in the inertial range are related only through nonlinear coupling of modes in the dynamical system. In a quasistationary state, a strong phase mixing of many modes occurs, which leads to chaotization. Thus, the connection between large and small cells becomes independent of a chosen cell and is independently maintained for the size ratio of two cells. Because $\ln(l_2/l_1) < 0$, the function $\zeta(q)$ in Eqn (15) must be a nonlinear function of the moment order q. Physically, this is explained by symmetry breaking of the Navier–Stokes and MHD equations under time reflection $t \to -t$, $u \to -u$, which reverses the energy flux. This symmetry breaking is provided by the term with viscosity, which is responsible for the nonlinearity of the function $\zeta(q)$.

In the most general log-Poisson model by She–Leveque–Dubrulle (ShLD) [69, 70], it is assumed that there exists a limit value ε_l^∞ associated with the most dissipative structures. The dimensionless dissipation energy $\pi_l = \varepsilon_l/\varepsilon_l^\infty$ is introduced and three similarity hypotheses are adopted:

1) the scaling law of the structure function is the same as in the K62 model, $\zeta(q) = q/3 + \tau(q/3)$, $\langle \varepsilon_l^q \rangle \sim l^{\tau(q)}$ (ε_l is the mean dissipation rate measured inside the cells, for example, a sphere or a cube, of size l) and describes the local inhomogeneity (intermittency);

2) the hierarchy of moments of the mean dissipation rate has the power-law dependence

$$\frac{\langle \pi_l^{q+1} \rangle}{\langle \pi_l^q \rangle} = A_q \left(\frac{\langle \pi_l^q \rangle}{\langle \pi_l^{q-1} \rangle} \right)^\beta \tag{16}$$

(presumably, this property is due to hidden symmetries of dynamical equations, the Navier–Stokes equation in hydrodynamics or MHD equations in plasma. The index β characterizes the degree of intermittency; in developed isotropic turbulence, $\beta = 1$, as in the K41 model, for example);

3) the scaling law of limiting dissipative structures has the form $\varepsilon_l \sim l^{-\Delta}$ for $l \to 0$, where Δ is a parameter related to the geometry of dissipative structures and boundary effects [70].

Hypotheses 1–3 are based on the assumption that there are power laws associated with self-similar symmetries of turbulence, i.e., the property of scale invariance holds. The analysis of hypotheses 1–3 allows deriving a formula for the scaling of structure functions. Below, we reproduce this derivation (see, e.g., [32]).

From Eqn (16), we have

$$\langle \pi_l^{q+1} \rangle = \langle \pi_l^q \rangle^{\beta+1} \langle \pi_l^{q-1} \rangle^{-\beta} . \tag{17}$$

We write the chain

$$\begin{aligned} &\langle \pi_l^2 \rangle = \langle \pi_l \rangle^{\beta+1} , \\ &\langle \pi_l^3 \rangle = \langle \pi_l^2 \rangle^{\beta+1} \langle \pi_l \rangle^{-\beta} , \\ &\ldots \\ &\langle \pi_l^q \rangle = \langle \pi_l \rangle^{\psi} , \end{aligned} \tag{18}$$

where

$$\psi = \sum_{m=0}^{q-1} \beta^m = \sum_{m=0}^{\infty} \beta^m - \sum_{m=q}^{\infty} \beta^m = \frac{1}{1-\beta} - \frac{\beta^q}{1-\beta} = \frac{1-\beta^q}{1-\beta} , \tag{19}$$

where

$$\langle \pi_l^q \rangle = \langle \pi_l \rangle^{(1-\beta^q)/(1-\beta)} \sim (\delta_l u)^{\Delta(1-\beta^q)/(1-\beta)} . \tag{20}$$

Then the qth-order moment of velocity can be expressed through the third-order moment

$$\langle \delta_l u^q \rangle \sim (\delta_l u^3)^{q/3} \frac{\langle \pi_l^{q/3} \rangle}{\langle \pi_l \rangle^{q/3}} = (\delta_l u)^{(q/3)(1-\Delta)+\Delta(1-\beta^{q/3})/(1-\beta)} , \tag{21}$$

$$\langle \delta u_l^q \rangle = \langle \delta u_l^3 \rangle^{\zeta(q)} , \tag{22}$$

$$\zeta(q) = (1-\Delta)\,\frac{q}{3} + \frac{\Delta}{1-\beta}\,[1-\beta^{q/3}] . \tag{23}$$

For an isotropic three-dimensional turbulence, She and Leveque (ShL) [69] assumed $\Delta = \beta = 2/3$, which yields the scaling law

$$\zeta(q) = \frac{q}{9} + 2\left[1 - \left(\frac{2}{3}\right)^{q/3}\right] . \tag{24}$$

We briefly describe the cascade in the log-Poisson model. We consider a multiplicative turbulent energy cascade in a system with a hierarchy of turbulent eddies or velocity fluctuations with different scales and amplitudes. We divide the entire volume into small cubic cells of size l_0 and introduce the energy dissipation rate ε_l in each cell. In the stationary case, the dissipation energy flux averaged over all cells is equal to the input energy flux on the largest scales. In the basic cascade treatment by Kolmogorov, the dissipation flux is constant. Next, we separate each cell into cubic boxes of size λl_0, where $0 < \lambda < 1$, and repeat the procedure on all scales using the same factor λ. As a result, we obtain a hierarchy of cells as shown in Fig. 4. We consider two levels of hierarchy: l with the flux ε_l and $l' = \lambda l$ with new cells. We assume that a fraction y of these cells has the energy dissipation flux $\varepsilon_1' = \beta_1 \varepsilon_l$, and the fraction $1-y$ has the dissipation energy flux $\varepsilon_2' = \beta_2 \varepsilon_l$. If the energy flux down the cascade is conserved, then $y\beta_1 + (1-y)\,\beta_2 = 1$. We assume that the division by cells is random, i.e., a fixed point of observation can fall into any of the newly created cells with equal probability. After a large number m of cell splitting, the scale $l_m = l_0 \lambda^m$ is reached. The moment of energy $\varepsilon_l^q \gtrsim l^{\tau(q)}$ averaged over the entire volume with the scaling law

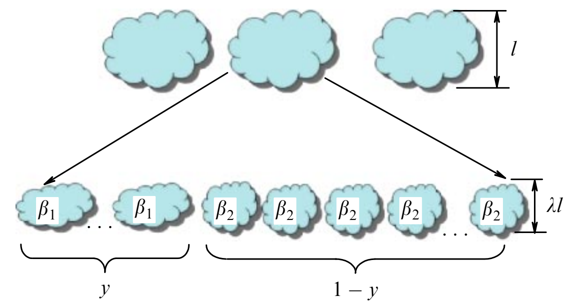

Figure 4. Diagram of a random anisotropic multiplicative cascade in the log-Poisson model.

$$\tau(q) = \frac{\lg(W^q)}{\lg l} , \tag{25}$$

where $W = \varepsilon_{i+1}/\varepsilon_i$ is the cascade factor describing the process and

$$W = \begin{cases} 0 & \text{with probability} \;\; 1 - y\beta_1 - (1-y)\,\beta_2 , \\ 1/\beta_1 & \text{with probability} \;\; y\beta_1 , \\ 1/\beta_2 & \text{with probability} \;\; (1-y)\,\beta_2 , \end{cases} \tag{26}$$

allows finding the value β_1 with probability y and β_2 with probability $1-y$. We now assume that $y \ll 1$ and the cascade develops with a small parameter $\lambda = 1 - C_0/y$. For $y \ll 1$, $\beta_1 < 1$, and $\beta_2 > 1$, the structures with β_1 are the most intensive and singular structures. Using Eqn (26), we obtain

$$\tau(q) = C_0(\beta_1 - 1)\,q + C_0(1 - \beta_1 q) . \tag{27}$$

The parameter C_0 is associated with the fractal dimension of the structures whose energy fraction is β_1. The number of such cells is $N_m = N_0\left[(1-y)/\lambda^3\right]^m$, and the cubic cell size on the mth level of the hierarchy is $l_n = l_0 \lambda^m$. The fractal dimension calculated by box-counting is

$$D = -\lim_{m\to\infty} \frac{\lg(N_m)}{\lg(l_m/l_0)} = 3 - C_0$$

for $y \ll 1$.

The value of C_0 is the codimension of the structure that covers only cells characterized by the parameter β_1. We have $C_0 = 2$ for one-dimensional (filamentary) structures and $C_0 = 1$ for two-dimensional structures like layers (we note that this definition of the dimension is different from definitions used in geophysics, for example). For the energy dissipation rate, we can use the Kolmogorov formula $\varepsilon_l \approx (\delta_l u)^3/l$. Then the scaling law for the velocity structure function in Eqn (22) is

$$\zeta(q) = \left[1 - C_0(1-b)\right] \frac{q}{3} + C_0(1 - b^{q/3})\,. \tag{28}$$

A comparison with Eqn (23) yields a relation between C_0 and Δ. The parameter $\beta = \beta_1$ characterizes the degree of intermittency, which can be determined from numerical simulations or from experiment (in the $\beta = 1$ case without intermittency). Based on experimental data on hydrodynamic turbulence, it is assumed that one-dimensional filaments are the limiting dissipative structures in hydrodynamics: only filamentary structures appear to be mechanically stable on small scales in hydrodynamic systems (see [3]).

The logarithm of the energy dissipation rate ε_l obeys the Poisson distribution (which is why the model is called log-Poisson):

$$\mathrm{P}(y, \mu) = \frac{\mu^y e^{-\mu}}{\Gamma(y+1)} \quad \text{with} \quad y = \frac{\ln \varepsilon_l}{\ln \beta}\,, \tag{29}$$

where $\mu > 0$ is the Poisson distribution parameter.

We recall that the Poisson distribution (PD) (see [66]) is one of the most important probability distributions of integer random values. For example, the PD well describes the radioactive decay of atoms and many other physical phenomena.

A note should be made on the practical application of log-Poisson models for interpretation of experimental data. In [85], a stochastic multiplicative cascade is considered in which dissipative structures with different dimensions can be simultaneously formed, including a fractal, which yields a complicated topology. This process is described in probability theory by the Khinchin–Lévy model [85], which should be used in interpreting experimental results in the case where deviations of experimental scaling from formula (23) with fixed Δ and β are observed. Such deviations can be connected with a complicated geometry of dissipative structures or with the simultaneous presence of structures of different dimensions. In that case, the process can be characterized by the adjustable values Δ and β.

The Politano and Pouquet model. Politano and Pouquet [86] generalized the She–Leveque model to the case of MHD turbulence. They used the approach suggested by the two-dimensional MHD turbulence model by Iroshnikov–Kraichnan by assuming two-dimensional dissipative structures. The Politano–Pouquet model predicts the scaling law [86]

$$\zeta(q) = \frac{q}{8} + 1 - \left(\frac{1}{2}\right)^{q/4}. \tag{30}$$

A stochastic multiplicative cascade is also considered in other models, for example, in the log-Lévy model [82, 83, 87]. Essentially, the stochastic multiplicative cascade is parameterized in this model the same as in the log-Poisson model. But the log-Lévy model does not suggest any physical illustration of a turbulent process, for example, in terms of the geometry of dissipative structures.

As noted above, phenomenological cascade models of turbulence with intermittency are not directly derived from equations of motion (for example, those describing the edge plasma in tokamaks); the cascade properties are related to the structure and symmetries of the dynamic equations. Another assumption concerns the nature of dissipative structures: in a three-dimensional turbulent flow of an incompressible neutral liquid, only one-dimensional filamentary structures,

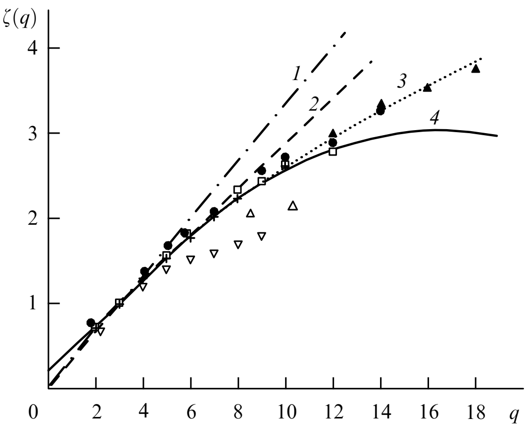

Figure 5. Experimental scaling laws of hydrodynamic turbulence and a comparison with (1) the K41 model, (2) the β-model, (3) the She–Leveque log-Poisson model, and (4) the log-normal model (from book [24]).

as noted above, are stable on small scales (see [3]). In two-dimensional models of incompressible fluids and in the Iroshnikov–Kraichnan model of MHD turbulence, dissipative structures can be two-dimensional (sheets, layers, and so on), and therefore their predictions can be different from those of three-dimensional models.

The cascade log-Poisson models satisfactorily describe experimental measurements of hydrodynamic turbulence with intermittency; the nonlinear scaling law of the structure function is close to the model scaling law (Fig. 5). But log-Poisson models have not yet been widely used to describe strong plasma turbulence.

Extended self-similarity. Extended self-similarity (ESS) was discovered experimentally in studies of low-scale hydrodynamic turbulence in a wind tunnel [81]. At relatively low Reynolds numbers, when $S_q(l) \sim l^{\zeta(q)}$ in the usual representation of turbulence and the inertial range is not seen, the dependence

$$S_q(l) \sim S_3(l)^{\zeta(q)/\zeta(3)} \tag{31}$$

was found for an extended range of scales $l \geqslant 5\eta$, where η is the Kolmogorov dissipation scale. This property (which can be called the generalized self-similarity) is observed almost down to those scales where dissipation occurs. This phenomenological observation led to the criterion of the generalized self-similarity in the form

$$S_q(l) \sim S_p(l)^{\zeta(q)/\zeta(p)} \tag{32}$$

(for any pair of structure functions), assuming the log-Poisson statistics of turbulence [69, 70]. Presumably, this self-similarity is a manifestation of hidden statistical symmetries.

To test the log-Poisson model hypotheses on the existence of power laws, we can study the scaling law of relative moments $\Pi_q(\tau) = S_{q+1}(\tau)/S_q(\tau)$ and analyze the dependence in the form

$$\Pi_{q+1} = (\Pi_q)^{\delta_q}\,. \tag{33}$$

The similarity hypothesis in the ShLD model modifies the similarity hypothesis adopted in the K62 model [55]:

$$\zeta_q = (\zeta_3 + \delta_0)\,\frac{q}{3} + \tau_{q/3}\,. \tag{34}$$

The ShLD and K62 hypotheses coincide at $\zeta_3 = 1$ and $\delta_0 = 0$. Both conditions are satisfied in the case of three-dimensional turbulence and are violated for two-dimensional turbulence [32].

The log-Poisson model has the advantage of taking the effect of the dissipative range into account when boundary effects play a significant role in a system with a relatively low Reynolds number and a restricted inertial range is observed. The generalized self-similarity property takes boundary effects into account; the scale invariance is here formed not in an infinite space but on a finite interval of scales. This naturally allows analyzing the effects of viscosity (dissipation) and the properties of dissipative structures, in particular, their dimensionality. For example, the log-Poisson model of isotropic three-dimensional hydrodynamic turbulence assumes that one-dimensional filamentary structures are responsible for dissipation. In the log-Poisson model, which takes the empiricism of the Iroshnikov–Kraichnan model into account, two-dimensional dissipative structures are assumed [86, 88].

1.4 Features of transport in turbulent boundary layers

Intensive experimental research on low-frequency plasma turbulence started after Bohm derived his famous semi-empirical formula for the transverse diffusion coefficient in a strong magnetic field (see [12]):

$$D_{\mathrm{B}} = \frac{1}{16}\,\frac{k_{\mathrm{B}} T_{\mathrm{e}}}{eB}\,, \tag{35}$$

where k_{B} is the Boltzmann constant and T_{e} is the electron temperature.

This formula suggests that the dependence on the magnetic field is weaker ($D_{\mathrm{B}} \sim 1/B$) than in the classical diffusion ($D \sim 1/B^2$), i.e., suggests an anomalous (enhanced) diffusion of plasma in a magnetic field. Bohm's formula satisfactorily described experimental observations of the plasma diffusion in a voltage arc and subsequently was widely used in describing anomalously large losses in magnetic traps in FDs [12, 16, 89]. The role of low-frequency turbulent electric fields and density fluctuations in the transport phenomena across the magnetic field was clarified. The anomalous diffusion is a result of turbulence. In turbulent eddies, plasma moves across the magnetic field with the drift velocity $V_{\mathrm{T}} \sim E/B$. The electric field can be estimated approximately as perturbations of the potential divided by the characteristic space scale δ_{T} of turbulent eddies. This scale can be used in estimating the diffusion coefficient D. The thermal energy of a turbulent plasma is the energy reservoir for the perturbations of the potential, and therefore the potential perturbation can be estimated as $k_{\mathrm{B}} T/e$ by an order of magnitude. Then the turbulent diffusion coefficient is $D = \delta_{\mathrm{T}} V_{\mathrm{T}} \sim k_{\mathrm{B}} T/eB$, which coincides with Bohm's formula (35) up to a numerical factor.

In TBLs, the transport is not the diffusion. In FDs, it was found that most of the plasma flow (up to half) across the magnetic field can be transported by coherent turbulent structures (the studies were carried out in tokamaks T-10 [90], TF-2 [21], DIII-D [92], and others). Such a transport is characterized by the effective diffusion coefficient attaining tens of 'Bohm's' values. Here, the turbulent flow is highly inhomogeneous in space and exists even in the region with an unfavorable curvature of the magnetic field [93].

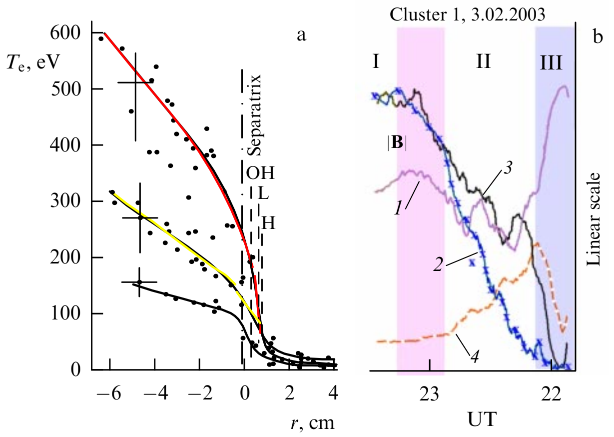

Figure 6. The transport barrier in the periphery zone of tokamak Asdex. The barrier value changes in the improved confinement regime (H-mode). The electron temperature profile in (a) tokamak [94], (b) the Earth magnetosphere [95] (measurements by the Cluster I spacecraft 03.02.2003). I — the dense solar wind plasma region, II — hot stagnation turbulent zone, III — magnetosphere, *1* — magnetic field strength $|\mathbf{B}|$ (the maximum indicated by a line is the magnetic barrier), *2* — velocity, *3* — density, *4* — temperature of ions.

Experiments revealed that the turbulence and the induced turbulent flow are due to transport barriers at the edge of the plasma discharge (Fig. 6a). When the plasma energy content exceeds some value, spontaneous transitions to the high confinement regime (H-regime) are observed, where the turbulence level and turbulent transport change [94].

The transport barrier is also observed in the TBL of Earth's magnetosphere [95, 96]. As an example, Fig. 6b shows the transition from a dense solar-wind plasma bypassing the magnetosphere (region I on the left), which is a topological analog of the central plasma in tokamaks (cf. zone I in Fig. 1a), to the outer magnetosphere (region III on the right), which is an analog of the near-wall zone in tokamaks. Both density (*3*) and velocity (*2*) of the plasma decrease in the magnetosphere, almost to zero. But the transition itself (the region similar to region II in Fig. 1a) contains two substructures:

a) a magnetic transport barrier (*1*, see the plot of $|\mathbf{B}|$) with a relative maximum in $|\mathbf{B}|$ at 23 UT, when plasma pressure is dominated by the magnetic field pressure produced in the Alfvenic collapse of the magnetic field lines that are forced down by the incoming flow to the magnetic obstacle and are upturned by the flow [95];

b) a hot stagnation turbulent region (II, see the significant velocity decrease of the plasma and its heating in the ion temperature plot *4*), apparently similar to region III in Fig. 1a.

As shown in [19, 20], up to 80% of the plasma flow incident on the transport barrier can be reflected by plasma turbulence, whose mean amplitude is comparable to the main field (which is often observed in the vicinity of the outer polar cusp). Here, turbulence not only can lead to an anomalous diffusion (which provides up to 10% of the diffusion flux in the total flux [19, 20]) but also can create the transport barrier itself. Such a mechanism of the self-consistent regime is also discussed in the literature in describing the periphery transport and transport barriers (H-regimes) in tokamaks and other fusion devices (see, e.g., [97]). Intermittency in a small-scale turbulence with non-Gaussian statistics that provides the anomalous transport exactly on small scales (in comparison with large-scale coherent structures; see below) apparently plays a dominant role in sustaining this regime. In other words, the local (small-scale) superdiffusion with 'correctly' chosen parameters and statistical properties can effectively destroy the medium-scale structure of the boundary layer, which contains middle-scale 'intermittent' bursts with the intensity far exceeding the Gaussian statistics predictions. Here, the anomalous small-scale transport most likely predictions smears the boundaries and the medium-scale bursts of the plasma flow themselves (see the description of the effect of small paddles in the case of two rotating cylinders in [5]).

The model of self-organized criticality (SOC) [98] is discussed in the literature concerning anomalous transport processes. Most of the existing experimental results on TBLs in laboratory and magnetospheric plasmas are not described by the standard SOC model (see, e.g., [99]). The applicability of a modified SOC model to the description of anomalous transport processes in Earth's magnetosphere is discussed in [96].

The size of boundary layers and transport barriers in laboratory FDs is small, about several centimeters across the magnetic field, and it is difficult to study them experimentally. That is why detailed experimental research on turbulence and transport barriers in the TBL of the magnetosphere by space probes will help develop new approaches to describing and controlling plasma transport in fusion reactors. This review is one of the first steps in this direction.

2. Experimental data

2.1 Studies of hydrodynamic turbulence

During the last hundred years, developed hydrodynamic turbulence has been studied by many researchers; the most significant results were obtained by A N Kolmogorov, G I Taylor, L Prandtl, T von Kármán, A M Obukhov, and others. In spite of significant efforts, the treatment of the problem 'from first principles' based on the Navier–Stokes and continuity equations did not led to the formulation of a complete rigorous theory of turbulence in liquids and gases. Therefore, Kolmogorov suggested the most promising and realistic approach where hypotheses rely on the results deduced from experimental data. Such models describe only special classes of turbulent flows. Such an approach enabled new data to be obtained and basic hypotheses suggested earlier to be generalized or modified, as well as new theories allowing further progress and describing more general turbulent flows to be formulated.

For turbulence at very high Reynolds numbers (so-called developed turbulence), two principal results were obtained, which were assumed to be universal. These are the Kolmogorov–Obukhov scale invariance law for the local structure of developed turbulence, the famous K41 model [1, 2], and the universal von Kármán–Prandtl logarithmic law for turbulent flows with the shear restricted by walls (shear flows or flows with the velocity gradient, including the TBL; see [8]).

Properties of flows in turbulent boundary layers were systematically considered by Monin and Yaglom (e.g., [3, 100]); the importance of the structure of the flow was stressed as early as the 1950s (see, e.g., [101]). In the last few years, the relation between the flow structure and the TBL scaling properties has been discussed in reviews [102, 103]. From the very beginning, the study of this problem has been focused on the properties of the near-wall turbulence at large Reynolds numbers.

The laboratory experimental data on the developed turbulence at very high Reynolds numbers is still insufficient to make definitive conclusions on the local structure of turbulence, and geophysical (atmospheric and oceanic) data is not clear enough (see, e.g., the remark on this subject in review [8]). Nevertheless, in recent decades, solid experimental evidence has been obtained that strongly changes the perception of basic hypotheses of turbulence. This concerns, first of all, the role of intermittency and the correction of the universal logarithmic law by von Kármán, which requires a revision of the TBL theories based on this law.

The universal logarithmic law is based on von Kármán's hypothesis of the independence of the velocity gradient in the intermediate region of the boundary layer from viscosity (this assumption was first clearly formulated by Landau [6]). The intermediate region of the boundary layer is the zone between the 'viscous underlayer' (i.e., adjusting directly to the wall with large velocity gradients, where the viscous stress is comparable to that produced by turbulent eddies) and the central zone of the flow (for example, near the flow axis in the cylindrical case). Based on this hypothesis and on dimensionality considerations, one can deduce a 'universal', i.e., not depending on the Reynolds number, law of the velocity distribution in the intermediate region (see, e.g., [8] for the derivation) — the von Kármán–Prandtl law

$$U^+ = \frac{1}{\kappa}\ln(y^+) + C\,, \tag{36}$$

where $U^+ = u/u_*$, $y^+ = u_* y/\nu$, $u_* = (\tau/\rho)^{1/2}$ is the friction velocity, y is the distance from the wall, ρ is the density, and τ is the viscous stress on the wall. In this law, the constants C and κ are assumed to be independent of the Reynolds number and must coincide in all high-quality experiments. However, experimental data accumulated in the last few decades calls for the revision of this law and the underlying hypothesis (see [8]). Even allowing for a very broad range of values of C and κ (from 4.1 to 6.3 for C and from 0.38 to 0.44 for κ), law (36) was found to apply in a very narrow range (see [3] and the data for flows in wind tunnels in [104]). For example, in some wind-tunnel experiments (see [105]), the coefficient C was observed to depend on the Reynolds number.

The classical scaling laws (see [106]) were proposed for verification in [8, 107–109]). To describe experimental data on turbulent boundary layers, power-law dependences of the mean velocity on the Reynolds number have been proposed, which means that the scale invariance property was used (see [8, 103, 110] and the references therein), in particular [8],

$$U^+ = \left(\frac{\sqrt{3} + 5\alpha}{2\alpha}\right)(y^+)^\alpha\,, \quad \alpha = \frac{3}{2\ln\mathrm{Re}}\,. \tag{37}$$

Based on these assumptions, many papers (see the references in [110]) have attempted to treat experimental measurements in TBLs using power laws in the form of asymptotic power series in the parameter $\varepsilon = 1/\ln\mathrm{Re}$. For variations of Re in a wide range, ε remains sufficiently small. A power law reflects a nontrivial self-similarity because the self-similarity exponent depends on the Reynolds number. Such a scale invariance (dilatational symmetry) produces the intermittency observed in many experiments.

Discussions of the applicability of the logarithmic or power law in TBLs and the universality of properties of the near-wall flow (in the sense that the effect of the outer flow on the near-wall flow is fairly small) [107, 111] stimulated serious experimental research with high Reynolds numbers and a revision of basic scaling relations. Recent reviews of these studies are given in [103, 112].

Another important question in studies of near-wall turbulence is related to the observation of coherent structures in TBLs, starting from horseshoe-like eddies. Studies of coherent structures (see reviews [103, 113–115]) revealed that the turbulent flow in the near-wall region sometimes violently interacts with the outer flow via sudden ejections of near-wall liquid into the outer region (in the form of 'bursts'), and near-wall motion is clearly modulated by the expansion of structures from the outer layer. The concept of 'active' and 'passive' motion was put forward as early as the 1950s (see, e.g., [101]). In this concept, fluctuations across the main flux (responsible for the momentum transport) and longitudinal fluctuations are considered. To explain the properties of intermittent turbulent flows, various models have been proposed (multifractal, log-Poisson, log-Lévy, etc.; see, e.g., [71, 82]), which are also applied to describe statistical characteristics of turbulent flows.

In [116–120], a theory was proposed based on the Navier–Stokes equation in the limit of the infinite Reynolds number. In this model, due to the infinite speed of sound, the boundaries (walls) are assumed to affect all points in the flow, regardless of the volume. The 'large-scale' component of pressure is considered here; it is responsible for the development of one-dimensional vortex structures — filaments, which provide the intermittency property. The vorticity takes maximum values in the filaments. In this model, the Lagrange structure functions of velocity $K_n(\tau) \propto \tau^{\zeta_n}$ are calculated on the incremental time scale τ, which is small compared to the correlation time of large-scale turbulence, $\zeta_n = n - \Lambda_{2n}/\Lambda_4$, where Λ_{2n} is the exponent describing the time dependence of the vorticity moment $\langle \omega^{2n} \rangle \sim \exp(\Lambda_{2n} t)$ and ω is the vorticity. The exponents Λ_{2n} are calculated numerically, in particular, $\Lambda_2 = 2.52$, $\Lambda_4 = 6.12$, and $\Lambda_6 = 10.43$. The obtained analytic expressions for ζ_n have no fitting parameters and are in agreement with experimental data [12] and numerical calculations [120].

Below, we present a set of experimental observations of intermittency in hydrodynamic flows in TBLs. Of course, we have no intention of presenting a full review of the results (see, e.g., [103, 122] and the references therein), and our aim is to show the results that can be considered examples of the universal properties of intermittency in small-scale turbulence.

Experimental measurements of developed turbulence were carried out at different temperatures in gaseous media (tunnels, tubes, and so on) and liquids (tubes, channels), including liquid helium [122]. To study intermittency, flows with different geometries were used: jets, flows above grids, mixing layers, duct flows, and cylinders with Taylor's Reynolds numbers from 30 to 5000 (see Table 1) [100]. We note that the so-called Taylor's microscale Reynolds number $R_\lambda = \langle u^2 \rangle \lambda / \nu$, where λ is Taylor's microscale, is frequently considered in hydrodynamics. Studies of the near-wall turbulence with high Taylor numbers were carried out at the Superpipe device in Princeton [255], in the atmosphere above the desert in the SLTEST project (at the Great Salt Lake in the USA [266]), and in other experiments (see [267–269]).

Turbulence intermittency was observed in turbulent flows with Reynolds numbers $R_\lambda \sim 10^2 - 10^4$ (Table 1).

Most experimental measurements in hydrodynamics were made using local probes in one or several points. Velocity, temperature, pressure, and other quantities were measured as a function of time. Such measurements are treated as a spatial slice of the flow, assuming that the Taylor hypothesis, whose limitations are not yet fully understood, is valid (see [134]). In the last few years, data were obtained on the space–time structure observed by the laser fluorescence method [135], as well as by the visualization of the velocity flow [136].

For measurements in a flow with high Reynolds numbers, it is important to avoid the effect of compressibility for gases and cavitation for liquids. Hence, in addition to usual liquids, low-viscosity fluids are used, including HeI in cryogenic experiments, which provide data in a broad range of Reynolds numbers. Modern methods of turbulence visualization allow registering all stages of the development and existence of turbulence. The visualization using hydrogen bubbles is used: the bubble generator is placed at different points in the boundary layer, and the bubble sheet is

Table 1. Parameters of the experimental turbulent flows (from [128–133]). Λ is the integral scale, η is the Kolmogorov length, u'/U is the fluctuation level (u' is the rms deviation of velocity fluctuations and U is the mean velocity), l_W is the length of the wire, f_a is the low-frequency filter frequency, and $f_\eta = U/2\pi\eta$ is the Kolmogorov frequency.

Exp.	Configuration	Λ	η	R_λ	u'/U, %	l_W/η	f_a/f_η
1	Flow	10 cm	2.5 – 50 μm	200 – 500	20 – 40	0.1 – 3	0.5 – 5
2a	Streams	20 cm	0.28 mm	428	26	2.5	7
2b	Air tunnel	10 cm	0.35 mm	3050	7	1.2	3
3	Streams	2 cm	7 μm	580	25	3	7
4a	Cylindrical flow	6 – 10 cm	0.2 – 0.5 mm	100 – 300	15	1 – 2.5	7
4b	Streams	10 cm	0.1 mm	800	30	5	7
5a	Streams	7.5 cm	0.095 mm	810	16	2	1
5b	Grid	17 cm	0.19 mm	530	8	1	1
6	Streams	4 – 8 cm	22 – 48 μm	240 – 330	20 – 25	0.6 – 1.3	—
7	Grid	4 mm – 1 cm	100 – 250 μm	35 – 110	1.5 – 8	3 – 10	1 – 3

registered with a video camera under different aspects and illumination. New methods of the near-wall turbulence diagnostics were developed and used, such as particle image velocimetry (PIV) (see [103, 126]).

In a hydrodynamic turbulent flow, the kinetic energy dissipates via molecular viscosity. Batchelor [137] showed that the non-Gaussian behavior of the distribution function (PDF) of dissipating quantities increases as the scale decreases. This concerns the dissipation region. For the inertial range, variations in the Reynolds number do not affect the statistics, and intermittency shows up as a flattening of the PDF on small scales.

Intermittency is a typical property of fluctuations in TBLs (see Fig. 7) (see, e.g., [138–140]). In real experiments, the turbulent flow is essentially three-dimensional. Fourier spectra of the velocity pulsations in TBLs are broad-band, ranging from 10 Hz to 10 kHz [141].

Statistical properties of turbulent pulsations are described by non-Gaussian statistics (see, e.g., fluctuations of pressure in water in Fig. 7b). The intermittency of the near-wall turbulence can be described by a multifractal statistics. The PDF in Fig. 7c demonstrates the multifractality, which is the dependence of the non-Gaussian shape on the scale at which velocity differences are measured. In turbulent boundary layers, the deviation from the Gaussian statistics increases in approaching the wall. Intermittency and multifractal statistics are characterized by a broadened singularity spectrum [142] (Fig. 8), which is reproduced in numerical simulations [143]. The multifractality property of hydrodynamic turbulence is found in atmospheric and oceanic flows [144–150]. In the multifractal treatment of turbulence, dissipative effects are introduced self-consistently, in both the Eulerian and the Lagrangian descriptions (see review [151]). The multifractal formalism well describes intermittency in turbulence; for example, it predicts the enhancement of intermittency in the so-called intermediate viscosity range [152, 153]. The consideration of a passive scalar in the Lagrangian formalism (the experiment, theory, and numerical simulations) is reviewed in [154].

The extended self-similarity of hydrodynamic turbulence with intermittency was empirically found in [81]. This property is expressed in the form of the power-law dependence $S_q \sim S_3^{\zeta(q)/\zeta(3)}$ of the structure functions of different orders. It characterizes fluctuations of the transverse and longitudinal velocity components (Fig. 8) in turbulent flows with intermittency in a wide range of Reynolds numbers. Using the ESS property, it is possible to estimate scaling laws of the structure functions $\zeta(q)$ with good accuracy. Experimental data are characterized by a nonlinear functional dependence $\zeta(q)$ on the moment order q (see Fig. 8); this nonlinearity is due to intermittency. We recall that for the Kolmogorov turbulence K41, the scaling law has the linear form $\zeta(q) = q/3$. To interpret the nonlinear spectrum $\zeta(q)$, log-Poisson models are used. In TBLs, the nonlinearity increases in approaching the wall (intermittency becomes stronger); see Table 2. Far from the walls, the experimental data are well described by the She–Leveque model for three-dimensional turbulence with intermittency, but a significant increase in the nonlinearity parameter is observed in approaching the wall (Table 2).

The visualization of the developed turbulence demonstrated that long-lived filamentary structures of different lengths exist in the flow [140, 155, 156]. Empirical observations evidence that the diameter and the lifetime of a filament

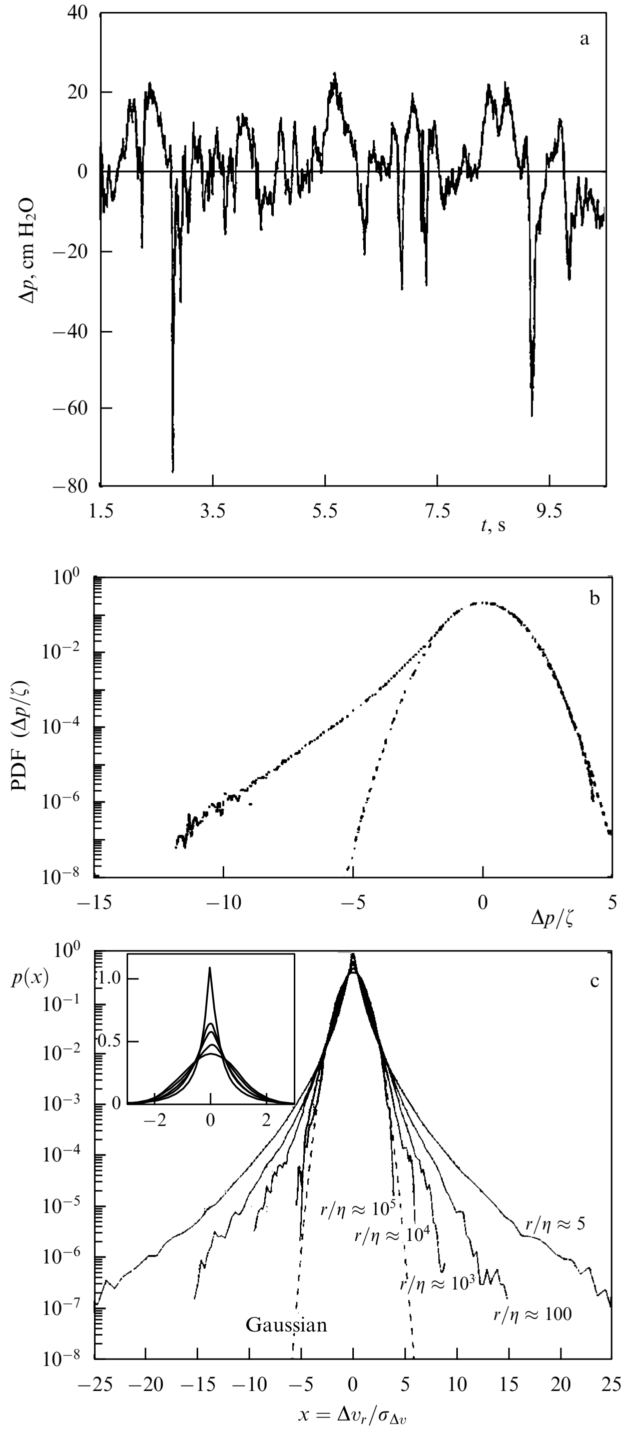

Figure 7. Pressure change with time in a neutral liquid, water [138]. (a) Three-dimensional turbulent flow is generated by a cylinder rotating with the frequency 2.7 Hz, Re = 308,000. (b) PDF of pressure fluctuations in water: the turbulent flow is generated by a cylinder rotating with the frequency 3.8 Hz, Re $= 1.2 \times 10^5$ (the dashed curve shows a Gaussian fit, the abscissa is in units of rms deviations) [138]. (c) PDF of the velocity difference obtained for the atmospheric turbulence at the altitude 30 m above the ground. Half-logarithmic and linear scales are respectively used for the main figure and the inset. Each curve is obtained for a different distance r in the direction across the velocity. The minimum distance (about 2.5 mm) corresponds to the minimum scale of fluctuations and is about five Komogorov scales η. The maximum distance is about 50 m. The dashed curve shows a Gaussian fit [142].

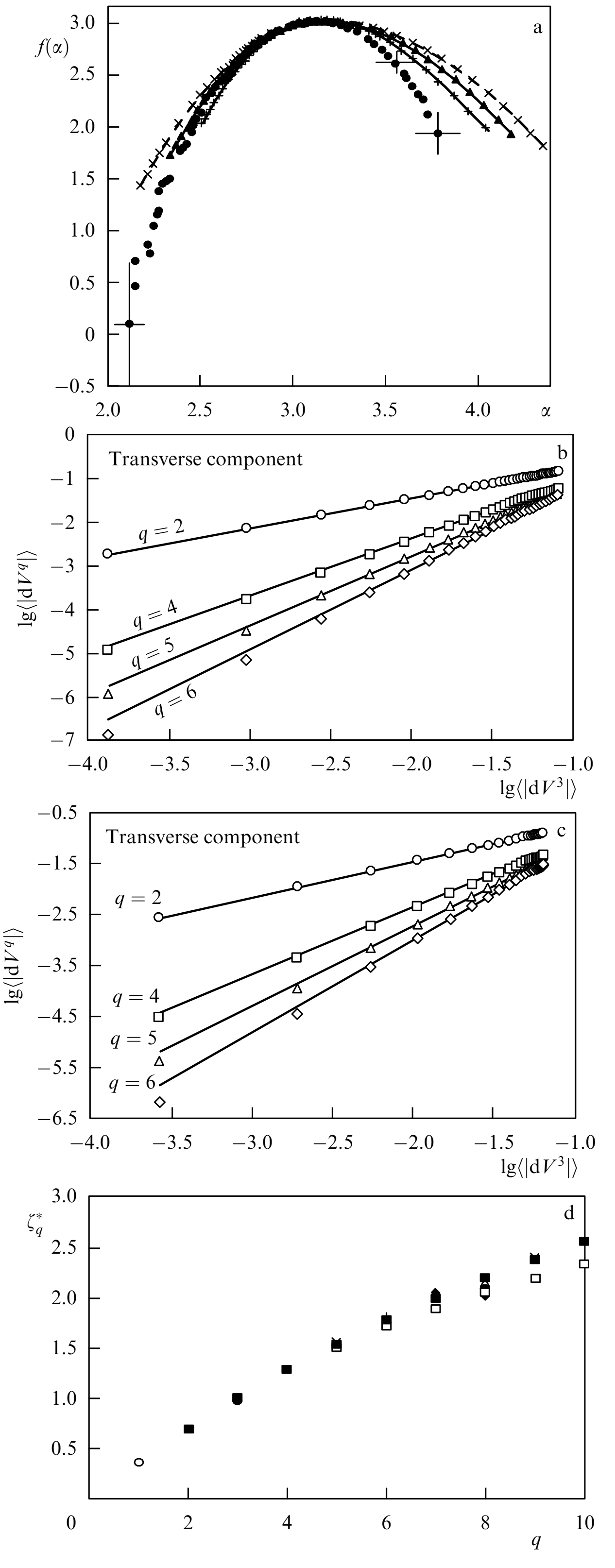

Figure 8. The singularity (multifractality) spectrum. (a) Black dots are the experimental data in [142], black triangles and crosses are the model of the three-dimensional turbulent flow with different parameters in [143]. (b, c) The extended self-similarity demonstration; the plot of the first six moments of the longitudinal and transverse velocity. The solid lines show the best fit approximation of data by a linear law (from [139]). (d) The structure function scaling law for different experiments on Table 1: □ — experiment, × — 2a, • — 2b, ◆ — 3, □ — 5a, △ — 5b, ○ — 6, + — 7 (from [123]).

Table 2. The scaling law of the log-Poisson She–Leveque model and experimental data in an air channel (from [123]), calculated with the use of ESS. A significant increase in intermittency in approaching the wall, $y^+ = 15$, is observed.

q	ζ_q, She–Leveque model	ζ_q, experiment, $y^+ = 310$	ζ_q, experiment, $y^+ = 15$
1	0.37	0.37	0.43
2	0.70	0.70	0.75
3	1.00	1.00	1.00
4	1.28	1.27	1.19
5	1.54	1.52	1.34
6	1.78	1.75	1.48

depend on its length: the longer the structure is, the larger its diameter and the longer its lifetime. The orientation of filaments in the flow can be different, but in the near-wall region, they are predominantly extended along the wall (Fig. 9) [155]. Sometimes, structures of a peculiar form are observed. Long-scale structures, along with lambda-structures, were observed in a turbulent boundary layer in a duct flow [157] and in other experiments (see [115]). We note that systems with vortex filaments have been discussed in models of intermittency for a long time (see [156]), including the case of high Reynolds numbers. Here, both large-scale and small-scale (down to the Kolmogorov scale) structures are considered (see the discussion in [2, 156]).

A significant new result obtained in recent years is the experimental observation of very large-scale motion (VLSM) in a flow. The size of moving structures along the flow is around ten radii of the pipe (or the near-wall thickness) [103, 158, 159]. The VLSM structures contribute to the spectrum at low wave numbers (Fig. 9) [158]. These structures contain a significant fraction of the overall energy of the flow, which increases with the Reynolds number. At high Reynolds

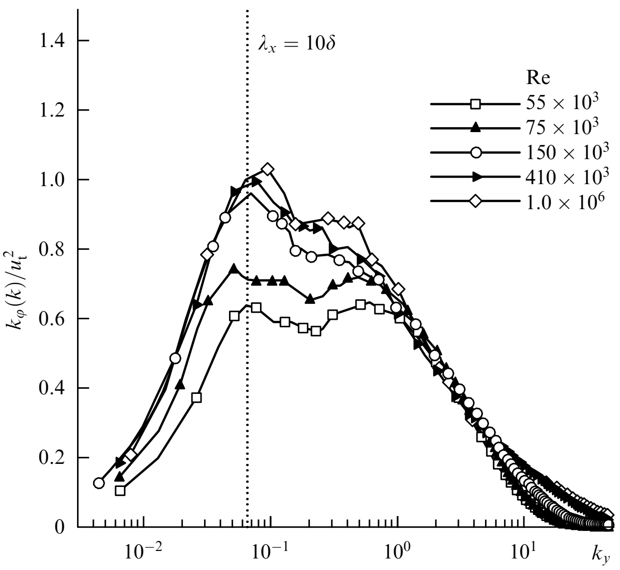

Figure 9. The spectrum of the parallel velocity component for $r/R = 0.1$ in the Superpipe device for different Reynolds numbers (from [160]). The vertical line shows the wavelength $\lambda_x/R = 10$ corresponding to large-sclae VLSM structures.

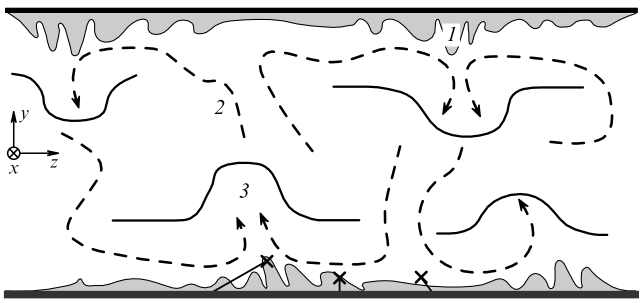

Figure 10. Schematic of the interaction of large-scale structures with near-wall eddies in a flow with low Reynolds numbers in a channel [162]: *1* — near-wall coherent structures, *2* — rotation of large-scale structures, *3* — the region of low velocities of large-scale structures.

numbers, the energy of VLSM structures can be about half the total fluctuation energy in the flow.

The large-scale VLSM motion is responsible for the small-scale structuring and the fluctuation energy enhancement, and is the reason for the modulation of the near-wall turbulence cycle, which was previously considered to be autonomous. The VLSM structures are observed in the velocity and large-scale pressure fluctuations. Presumably, the VLSM structures result from statistical merger of many near-wall structures, in a way similar to percolation of structures, which fully cover the medium once the probability of the percolation exceeds some threshold value (see [103]). The role and importance of the VLSM structures in producing turbulent energy remain an open issue. If a significant fraction of energy in the intersection zone is due to VLSM, their role in providing the so-called universal scaling law is obvious (see [103]). Also unsolved is the issue of the nonlinear coupling of these large-scale and small-scale fluctuations.

The interdependence of processes in the near-wall zone and large-scale structures was considered and registered earlier (see, e.g., [161]). Recent experimental and numerical studies, including observations of coherent VLSM structures, have provided a detailed description of this process. The schematic interpretation shown in Fig. 10 (taken from [162]) describes the nature of such an interaction and is confirmed by other studies (see [163]). As can be seen from the diagram, the small-scale turbulent activity near the wall depends on the propagation direction of large-scale structures.

The appearance of large-scale coherent structures is explained by a theoretical treatment of the appearance and development of turbulence. It is known that the laminar–turbulent transition in boundary layers of low-level turbulent flows is related to the growth of so-called Tolmin–Schlichting waves (see [164] and review [115]). Such a two-dimensional wave is distorted on the nonlinear stage of the growth, resulting in the appearance of the characteristic lambda-structures [165, 166]. In more complex flows, they also appear in the form of horseshoe-like (omega structures), hairpin, and other types of eddies. They share a common property of displaying two counter-rotating eddies (legs of the structure) looped via a 'head'. The appearance and development of these structures are considered in many numerical and experimental studies (see [115, 167] and the references therein). It is shown that the emergence and reproduction of near-wall turbulence are the same in various types of flows [115, 167] and are due to the appearance, growth, and destruction of coherent forms like lambda structures, omega structures, and ribbon-like structures (see Fig. 11). These structures are observed in experiments. Figure 12 presents the spatial picture of the development of a secondary high-frequency perturbation at the nonlinear stage of a sine-like instability in a ribbon-like structure, obtained using a thermometric visualization. This procedure allows considering the flow structure and revealing the smallest coherent forms, including the lambda structures. Azimuthal lambda structures in a 3D-flow are observed, for example, during the interaction of an annular eddy with ribbon-like structures (Fig. 13).

In recent years, the effect of wall roughness on the TBL properties (see [103, 115]), which is connected with a decrease in turbulent friction in aircraft, has garnered significant interest. Experiments over the last few years have evidenced that most (but not all) types of surface roughness lead to a relation between the hydraulic friction coefficient and the Reynolds number in the framework of the Nikuradze model, which considers one-grain homogeneous roughness. In addition, recent experiments have revealed the influence of a rough wall on the central part of the flow. It is noted that the existing methods of estimating the transport in pipes and channels (for example, the Moody charts) do not describe many experi-

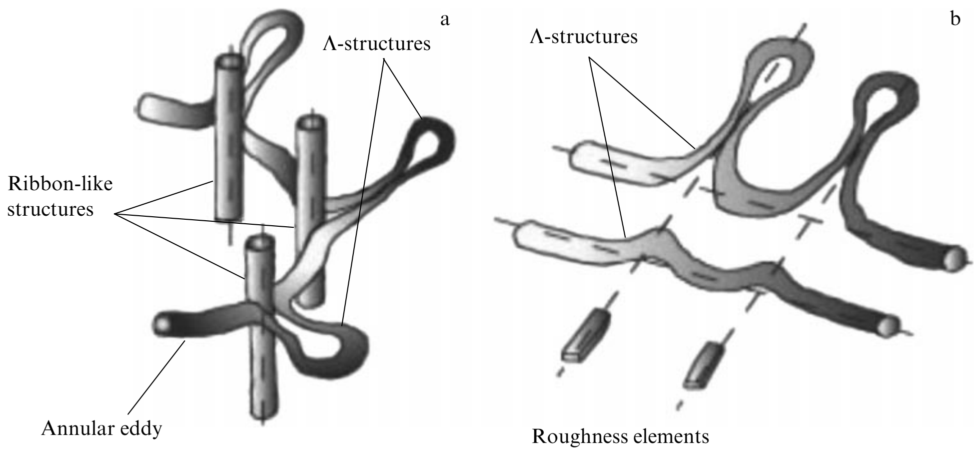

Figure 11. (a) Schematic of a three-dimensional distortion of an annular eddy on local flow inhomogeneities and (b) a two-dimensional instability wave on roughness elements [168].

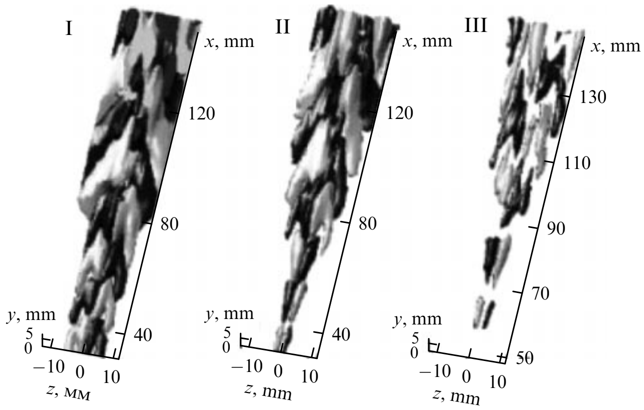

Figure 12. Spatial patterns of the development of a secondary high-frequency perturbation at the nonlinear stage of a sine-like instability. Shown are iso-surfaces of equal amplitudes: $0.4\% U_\infty$ (I), $1.3\% U_\infty$ (II), $6.4\% U_\infty$ (III). Darker gray scale shows velocity defects [169].

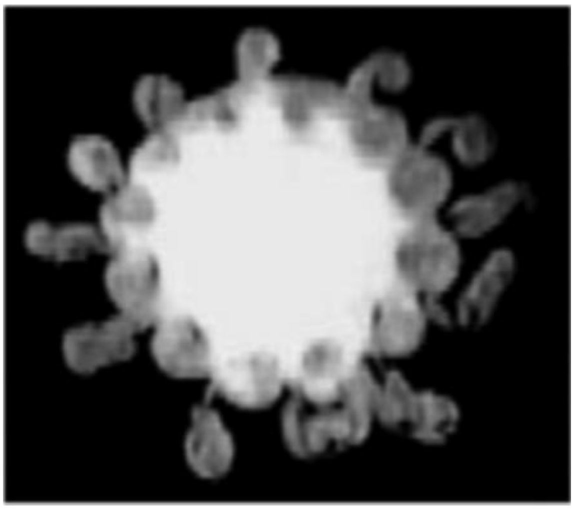

Figure 13. Vizualization of the cross section of an annular flow in the process of interaction of an annular eddy with ribbon-like structures generating azimuthal lambda structures [170].

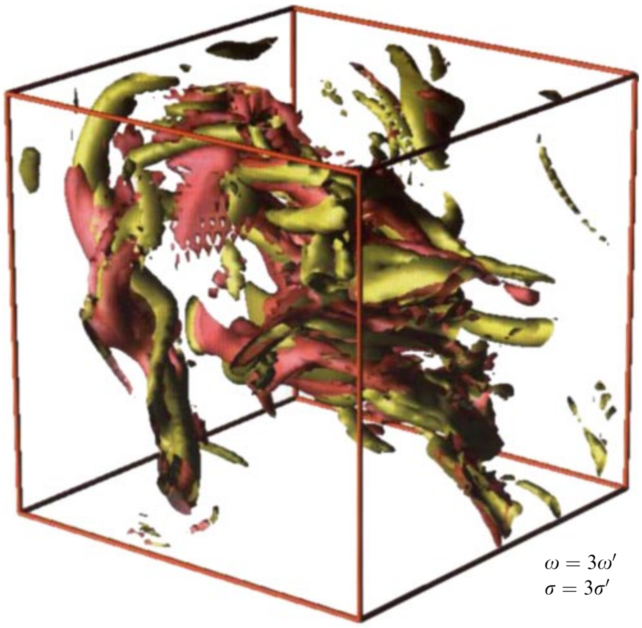

Figure 14. Results of numerical simulation of a turbulent flow [122]. The large-amplitude vorticity (more than three standard deviations) shows up as tubes (shown in yellow online). The large-amplitude dissipation (shown in red online) is not organized so clearly, but is concentrated near the tubes.

ments with a specific wall roughness. A review of studies of turbulence in flows restricted by a rough surface is given in [171]. To handle a turbulent flux (which can be practically used, for example, to decrease the drag of aircraft), different methods of control of disconnected flows are used, involving localized sources of perturbations in the region of the flow disconnection, acoustic effects and waving or other shaping of the streaming surface, the inclusion of rough-surface riblets, and so on. Micro-electromechanical systems (MEMSs) utilize microsensors for adaptive and selective real-time control by individual perturbations and structures in the near-wall zone of the boundary layer (see reviews [115] and [172]).

Numerical experiments. For numerical simulation of turbulent flows, different methods are applied, including the most promising one, the so-called method of large eddy simulations (LESs) (see, e.g., [122, 123, 174]). The direct reliable modeling of turbulent flows based on numerical solution of the full Navier–Stokes equations is also used (see [175]).

Intermittency has been observed in numerical two- and three-dimensional simulations of Navier–Stokes equations (Fig. 14). Even in the case of global homogeneity and isotropy, large-amplitude structures (at the level of more than three standard deviations) are organized in the form of tubes, and the large-scale dissipation is also localized near these tubes. The reason for such a concentration of dissipation is unclear, and the qualitative characteristics and scaling laws describing these structures are also unknown. In principle, the multifractal formalism describes processes involving such structures with different geometries, the tube- and sheet-like structures in particular. This method is the most promising for treating turbulence with intermittency (see [103, 112, 153]).

Numerical calculations in TBLs are reviewed in [103, 176, 177]. Numerical simulations have confirmed that about half the energy in the viscous sublayer is transferred by coherent structures. Simulations have revealed that the structure of near-wall flows is more complicated than predicted by many theoretical models. Numerical experiments enabled the description of the three-dimensional momentum cascade and self-similarity in a broad range of scales in the logarithmic layer. As the Reynolds number increases, the smallest scales play an increasing role in the process.

Recent numerical calculations have revealed a significantly nonlinear interaction of large-scale and small-scale fluctuations, the role of this interaction in the intermittency formation, and a significant cross-propagation of perturbations from the central zone toward the wall, influencing the shear stress fluctuations on the wall (see [178–180]). This effect of the central region on the near-wall zone increases as the Reynolds number increases [181]. An example of this effect is shown in Fig. 15 [182], where correlations of the flow velocity in all of the logarithmic range and the shear stress on the wall are observed.

One more numerical result should be noted. Previous calculations were aimed at reaching viscous scales by assuming that smaller scales can be neglected in the dynamics. The

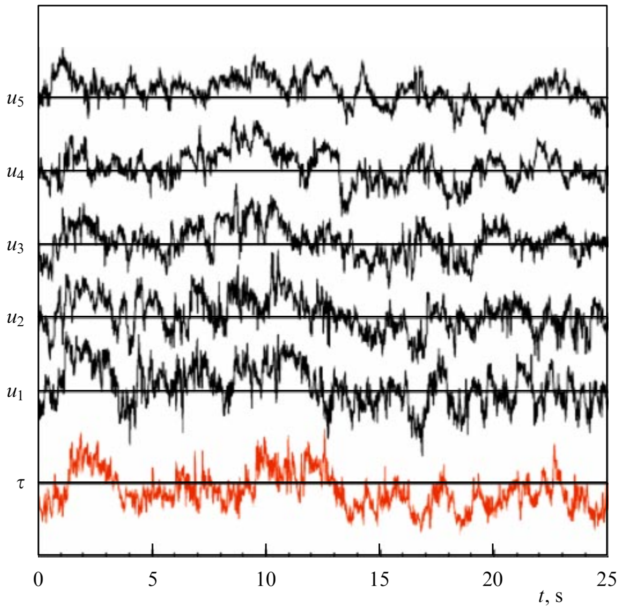

Figure 15. Fluctuations of velocity u in five regions (normal to the flow boundary) in the logarithmic zone and the shear stress tension τ at the boundary. Experimental measurements in the atmospheric near-surface layer (SLTEST) at a very high Reynolds number Re $\sim 10^6$ [182].

analysis of numerical results carried out in the last few years has led to the conclusion that smaller scales become important as the Reynolds number increases. The smallest dynamically important scale can be significantly lower than the Kolmogorov scale [183].

The study of particle motion in a turbulent flow, i.e., the Lagrangian description of turbulence, has recently led to impressive progress in the understanding of the statistical properties of turbulence and the role of small-scale structures (see reviews [184–186]). Experimental results were obtained for Reynolds numbers $R_\lambda \sim 350-900$ in experiments with counter-rotating disks. Numerical modeling of isotropic homogeneous turbulent flows was carried out for $R_\lambda \sim 280$, and the results were compared with experiment [185]. Figure 16 [187] shows the results of experimental observation of high-velocity flows and numerical modeling. Such Lagrangian observations led to a surprising conclusion: the most intensive fluctuations turned out to be related to motion in small-scale eddies and survive on time scales much longer than the eddy turnover time (see [188]).

To conclude the review of studies of hydrodynamic turbulence, we note that the problem of separation of scales, if it is present in flows bounded by walls, is the basic property of all scaling theories of the TBL. To confirm this hypothesis, reliable experimental data at high Reynolds numbers are required. The accuracy of experimental measurements is still insufficient to choose between alternative hypotheses, even for the mean velocity scaling law. New experimental devices allow measurements with higher Reynolds numbers. Nonetheless, the possibility of resolving and characterizing all scales and structures, and not simply increasing the Reynolds number in an experiment, appears to be more attractive. In many types of turbulent hydrodynamic flows, large-scale filamentary structures and intermittency, as well as multifractality and generalized self-similarity, are usually observed; this evidences a strong nonlinear coupling between large-scale and small-scale fluctuations. Recent numerical experiments have allowed better understanding the dynamics in the near-wall zone; however, much effort is required to reach the experimental parameter values in numerical calculations. Thus, the interest in the TBL problem persists. Experimental data about the character of turbulence and intermittency in other media, including plasmas, can provide additional support for the existing hypotheses and theories of hydrodynamic TBLs.

2.2 Measurements in Earth's magnetosphere

General characteristics of the magnetosphere boundary. A typical crossing of the entire magnetosphere and its outer boundary layers by the Interball-1 spacecraft on March 16–17, 1998, from the bow shock (BS) through the magnetosheath (MSH) to the magnetopause (MP) and back, is shown in Fig. 17a (see [29], Vol. 1, pp. 398–412, upon which this section is based). The characteristic subregions near the MP are presented in Fig. 17b relative to the upper half-plane *8* (summer in Fig. 1c): external and internal cusps and the external throat (ET) *6* of the cusp, and the turbulent boundary layer (TBL) *7*. The ET is located outside the MP (*6*), the external cusp (*4*) is inside the MP, and the internal cusp (*3*) lies deeper inside the magnetosphere. We identify the MP as the innermost current sheet where the magnetic field

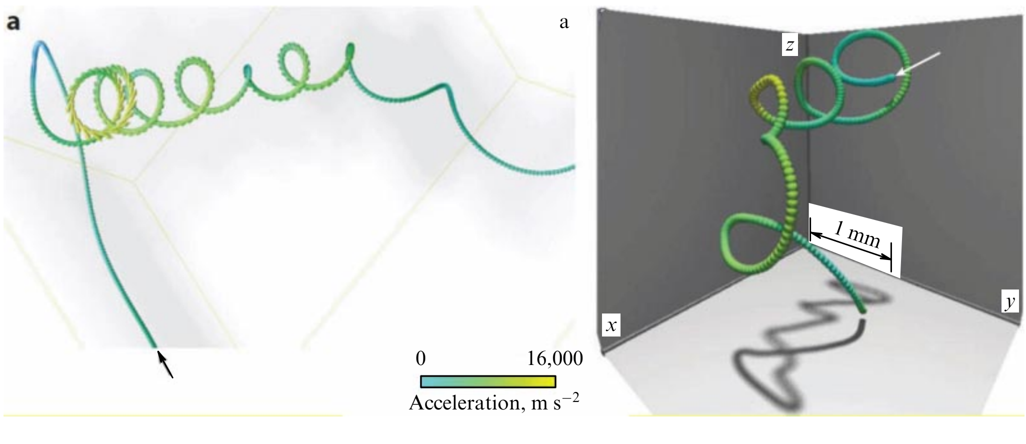

Figure 16. (a) The trajectory of a fluid element in a small-scale vortex tube (filament), from a numerical simulation at $R_\lambda \sim 280$. The color (online) and arrows show the amplitude and direction of acceleration [153]. (b) Experimentally measured trajectory of the acceleration of a 46 μm particle in a turbulent flow at $r_\lambda = 970$, taken at the registration rate of 70,000 frames per second [187].

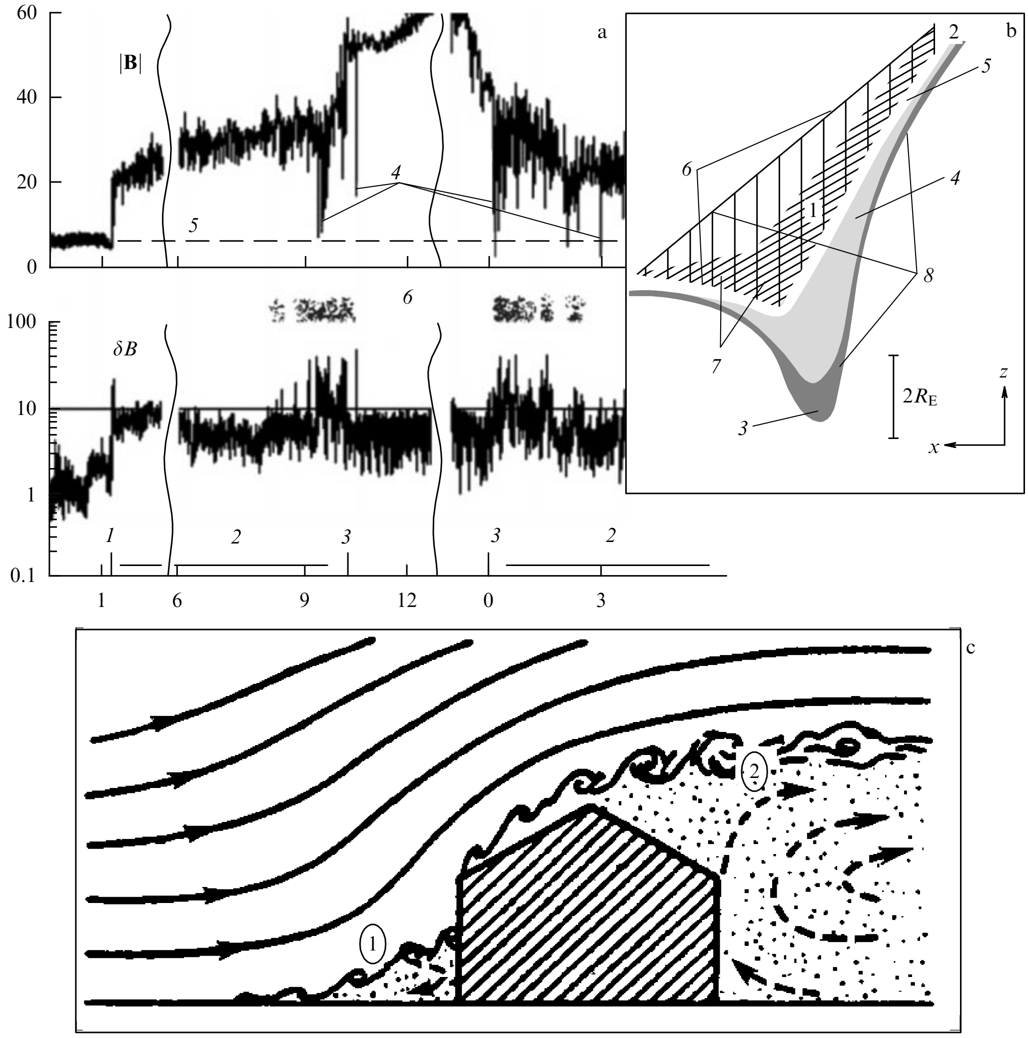

Figure 17. (a) The magnetosphere crossing by the Interball-1 SC on March 16–17, 1998, from the bow shock (BS — *1*) through the magnetosheath (MSH — *2*) to the magnetopause (MP — *3*) and return. The figures mark: *4* — diamagnetic bubbles, *5* — solar wind, *6* — TBL. Top: the magnetic field modulus $|\mathbf{B}|$. Bottom: the peak-to-peak magnetic field fluctuations δB. (b) Boundary layers at the magnetosphere boundary near the polar cusp (see the upper half-plane 8 in Fig. 1c): *1* — open cusp throat, *2* — high-latitude TBL behind the cusp, *3* — inner cusp, *4* — outer cusp, *5* — magnetopause, *6* — inner throat, *7* — TBL, *8* — stagnation zone, R_E is the radius of Earth. (c) Diagram of turbulent boundary layer formation during the streaming of an obstacle by a hydrodynamic flow [189]; 1 — stagnation zone, 2 — turbulent wake.

turns from the direction determined by the solar wind (SW) to that controlled by the geomagnetic dipole [190]. In a turbulent transition, the MP can correspond to an extended zone in which the mean direction of the magnetic field loses correlation with the interplanetary magnetic field (IMF) in the SW.

The MP thickness determined from the change in the maximum field component varies in a wide range from 50 to a few thousand km, with the mean 1600 km and the median 800 km. The ion gyroradius and the inertial length lie in the range 40–80 km, which is smaller than the determined thickness of the MP. However, the main turn of the field direction in approximately half the cases occurs on scales 2–3 times smaller, which leads to a significant effect of the finite value of the gyroradius. The MP velocity ranges from 0 to 300 km s^{-1}, with the median $\sim$ 50 km s^{-1} and the mean $\sim$ 60 km s^{-1}, although the velocity behind the cusp is not higher than 70 km s^{-1}.

The external cusp is the region with three different ion populations, including the freshly injected ions from the magnetosheath, the MSH ions reflected from the ionosphere, and quasi-perpendicular ions trapped in the local minimum of the magnetic field near the cusp (cf. [191]). It is also characterized by moderate magnetic noise, whereas in the internal cusp, this noise is observed only on the boundaries.

In the cusp, the MP can be concave (see the upper half-plane in Fig. 1c), which was predicted in [192] and discovered by the HEOS-2 spacecraft (SC) [189]. The measurements by the Interball-1 and Cluster SC show that the average cusp depth is $2R_E$ (R_E is the radius of Earth), reaching $5R_E$ [193, 194]. The MSH plasma in the ET (relative to the MP) is strongly perturbed and broken down.

The TBL is the region outside of and/or on the MP, mainly above the polar cusp and downstream (Fig. 1c). Here, the energy density of magnetic fluctuations at ultra-low frequencies (ULFs) is comparable, within an order of magnitude, to the kinetic energy density of ions and the magnetic field. In the TBL, the ULF power is several times greater than in the MSH, and greater than inside the MP by one to two orders of magnitude. ULF oscillations near the

MP can independently lead to micro-reconnection of the magnetic field and local plasma entering over the entire MP, even without a global magnetic field line reconnection (i.e., a change in the mean field topology). The potential role of magnetic reconnection, both stationary and pulsed, is discussed in detail in review [29]. MHD modeling and measurements by many satellites confirm the direct entering of solar wind plasma near the minimal magnetic field at the cusp and in the 'sash' — the continuation of the cusp into the magnetosphere tail for a transverse interplanetary magnetic field. A deep penetration of the solar wind plasma into the plasma sheet, up to the midnight sector, also occurs on the boundary of the neutral layer in the geomagnetic tail for a small magnetic field [29].

The external cusp and turbulent boundary layer as the principal region of plasma entering the day magnetosphere. Haerendel [190] considered data obtained by the HEOS-2 satellite that evidenced eddy convection in the stagnation zone over the polar cusp and its possible consequences for the plasma entering the magnetosphere and the magnetic reconnection. He suggested that the reconnection is not a laminar process but a subsidiary product of the eddy convection (the so-called 'secondary' reconnection on smaller scales) that results from the flow interaction with a local obstacle, the rear wall of the cusp (Fig. 17c). The 'eddy' diffusion coefficient estimated from previous observations was $D_{\mathrm{ed}} \sim 5 \times 10^{10}\ \mathrm{m}^2\ \mathrm{s}^{-1}$. The search for predicted properties of the magnetic reconnection already in 1978 led to quite definitive conclusions (we here follow paper [190], which is very important for the understanding of the physics of plasma boundary layers): the transition from laminar outer flows to the boundary layer occurs via turbulence, inverse flows, and the formation and separation of eddies. The mean velocity of the flow in the boundary layer is lower than outside the MP, and the flow is irregular and not directed from the subsolar point, even for the southern IMF (the negative B_z). Therefore, the cusp is unlikely to be a result of reconnection at the subsolar point. The independence of the cusp from the IMF is one of the main reasons to consider reconnection near the cusp to be a secondary process. In the classical reconnection model, free energy is stored in a magnetic configuration with an X-type neutral point (or a line in three dimensions). The magnetic energy is transformed into the turbulent energy of waves and the kinetic energy of the outflow plasma. If macroscopic turbulent convection is present, there are additional sources of free energy sustaining turbulence. Anomalous diffusion in the region of locally counter-directed fluctuating fields is very likely to initiate a secondary reconnection, which opens way for plasma from the MSH to closed field lines. Indeed, according to the Interball-1 data, in the center of the turbulent boundary layer, there are scales comparable to the electron gyroradius (see Fig. 18a), which evidence a violation of the freeze-out of electrons, i.e., the effective reconnection [29]. The rest is similar to the classical picture of magnetic reconnection, with two differences: 1) the characteristic length must be of the order of the convective cell size ~ 1000 km; 2) instead of being stationary, the reconnection must beat on the timescale $t \sim 20$ s [189]. In the cusp throat, the main difference from a stationary

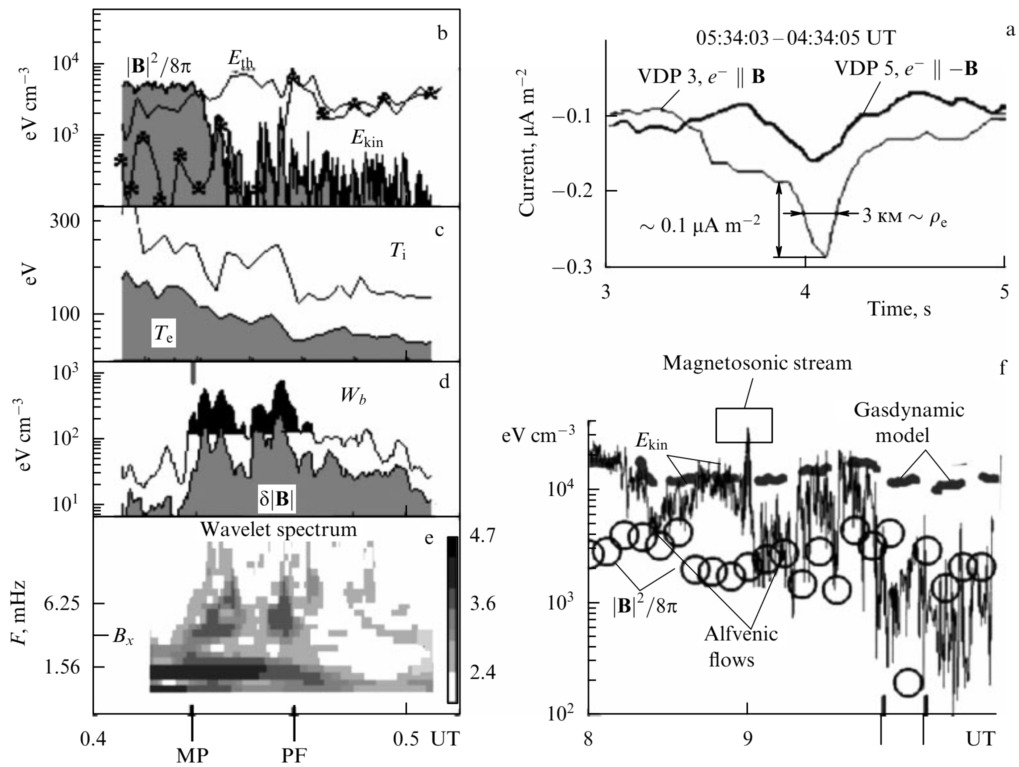

Figure 18. Probing the turbulent boundary layer structure and cusp by the Interball-1 SC. (a) the current sheet with the size $\sim \rho_{\mathrm{e}}$ (electron gyroradius, see [193]) in the TBL according to the Faraday cylinders data (VDP), 21.04.1996. (b) The energy density of ions (E_{th} and E_{kin} are the thermal energy and kinetic energy) and the magnetic field ($|\mathbf{B}|^2/8\pi$), 02.04.1996 (see [17]). (c) Temperature of ions T_{i} and electrons T_{e}, 02.04.1996. (d) The total power density W_{b} of magnetic fluctuations and power of the compressible waves $\delta|\mathbf{B}|$, 02.04.1996. (e) Wavelet spectrum of B_x, 02.04.1996. (f) The kinetic energy density of ions E_{kin} (the dashed curve shows the model fit) and the magnetic field energy density $|\mathbf{B}|^2/8\pi$ (circles); the accelerated magnetosonic stream is shown by the quadrangle, 19.06.1998 (see [19]).

reconnection on a smooth MP shows up in the absence of regular directed flows and the independence of reconnections in different hemispheres. As a rule, the region with locally antiparallel magnetic fields is found there, and therefore the 'annihilation' of the mean magnetic field can proceed more efficiently on the medium scales (between MHD- and gyro-scales), which does not rule out the simultaneous reconnection far from the cusp on the global scale comparable to the curvature radius of the magnetopause [21].

Interaction of a plasma flow with the cusp and its topology. Figure 17a shows the entrance of the Interball-1 SC from the SW into the magnetosphere, including the BS, MSH, and MP at the entrance and exit. On the BS, fluctuations have a narrow maximum, and above the MP, a broad zone of more intensive waves, a turbulent plasma layer is present where depressions of $|\mathbf{B}|$ occur below the IMF layer — the so-called diamagnetic bubbles (DBs).

According to data obtained by Interball-1 in 1995–2000 (651 TBL crossings during about 400 MP intersections [19]), the TBL is present in $\sim 80\%$ of high-latitude MP crossings (with the mean amplitude ~ 20 nT). On the day side, the events are concentrated on high latitudes ($|Z| > 4R_{\mathrm{E}}$, where Z is the coordinate along the magnetic dipole) above the cusps and downstream, which is related to the TBL. The most intensive events are approximated by an effective disc with the diameter $6R_{\mathrm{E}}$ above the cusps with the mean value of the maxima ~ 22 nT and the characteristic threshold > 10 nT. Most high-latitude events with the fluctuation threshold 7 nT are observed in the near tail or correspond to SW perturbations. The summer TBL (see the 'summer' half-plane in Fig. 1c) and MP have a depression above the cusp with the depth $\sim (1-3)R_{\mathrm{E}}$. The location of the TBL has not been found to have obvious dependences on the B_z component of the IMF.

The high-latitude Interball-1 data on the sunward magnetic dipole tilt demonstrate the regular presence of stagnation plasma in the cusp throat above the convex MP [19], which corresponds to the predicted interaction of the MSH plasma flows with the open cusp throat resulting in the formation of the TBL [189].

On June 19, 1998, the Polar SC was located above the cusp in the northern stagnation zone outside the MP (dipole tilt: $+20°$); the Interball-1 SC registered such a plasma in the diamagnetic cavity inside the MP, the 'plasma cloud' (PC), for negative dipole tilts in the southern hemisphere [21]. Figure 18f shows the magnetic $|\mathbf{B}|^2/8\pi$ (circles) and the kinetic E_{kin} (black line) energy densities; the dashed curve shows the prediction of the gasdynamic GDCF model for E_{kin} [19]. The mean flow in the MSH down to the MP (at $\sim$09:53 UT) is subsonic and super-Alfvenic ($E_{\mathrm{kin}} > |\mathbf{B}|^2/8\pi$). Immediately inside the MP, energetic electrons produce a high count rate, which is characteristic of the boundary of closed magnetospheric field lines. The IMF B_z became northern 10 min before the MP. The ratio of the ion thermal pressure to the magnetic pressure $\beta_i > 1$; for example, at 09:56 – 10:03UT, $\beta_i \sim 15$.

The scheme of the SW flow interaction with the tilted dipole on the bottom half-plane (*9* — winter, Fig. 1c) is as follows: the MP in the southern hemisphere (winter, the dipole is tilted away from the Sun) has no depression, and the Polar SC data confirm the configuration shown in Fig. 1c for the sunward dipole tilts in the summer hemisphere (cf. [21]). As is shown in [19], the ET is registered for positive magnetic dipole tilts and the PC is registered for negative tilts. For example, the maximum number (20 PCs) is observed for the inclination angles between -15 and $-25°$, 77% of the PCs were registered for the tilt angles $< -5°$, 6 appearances of the ET are observed for negative tilt angles, and 21 cases are found for positive dipole tilts ($> |5|°$). In most cases, energetic particles confirm that PCs correspond to a closed topology. PC appearances were found to be independent of the magnetic turn angle on the MP, whereas in $> 65\%$ of cases, the IMF component was $B_z > 0$. Therefore, at the absolute dipole tilt angles $> 10°$, the cusp throat tends to be open for the sunward dipole tilts, and the TBL outside the convex magnetopause separates the stagnation and magnetosphere plasma (1); for the dipole tilts away from the Sun, the cusp throat tends to be closed together with the stagnation plasma of a smoother MP (2). However, in $\sim 2/3$ of cases (especially at tilt angles $< 10°$), the large-scale structure of the cusp throat is irregular. It was shown in [192] that the common property of open field lines and PC is that the captured ions from the MSH are frequently seen even at low β and in the regions of smaller scales (see the diamagnetic lobes above). High values $\beta_i \sim 2-15$ and the direct interaction of the PC plasma with incident MSH fluxes are distinctive features of the PC from the external cusp. The mean location of PCs is related to the region of locally antiparallel magnetic fields near the MP, which corresponds to the location of the minimum of $|\mathbf{B}|^2/8\pi$. PCs are also regularly detected by the Cluster satellite.

We next consider the kinetic energy loss by a plasma flow in the TBL above the magnetopause observed on June 19, 1998. The main issue is how a virtually nonmagnetized PC interacts with the incident collisionless plasma flow, because the magnetic pressure in the PC is low. Inside the MP at a distance of the order of the ion gyroradius, charged particles in the magnetic field are reflected or change their direction of motion. But in front of the MP, the MSH flow deviates only due to the local electric fields and waves. The electric field E_{n} normal to the MP can be sustained by a surface charge on the MP. This field deflects the MSH plasma flow by accelerating it along the magnetopause due to the drift in the crossed electric and magnetic fields. When E_{n} (the component normal to the MP electric field) increases in the positive (anti-solar) direction upon approaching the MP, the inertial drift, as well as effective collisions caused by the interaction with nonlinear waves, can decrease the normal component of the ion velocity. In this case, the waves provide the main interaction of the MSH plasma with the PC.

Spectral maxima at 1–2 mHz are seen everywhere in the MSH; they strengthen closer to the MP. It can be seen from Fig. 18d and e that at the frequency ~ 1.3 mHz, the density mostly contributes to oscillations, which is related to the resonance of fast magnetosonic waves between the MP and the bow shock [19]. The characteristic frequency in Fig. 18e can also be related to these oscillations. They can show up everywhere, from the magnetospheric boundary to the auroral ground stations. Beyond the MP, density fluctuations are also synchronized by this resonance, and at a frequency ~ 3 mHz, waves appear that are much more poorly seen in the density fluctuations, which is typical for Alfven waves.

The concept of the incident plasma interaction with a surface charge at the boundary was applied in [21] to the observation of a stream that appeared at 09UT on 19.06.1998. Plasma acceleration in an inhomogeneous external transverse electric field at the boundary layer edge is described quantitatively in the inertial drift approximation, with the drift velocity given by

$$\mathbf{V}_{\mathrm{d}}^{(1)} = \frac{1}{M\omega_{\mathrm{H}}^2}\,\frac{\mathrm{d}\mathbf{F}}{\mathrm{d}t} = \frac{Ze}{M\omega_{\mathrm{H}}^2}\,\frac{\mathrm{d}\mathbf{E}}{\mathrm{d}t}\,, \tag{38}$$

where M, ω_{H}, and Ze are the mass, the cyclotron frequency, and the particle charge, $\mathbf{F}$ is the force across the magnetic field, and $\mathbf{E}$ is the electric field. In Fig. 18f, with the mean plasma velocity $\mathbf{V} \sim (-170, -70, -80)$ km s^{-1} at 08:55UT, the electric field at the instant of the stream observation reaches 8 mV m^{-1}. The energy increment under the inertial drift in (38) is $\delta E_{\mathrm{kin}} \sim \delta(M(|\mathbf{V}_{\mathrm{d}}^{(0)}|)^2/2) \sim 30$ keV cm^{-3}, where $\mathbf{V}_{\mathrm{d}}^{(0)} = c[\mathbf{E}\times\mathbf{B}]/B^2$ is the electric drift velocity (c is the speed of light, and $\mathbf{E}$ and $\mathbf{B}$ are the electric and magnetic field vectors). Formula (38) implies that ions and electrons drift in different directions, which explains the appearance of 'intermittent' current sheets with an anomalously large statistics of large turn angles of the magnetic field in the TBL (see the next section) due to neutralization of transverse polarization charges by longitudinal electron currents [195]. Acceleration of the stream by the surface charge on the MP was also discovered in the data obtained by four Cluster SCs on 13.02.2001.

Thus, our data suggest the possibility of a transformation of the laminar flow behind the bow shock into nonstationary magnetosonic streams and decelerated Alfvenic flows, which reflects the whole synchronized picture of interaction in the outer boundary layer with the size of $(1-2)R_{\mathrm{E}}$ at the distance $\sim 10R_{\mathrm{E}}$ from Earth.

Properties of turbulence and small-scale processes and their role in plasma transport. We now turn to the role played by the above wave interactions on the scale of the entire external cusp. By interacting with the MP, inhomogeneities in the flow generate Alfven waves, some of which are reflected backward, are focused by the concave MP, and interact with the incident flow [17]. As a result, a series of cascades emerges self-consistently, which are synchronized at certain frequencies f_l. The characteristic spatial scale for waves with the frequency 1.5 mHz is estimated to be $L \sim V_{\mathrm{A}}/f_l \sim (3-7)R_{\mathrm{E}}$ (V_{A} is the Alfven velocity), which is comparable to the TBL size (see Fig. 17) and the width of the MSH on the day side. As follows from the Rankin–Hugonio relations, the ion heating in the TBL on the bow shock, as estimated from the magnetosonic Mach number in the MSH, from the Alfven Mach number relative to the velocity projection normal to the incident flux ($\mathrm{M_M} \sim \mathrm{M_{An}} \sim 1.2$), and from the total velocity ($\mathrm{M_A} \sim 3.5$) is 1, 6, and 5, respectively. The observed ion heating in the TBL is higher than on an inclined shock (by 2.2 times), but is smaller than the maximum possible value. Hence, the energy transformation is different from a shock-wave one: the entire perturbed region contains 'long-range' cascades, vortex trains, and coherent structures.

In the TBL, the effective reconnection of fluctuating fields occurs, which allows plasma to enter the MP and provides the transfer of the magnetic flux from the day side to the night side of the magnetosphere. A necessary condition for the reconnection is the presence of structures with a scale comparable to the inertial length or the electron gyroradius, which have close values in the MP. Figure 18a shows an example of detection of such an electron flux in the TBL on April 21, 1996, using the data obtained by oppositely directed Faraday cylinders aboard Interball-1 [193]. This example is unique in detecting the microscale to within a factor of two, whereas all other similar measurements are made to within an order of magnitude (cf. [29]). The direct turbulent cascade in the TBL is the natural source of structures with the electron scale [189].

In addition to the microreconnection, a significant contribution to the transport process is made by the percolation of plasma (see [29]) through the structured boundary with the diffusion coefficient

$$D_{\mathrm{p}} \sim 0.66\,\frac{\delta B}{B_0}\,\rho_{\mathrm{i}}^2\omega_{\mathrm{Hi}} \sim (5-10)\times 10^9\ \mathrm{m^2\ s^{-1}}\,, \tag{39}$$

which yields the flux $(1-2)\times 10^{27}$ particles per second through the northern and southern TBLs, which is sufficient to fill up the magnetosphere with solar plasma (here, the possibility of superdiffusion is neglected; see below).

Studies of the statistical properties of perturbations in the TBL, in particular, the distribution function of the rotation angle of the magnetic field vector in the plane of maximum magnetic variations in the TBL of 19.06.1996, evidence a non-Gaussian statistics for large rotation angles, with the distribution function being approximated at large angles by a symmetric Lévy function with the characteristic index $\alpha \sim 1.17$ ($\alpha = 2$ for the Gaussian distribution), which suggests a multifractal character of the observed intermittent turbulence [18]. The statistical properties of the distribution function of ion fluxes are similar to those of magnetic fluctuations.

The multiscale mixing and reconnection result in the magnetic field lines being connected via the TBL in the statistical sense, without the possibility of following individual field lines in an inhomogeneous nonequilibrium medium with two phases, the frozen MHD plasma and the almost nonmagnetized 'diamagnetic bubbles' encapsulated in nonlinear current sheets and vortices. This phase is responsible (in the statistical sense; see [17]) for the appearance of power spectra with the slope ~ -1.

Thus, the principal processes in boundary layers and the incoming flow are mutually related and globally synchronized by oscillations of the turbulent boundary layer and the magnetosheath as a whole and accelerated plasma streams. The streams modulate both the plasma flow in boundary layers and the reconnection of fields on the magnetopause. We are therefore dealing not with a consequence of additive responses to perturbations in the solar wind and the magnetosheath but with a complex multiscale nonlinear system. This qualitatively changes the system behavior, causes a 'catastrophic' reconfiguration of the flow and the magnetic topology, and leads to a dependence on the prehistory, to the appearance of anomalously strong correlations on large scales (intermittency), and to the formation of coherent structures providing effective energy transformation and plasma transport.

We also note that studies of plasma streams are at the initial stage, but in the physics of boundary layers, turbulence, and plasma streaming, they can be at least as important as the magnetic field reconnection, which has been the focus of cosmic plasma physics in the last few decades. In addition, as shown above, the statistics on the appearance of streams in magnetosphere boundary layers corresponds to the properties of the edge plasma in fusion devices: in both cases, intermittency, generalized self-similarity, and superdiffusion are observed.

2.3 Measurements in the plasma of fusion devices

Low-frequency turbulence of edge plasma has been measured in many tokamaks, starting from experiments on the first

TMP tokamak at the Kurchatov institute in 1956 (see [11]). Since the late 1970s, much effort has gone into measuring parameters of turbulence of the edge plasma in fusion devices (FDs) in order to understand the mechanisms of plasma transport across a magnetic field, which is anomalously high near the wall. The edge plasma in an FD is a very complicated object for study. Plasma probing (see [196–198]) is one of the effective plasma diagnostic methods. Mini-probes made of thermoresistive materials (usually of tungsten or graphite) are employed. They are referred to as electric or Langmuir probes (after Langmuir, who developed the method of plasma probing by such devices). Other methods include optical diagnostics (measurement of spectral lines of the main and admixture plasma components), bolometers, collective probes, thermo-pair probes, reflectometry, magnetic probes, beam diagnostics (lithium and helium beams), laser scattering, microwave reflectometry, and detection of optical emission by high-speed digital cameras [14, 199]. These diagnostic methods are used in different devices depending on the corresponding conditions, such as the size of the device and the diagnostic pipes, and the temporal and spatial scale of plasma parameter variations. The temporal and spatial resolution of the diagnostics are different, and each diagnostic technique has its own advantages. Langmuir probes [14, 198] are found to be the most effective in low-frequency plasma turbulence studies.

The near-wall turbulence parameters have been measured in tokamaks T-10 [200], TF-2 [201], FT-2 [202], DIII-D [203], TEXTOR [204], JET [205], Tore Supra [206], JT-60U [207], Asdex-U [208], MAST [209], and others [14], in stellarators L-2 [210, 211], LHD [212], and TJ-II [213], in linear systems [214, 215], reversed pinch devices [216], and in plasma devices NAGDIS-II [217] and PISCES [218].

Time measurements of the edge plasma demonstrate the characteristic structure with aperiodic bursts (pulsations) of the amplitude (Fig. 19), which is observed for fluctuations of density, electric fields, and transverse plasma flows due to the $[\mathbf{E} \times \mathbf{B}]$ drift. This feature of low-frequency turbulence is called intermittency and is observed by many researchers in all laboratory installations with magnetic confinement of a high-temperature plasma — tokamaks, stellarators, linear devices, and reversed pinch devices [14].

Turbulent fluctuations of the edge plasma display bursts of the specific amplitude shape with a fast growth and slow decay (Fig. 19b) on the timescales 50–200 μs. These characteristic bursts are observed in the edge plasma of FDs with various sizes and the topologies of the magnetic trap: tokamaks, stellarators, and linear devices. In the literature,

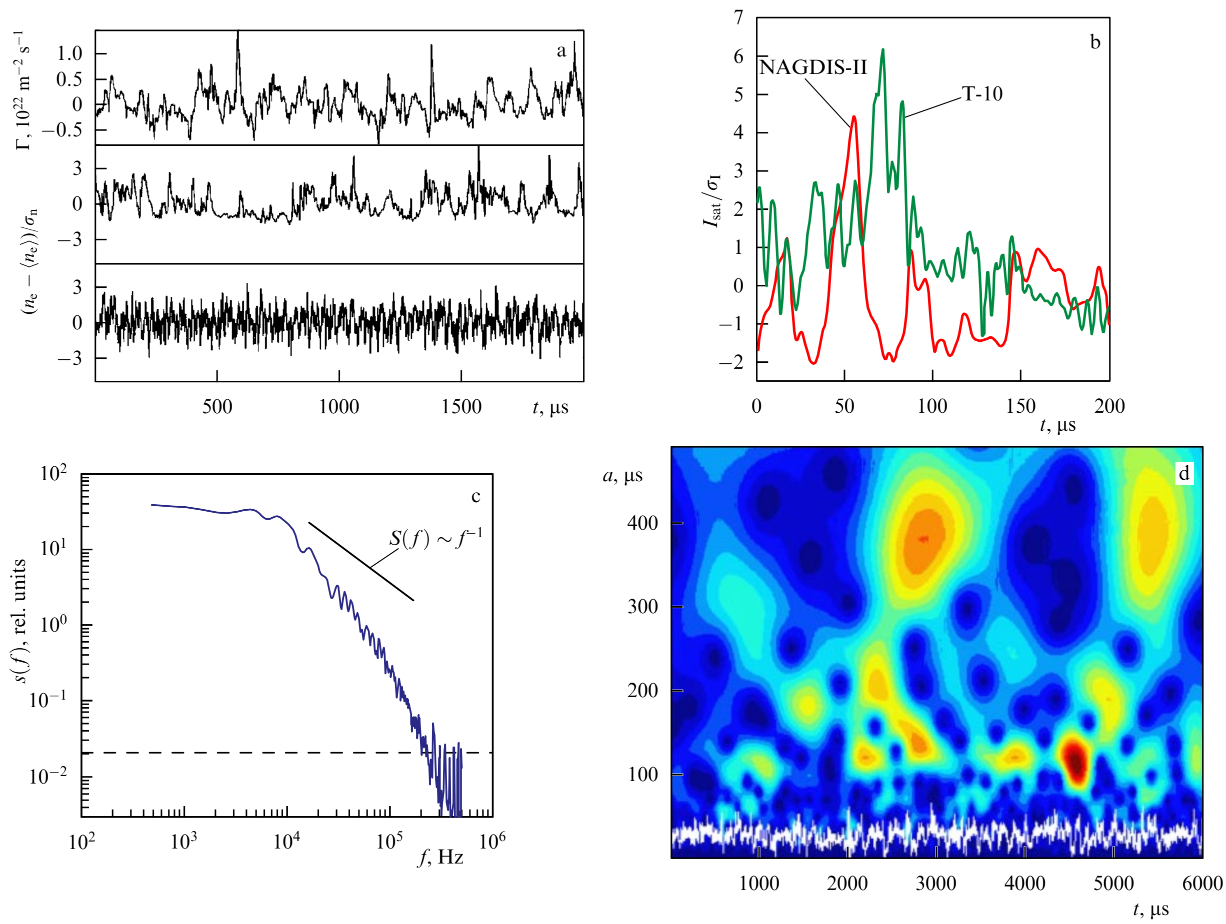

Figure 19. Fluctuating parameters of the edge plasma in the T-10 tokamak. (a) The cross particle flux Γ in SOL at the radius $t = 36$ cm (the upper panel); the plasma density n_e at the radius $r = 32$ cm (the middle panel) and at the radius $r = 29$ cm (the bottom panel). (b) Example of typical high-amplitude peaks of fluctuations in the edge plasma in the T-10 tokamak and NAGDIS-II. Shown is the ion saturation current (plasma density) normalized to the rms deviation. (c) The typical Fourier spectrum of plasma density fluctuations in the T-10 tokamak, SOL, $r = 36$ cm. The dashed line shows the noise level in the record. The $1/f$ law is shown for comparison. (d) The wavelet transform $|Y_\psi(t, a)|$ of the edge plasma density demonstrates a hierarchy of structures (online, the amplitude increases from blue to red color), the white color shows the experimental signal in the T-10 tokamak, $r = 32$ cm.

these structures are referred to as coherent structures, or bursts and blobs. The duration of these structures varies from $\sim 1\%$ to $\sim 15\%$ of the total signal time.

The characteristic properties of the radial dependence of the edge turbulence are largely the same in all FDs. The level of turbulence (the ratio of the amplitude of fluctuations to the mean level) increases toward the edge of discharge. Such a behavior is observed in devices of different sizes with different methods of plasma heating (see review [14]). The relative level of the electron density fluctuations increases from $\delta n/n \sim 5\%$ in the central regions of the plasma discharge to $\delta n/n \sim 100\%$ in the near-wall zone [14]. This growth occurs smoothly, including the crossing of the last closed magnetic surface. No reliable indications of the dependence of the fluctuation level $\delta n/n$ on the mean (chord) plasma density have been found. The relative fluctuations of the plasma potential ϕ normalized to T_e have approximately the same value as the density fluctuations. But in the TEXT tokamak, for example, the Boltzmann relation $e\delta\phi/T_e = dn/n$ is violated [14]. Fluctuations of the electron temperature are rather difficult to measure; $\delta T_e/T_e \sim (0/3-0.4)\,\delta n/n$ was measured in the DIII-D [203], TEXT [14], and TEXTOR [219] tokamaks. In the JET tokamak, $\delta T_e/T_e \sim 0.1$ in the near-wall zone [220]. Fluctuations of the magnetic field at the tokamak periphery are small, $\delta B_r/B_t \sim 10^{-5}-10^{-4}$ [221–223], they do not significantly affect the particle transport (although the contribution of magnetic field fluctuations can be indirect and can influence the low-frequency turbulence properties; see, e.g., [26, 27]). The frequency spectrum of the near-wall turbulence is broad, with a plateau extending up to some frequency that varies in the range $\sim 10-100$ kHz in different devices, and above this frequency, the spectrum shows a power-law decay with the exponent $\sim 1-4$ [14] (see Fig. 14c). The frequency spectrum varies with the radius. The form of the spectrum in the entire frequency range (from 0.1 kHz to 1 MHz) shows no reliably detected and justified dependence on the mean and local densities, or on the electron and ion plasma temperatures (or their gradients) at the discharge periphery.

Autocorrelation functions (ACFs) of signals have been studied in tokamaks [14], stellarators [224], and other plasma devices. ACFs decay not exponentially but in accordance to a power law $A(\tau) \sim \tau^{\nu}$ on the timescale $\tau < 10-20$ µs [225]. The power law exponent varies with frequency. For example, on a timescale about 10 µs, the plot can be approximated by a power law with the exponent $\nu = -(2.7-3.4)$. At longer times (up to 1–10 ms), oscillations are observed, which suggests the existence of long-range correlations. When approaching the wall, the ACF shape changes with radius; however, it is impossible to classify the properties of turbulence using the ACF shape.

In the traditional approach, the characteristic scale of spatial correlations is defined as the length at which the mutual correlation coefficient of signals from two spatially separated probes decreases to ~ 0.3. In tokamaks, such a characteristic correlation scale in the poloidal direction is $\sim 5-10$ mm [226].

The dynamics of the two-dimensional structure of the near-wall turbulence in tokamaks measured by a high-speed camera revealed that the turbulence evolves in both time and space [14]. In the Alcator-CMod [227], DIII-D [228], and NSTX [229] tokamaks and in the W7-AS stellarator, structures stretched along the magnetic field are observed.

In the literature, there are data on the scales of poloidal and radial correlations (estimated using the correlation functions method) $L_{pol} \sim 0.5-5$ cm and $L_{rad} \sim (0.5-1)\,L_{pol}$. The mean toroidal correlations $L_{tor} \sim 10-20$ cm and the relation $L_{rad} \sim (0.2-0.4)\,L_{tor}$ have been reported [14]. In some experiments, long-range correlations, up to several meters, are observed. However, these data are very nonsystematic, and give only approximate, qualitative information on the characteristic spatial scale of inhomogeneities.

We note that the spectral method detects only correlations connected with the translation symmetry — the invariance under time shifts. The long-range order of correlations caused by the scale invariance of turbulence can be discovered by using the wavelet analysis methods.

Wavelet transformation reveals the presence and hierarchy of coherent structures in the signal. The typical wavelet transformation for a turbulent signal in the T-10 tokamak is shown in Fig. 19d. The hierarchy of structures seen in Fig. 19d evidences the presence of a cascade process and self-similarity. Branching — a tree-like form — is observed, suggesting fractal properties of the process.

The spectrum of wave numbers (the k-spectrum) can be determined from two-point probe measurements. Measurements of the wave number spectra were carried out using multi-electrode probes and multipoint optical diagnostics [231–233]. The spectrum of poloidal wave numbers (integral over all frequencies) broadens similarly to the shape of the frequency spectrum (integrated over all k_{pol}), as is expected from the hypothesis of flux freezing. The form of the radial k_{rad} spectrum is difficult to measure due to a significant radial change in the mean plasma parameters on the correlation length scale. The structure of the edge turbulence along the magnetic field measured by Langmuir probes has the correlation lengths $L_{\parallel} \gg L_{\perp}$ along and across the field [234–236]. This is due to a high mobility of electrons along **B** and is confirmed in experiments in which optical emission is registered at the tokamak periphery [237, 238].

Poloidal wave vectors k_{pol} in the edge plasma in FDs change in the range $\sim 0.1-5$ cm^{-1}. This corresponds to the scaling interval $\langle k_{pol}\rangle \rho_i \sim 0.02-0.1$ (where $\langle k_{pol}\rangle$ is the averaged poloidal number and ρ_i is the local ion gyroradius, $T_i = T_e$) , i.e., to the typical low-frequency turbulence range [239–243]. The study of this scaling law is motivated by the simplest theoretical models that assume a linear increment of drift waves with a maximum near $\langle k_{pol}\rangle \rho_i \sim 0.03$. In the mixing length limit, the fluctuation level scaling is expected to be $\delta n/n \sim 1/(k_{rad}L_n)$, $L_n = n/(dn/dr)$. Such a dependence is found in some experiments with $r/a < 1$ [14]. But this scaling law does not correspond to observations of strong intermittency and a high level of $\delta n/n$ in the far SOL, where the radial gradient flattens.

The level of fluctuations is independent of the plasma current and the stability margin in ASDEX and TEXT tokamaks [244, 245].

In general, no universal scaling laws describing the properties of the low-frequency near-wall turbulence in a wide range of parameters have been reliably discovered experimentally.

The phase velocity in the poloidal direction in the edge plasma in tokamaks [246] reaches $\sim 1-10$ km s^{-1} (in the laboratory frame). Measurements showed that this velocity changes its direction: from the direction of the electron diamagnetic drift inside the last closed field surface to the ion drift direction in SOLs. That is, there is a strong shear (the change in the direction of motion) near the last closed magnetic surface (LCMS). This is observed in tokamaks with different configurations (limiters or divertors) and in L- and H-modes. Near the LCMS, the radial velocity is comparable to or less than the poloidal one on average. But the radial velocity toward the wall can exceed the poloidal one in the main SOL and can be as high as 1 km s^{-1}, i.e., a few percent of the local speed of sound. When approaching the wall, the radial velocity of coherent structures responsible for the intermittent turbulent transport in the SOL can decrease (in the DIII-D tokamak [247]) or can be constant (in the Alcator C-Mod tokamak [248]). A significant inhomogeneity of turbulence and the presence of coherent structures are typical features of near-wall turbulence, and it has been proposed to refer to such turbulence as structural turbulence (see [224]).

The transport of plasma across a magnetic field demonstrates the intermittency property. Intermittency in turbulent flows has been probed in tokamaks T-10 [90, 249], TF-2 [250], TEXTOR [231, 251], CASTOR [252], DIII-D [92], and MAST and Tore-Supra [209], in stellarators L-2 [224], LHD [253, 254], and others [14]. Intermittency of turbulence was observed in the L- and H-regimes. Most of the flow (up to 50%) can be transported by coherent turbulent structures (in tokamaks T-10 [90, 249], TF-2 [250], DIII-D [247], and others). The radial profile of the turbulent flow is not constant along the radius. Intermittency and superdiffusion are also observed in magnetospheric boundary layers [20, 255].

The statistical properties of plasma turbulence in tokamaks and other FDs have been studied starting from the 1990s. The probability density distribution function (PDF) of fluctuations of the plasma density and the cross flux of particles significantly deviate from the Gaussian law. The typical form of the distribution function of the amplitude of fluctuations is shown in Fig. 20 [256]. An asymmetry of the PDF and an excess over the Gaussian value at large amplitudes are observed (so-called 'thick tails'). These fluctuations occur with a higher probability than predicted by the classical Brownian process (known in the literature as 'white noise'). The presence of high peaks (with the amplitude exceeding three standard deviations; they are referred to as 'bursts' in the literature) evidence a significant intermittency in the system. The asymmetry of the PDF is observed for the plasma density, electric fields, and the radial plasma flow (Fig. 20). The continuity of the distribution function should be noted. This means that the turbulent process is not simply a sum of two independent processes, a 'white noise' and a 'coherent mode'. In that case, the PDF would have the corresponding form with a maximum at large arguments. In experiments, however, a monotonically decreasing PDF is observed [14]. At present, it is impossible to describe the experimental PDF by known analytic functions. The PDF tails can be described not by an exponential but by a power-law function: $P(x) \sim x^{-b}$ with a variable exponent b. As is known from the theory of probability (see [66]), such power-law dependences reflect the random process memory. Probability theory suggests different classes of random processes with memory. The distribution functions of such processes cannot be described by elementary functions, and many models allow only approximations of the distribution function by polynomials, or the distribution function is the solution of some equation. In the literature, the functional dependence of the experimentally observed PDF is discussed.

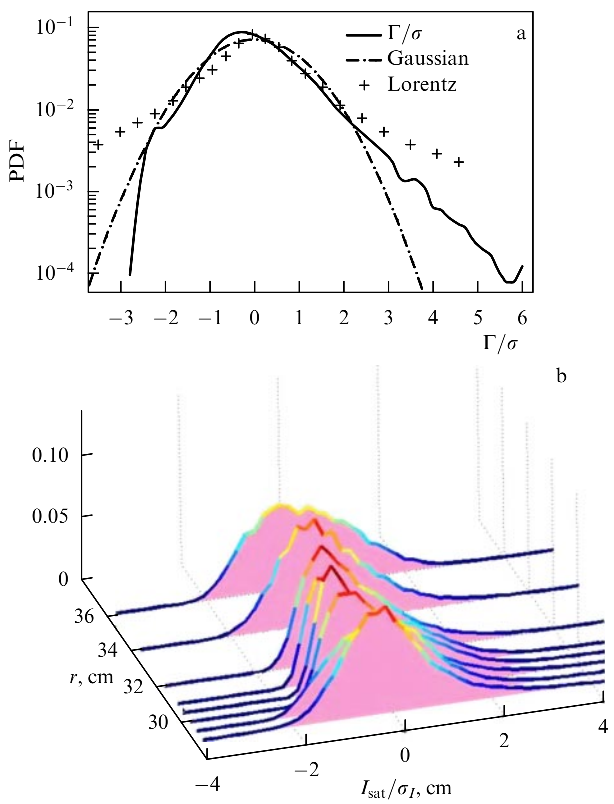

Figure 20. (a) The typical form of the probability density distribution function of the amplitudes of density and radial particle flux $\Gamma(t)$ fluctuations (normalized to the rms standard deviation value) on the semi-logarithmic scale. For comparison, the Gaussian approximation (the dashed-dotted line) and the Lorentz distribution (pluses) are plotted. (b) The radial dependence of the PDF of plasma density fluctuations in the edge plasma of the T-10 tokamak in the range from $r = 30$ to 36 cm.

Models are proposed that are based on mathematical models of complex stochastic processes with memory. There is a certain success in this field (see [224], [257]). The formalism of this approach is based on stochastic models of probability theory. The physical interpretation and the relation to the existing concepts and models of turbulence is often difficult because complicated probability theory constructions are required. Undoubtedly, the existing formalism of the description of turbulent processes should be completed by modern mathematical achievements, in particular, by the use of differential equations with noninteger derivatives [59, 60] and the application of Fokker–Planck–Kolmogorov-type equations to the description of anomalous diffusion and turbulence. In the framework of the traditional approach to turbulence, we can use the formalism of the distribution function moments by invoking modern achievements of statistical physics and probability theory that have been successfully applied in the hydrodynamic turbulence treatment [3]. On the one hand, this offers the possibility of comparing new results with older ones; on the other hand, this allows us to advance in the understanding of the physics of the process without loss of details and the connection with modern achievements of statistical physics and mathematics.

The shape of the distribution function of fluctuation amplitudes varies in different regions of the edge plasma, but typical properties, such as the asymmetry and thick tails, persist (Fig. 20b). The effect of wide flows (near the LCMS in T-10), which destroy coherent turbulent structures, also changes the PDF significantly, making it closer to the Gaussian one. It is difficult to classify the shape of the distribution function by using only its asymmetry and excess, and therefore experimental PDFs were classified using integral characteristics, such as the parameters of nonlinearity of the structure functions (see below).

Observations of the scale invariance and power laws in the edge plasma are a manifestation of the fractality of turbulence. As is known from the theory of fractal geometry, a fractal object can be characterized by a fractal dimension (or a set of dimensions). As we show below, the fractal structure of turbulence is very complicated. Depending on the detailed description, different indices characterizing the scale invariance of turbulence can be defined.

The correlation dimension is one of such indices [251]. The correlation dimension of the edge plasma turbulence in T-10, TEXTOR, and TF-2 tokamaks lies in the range from ~ 6 to ~ 15 [251, 258]. This relatively low fractal dimension (we recall that this dimension is equal to infinity for 'white noise') serves as an argument in favor of the fact that a turbulent process can be described by partial differential equations with a small number of variables (less than ~ 15, according to fractal dimension estimates).

The Hurst exponent is another indicator of self-similarity (scale invariance) and is used in the literature to characterize the fractal properties of turbulence. We have applied the fractal analysis with the use of wavelet methods [256] to estimate the Hurst exponent as one of the measures of the sigma self-similarity. The Hurst exponent H is interpreted as the diffusion coefficient of a particle in a turbulent medium: the rms deviation depends on time as $\langle \delta x^2 \rangle^{1/2} \sim t^H$. Here, it is assumed that the self-similarity properties do not depend on the scale of observation. This rough approximation allows comparing the process under study with the known theoretical models of stochastic processes for which the Hurst exponent is known. For Brownian motion (classical diffusion), the Hurst exponent is $H = 1/2$, i.e., the particle displacement law is $\langle \delta x^2 \rangle \sim t$. The Hurst exponent for the edge plasma turbulence is 0.6–0.8 [256] and demonstrates a tendency to increase toward the wall. Values $H > 1/2$ are typical of the edge plasma in FDs; such values of H are reported in the literature for D-IIID, Tore Supra [259, 260], and NAGDIS-II [261] tokamaks, and other FDs. This corresponds to a superdiffusion with the dominant contribution from large-scale fly trajectories.

To summarize, we note that experimental research on tokamaks, stellarators, and other FDs with different parameters of the central plasma (see [14]) has led to the conclusion that the properties of the edge plasma in different FDs (tokamaks, stellarators, and so on) are likely to be universal and also similar [255] to the properties of turbulence (intermittency, broadened spectra, long-range correlations) observed in the boundary layers of hydrodynamic flows [24] and in magnetospheric TBLs [20, 255].

3. Generalized self-similarity of turbulence with intermittency

3.1 Discussion of self-similarity in the Eulerian representation

In the Eulerian description of motion, a flow of an incompressible fluid at an instant t is characterized by the velocity field $\mathbf{u}(x_1, x_2, x_3, t) = \mathbf{u}(\mathbf{X}, t)$ at all points of space $\mathbf{X} = (x_1, x_2, x_3)$. In principle, equations of motion (for example, the MHD equations) allow finding the Euler variables $\mathbf{u}(\mathbf{X}, t)$ at any time $t > t_0$ from the given initial values $\mathbf{u}(\mathbf{X}, t_0) = \mathbf{u}_0(\mathbf{X})$.

To study some phenomena (for example, the propagation of test particles, surfaces, and lines in a turbulent flow), the Lagrangian description of fluid motion is sometimes used. In this approach, the motion of a fixed 'fluid particle,' a selected 'point' of a fluid element, is considered. Fluid volumes should have the linear size that is much larger than the mean distance between molecules, but be sufficiently small for the velocity and pressure inside this fluid element to be considered constant. The Lagrangian method describes the real motion of individual elements of a turbulent flow, and it appears to be even more natural than the Eulerian description. But the practical use of Lagrangian variables turns out to be much more complicated (in both theoretical calculations and experiments) than the use of Eulerian variables, and therefore hydrodynamic equations of motion in the Lagrangian form are used quite rarely [3]. Experimental research on turbulence in Lagrangian coordinates requires tracking the motion of microscopic volumes in a turbulent flow, which is very demanding and virtually impossible to realize in experiment.

In hydrodynamics and MHD turbulence of the interplanetary plasma, the Eulerian statistics in the framework of the Taylor hypothesis on the 'flow freezing' in a wide range of scales is assumed. This hypothesis is widely used to describe homogeneous and isotropic turbulence. In the edge plasma of laboratory fusion devices, anisotropy and boundary effects can constrain the application of Taylor's frozen turbulence hypothesis to study turbulence in Eulerian coordinates, and the Lagrangian chaos phenomenon should be considered (see [3, 262]). Chaotic motion is characterized by an exponential deviation of trajectories. In the Lagrangian chaos, the exponential growth of the distance between trajectories occurs only on the scale $l \gg \eta$, where η is the scale of minimal Eulerian structures (for example, dissipative turbulent eddies). In three-dimensional homogeneous developed turbulence, the Richardson law $\langle l^2 \rangle \sim t^2$ in the inertial range $\eta \ll l \ll L$ and the usual diffusion regime $\langle l^2 \rangle \sim t$ for very large scales $l \ll L$ are used to express scaling laws. To remain within the Euler approach in studying anisotropic turbulence with intermittency, a power law more general than the Richardson law was proposed [255]:

$$\langle l^2 \rangle \sim t^h , \tag{40}$$

where the exponent h can be scale-dependent (this property corresponds to the scale invariance and intermittency of turbulence). This property is considered in the multifractal formalism, which enables the unification of the Eulerian and Lagrangian descriptions of turbulence (see [24]), which allows overcoming the difficulty in interpreting experimental signals measured in one spatial point of a turbulent flow.

3.2 Turbulence and deterministic chaos

A large number of the degrees of freedom that are responsible for the appearance of chaotic dynamics is an essential feature of plasma. It was discovered and firmly justified that the complex space–time behavior of distributed media with an enormous number of degrees of freedom can be described adequately by a system of nonlinear equations of small dimensionality. MHD equations are used to describe plasma. The emergence of chaos can be signaled by the stability of waves and structures that appear in the system relative to small perturbations, nonlinear coupling of modes, dissipative effects, etc. If the dynamical stability is absent in the system, the deterministic description loses sense. These phenomena are considered by the theory of dynamical (or deterministic) chaos, which is a part of nonlinear dynamics (see, e.g., [64, 263]). The chaos (see, e.g., [264]) assumes the appearance of a qualitatively new regime with disorder and a complex structure. Much research has revealed that statistical laws are valid not only in very complex systems with a large number of degrees of freedom. The point is not in the complexity of the studied system or external noises but in the appearance of exponential instability of motion at some values of the parameters. In complex systems, the stationary periodic oscillations tend to a limit cycle. The cycles can be stable or unstable. Stable cycles form attractors, which 'attract' all nearby trajectories. Physically, this means that if the system departs from such fluctuations, they are nevertheless restored after a certain time. Oscillations of a pendulum provide an example of a stable cycle. If a system shows chaotic properties, a structure more complicated than an attractor emerges in its phase space — a strange attractor, a set with a very complicated (fractal) geometry that attracts nearby trajectories. Studies of nonlinear dynamical processes in physics and mathematics showed that systems with just a few degrees of freedom often demonstrate chaotic behavior.

Properties of the stochastic structure of plasma turbulence in a magnetic field are predicted by many theoretical models that involve the quasilinear approach (see, e.g., [265]). Such models, with some restrictions, can be applied to TBLs with strong turbulence.

The fractal structure of a chaotic system is characterized by a fractal dimension (also known as the Hausdorff dimension), which can take noninteger values (see [28, 266]). For white noise, its value tends to infinity.

Properties typical for chaotic systems are observed in plasma. Chaotic oscillations of the laboratory edge plasma in TF-2 [258] and TEXTOR [251] tokamaks were found to have fractal dimensions from ~ 4 to ~ 15. The dimension can vary in space, which reflects the complex structure of the edge plasma. According to theoretical considerations (see [266]), the dimension of the phase space is somewhat higher than that of the strange attractor in that space. A low value (from ~ 4 to ~ 15) of the fractal dimension suggests that the phase space of the system can be described by dynamical equations with a relatively small number of independent variables (less than 15).

The fractal dimension of the turbulent plasma in Earth's magnetosphere is estimated to be 4/3 for time oscillations and 5/3 for spatial distributions [28].

To illustrate characteristics of chaotic motion of a turbulent medium, methods studying the phase space topology are used. The most informative is the Poincaré map method (see [267]), which is based on two-dimensional sections of an N-dimensional phase space. The analysis of such two-dimensional maps helps understand the dynamics of systems described by differential equations. To construct the two-dimensional Poincaré maps, the Grassberger–Procaccia algorithm (see [251]) is applied, which allows constructing the multidimensional phase space from one experimental turbulent signal. In that phase space, the Poincaré map is constructed in the two-dimensional projection on the plane of two eigenvectors of the process with maximum eigenvalues.

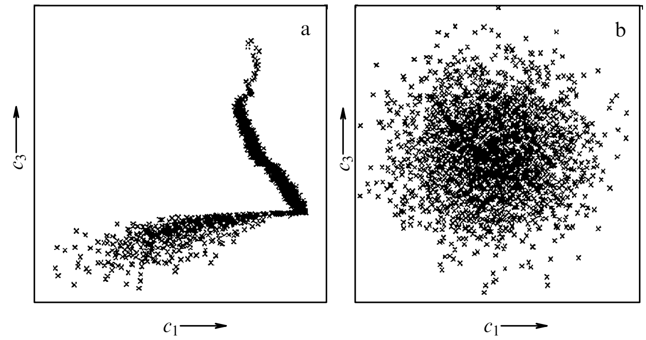

Figure 21. The Poincaré map for an attractor in the near-wall turbulence record in the plane of two eigenvectors (c_1, c_3) of the process. (a) the TEXTOR tokamak. (b) A model random process (white noise).

As is shown in the theory of nonlinear dynamics [267], the possibility of chaos arising in a two-dimensional map can be signaled by the presence of the so-called 'Smale horseshoe' — the horseshoe topology of the map with a fine structure. This is related to the presence of a homocline structure in the strange attractor, when the map is stretched along one direction and squeezed in the other direction. The presence of such an inhomogeneous topology must be due to chaotic trajectories (from the standpoint of nonlinear dynamics) and an infinite number of periodic trajectories in the phase space of the system. This horseshoe-like topology of the generalized phase space section is actually observed in T-10, TF-2 [268], and TEXTOR [251] tokamaks (Fig. 21). In some cases, oscillation properties can be similar to those of white noise. Such properties are usually observed in regions of shear flows where correlations are suppressed and plasma transport across the magnetic field is reduced.

Knowledge of the turbulence strange attractor properties is extremely important for the question of plasma confinement in FDs. Because no full theory of plasma turbulence is currently available, recommendations for effective plasma confinement in magnetic traps should be given by using advances in theoretical models and experimental data on the structure of turbulence. Experiments attempting to influence turbulence allow clarifying the properties of turbulence. It is known from experiments that plasma in laboratory FDs can be in qualitatively different states with different levels of fluctuations and correlation properties of turbulence (for example, the known L- and H-modes of plasma confinement in tokamaks), which points to several stable plasma states. Because the turbulent plasma state is related to the appearance of chaos in plasma dynamics, chaos control and suppression methods can be used to control plasma turbulence and turbulent transport in an FD (see [269]). The property of periodicity of oscillations in complex turbulent motion was noted by experimentalists and used to affect this motion. However, when choosing methods of influence on periodic (or quasiperiodic) modes, the nonlinear mode coupling must be taken into account, and therefore the methods of influence that are appropriate for trivial mechanical systems (for example, those similar to resonance build-up of a harmonic oscillator) are inappropriate to handle turbulence in most cases. Theoretical studies (see [269]) show that the dynamics of a chaotic system can be controlled by applying weak perturbations in order to switch the system from the chaotic oscillation regime to the required dynamical regime (thus stabilizing the system behavior). The transition from one stable state to another can be accomplished by different physical mechanisms of perturbing the system that are capable of driving it from the region of one strange attractor to the region of another one, or of significantly changing the system dynamics by forcing it to approach deterministic (regular) motion. These special perturbations can be realized using methods developed in recent years, for example, by the Grebogi–Yorke–Ott method [270, 271].

In FDs, perturbative methods of affecting plasma turbulence and plasma confinement in magnetic traps have been discussed for a long time. The aim is to reduce the radial transport using an external perturbation by keeping the stable plasma confinement conditions in the trap, which is a very complicated task because any (local or global) variation of the flow across the magnetic field by external forces changes the density, temperature, and pressure profiles in the plasma and hence changes the force balance. Such variations often break the stability of global plasma confinement in a magnetic trap. Methods of influencing the plasma parameters that are responsible for the linear stage of drift instabilities (the local pressure gradient or electric field) were considered. Such influence on local gradients can be performed by optimizing the pressure profile in the entire discharge, by choosing the optimal contribution of the power of the additional plasma heating, or by optimizing the gas injection regime or Pellet injection into the discharge periphery. There is some progress in this area, and all these methods, as a whole, relate to the arrangement of the entire discharge. However, it is also necessary to have the tools for local (resonance) control of the edge plasma parameters. For example, such a local handling by the plasma parameters and transport is important in the zone of periphery transport barriers determining the H-mode physics. Because plasma motion can be induced and controlled by electric and magnetic fields, the effective use of additional low-power devices (coils and electrodes) should not worsen the global confinement parameters. Experimental research has suggested edge plasma influence methods that can somewhat improve plasma confinement conditions. In tokamaks, these methods include the use of an external electric field by applying a potential drop (of a few hundred volts) to an electrode inserted into the edge plasma (so-called biasing), and the formation of a screw magnetic field by additional external coils, which ergodizes the periphery magnetic structure (the so-called dynamic ergodic divertor (DED) or ergodic divertor (ED) regime).

The effect of radial electric fields on the edge plasma in TF-2 [226], TEXTOR [251], and CASTOR [272] tokamaks changes the fractal structure of turbulence, increases disorder, suppresses correlations, reduces the radial plasma transport, and improves the plasma confinement.

Experiments carried out in TEXTOR [273], HYBTOK-II [274], and TF-2 [275] tokamaks revealed a significant influence of the dynamic ergodic divertor on the structure of turbulence. Electromagnetic fields of multipole windings of DEDs induce additional plasma rotation in the resonance zones. Alfven waves excited by a DED (with the windings playing the role of antennae here) dissipate on the Alfven resonance surfaces located on both sides of the tearing-mode resonance. That is, the rotating magnetic fields of the DED in the tokamak represent a system with phase control of dissipation processes and hence the plasma turbulence. Changing the rotation frequency in the external coils of the DED leads to the effect of periodic modulation of low-frequency plasma turbulence, which modifies its structure. The maximum effect occurs at the modulation frequencies close to the value determined by the time scale of turbulence. Different time scales can be chosen, for example, those determined by Alfven resonances or drift modes. The maximum effect occurs at frequencies corresponding to long-range correlations, which was observed in experiments with the dynamic ergodic divertor in the HYBTOK-II tokamak [274, 276]: in the narrow frequency range 5–25 kHz, the fractal structure of turbulence (Fig. 22) and the related correlations and the intermittency character change significantly. This frequency range corresponds to the characteristic times of long-range correlations.

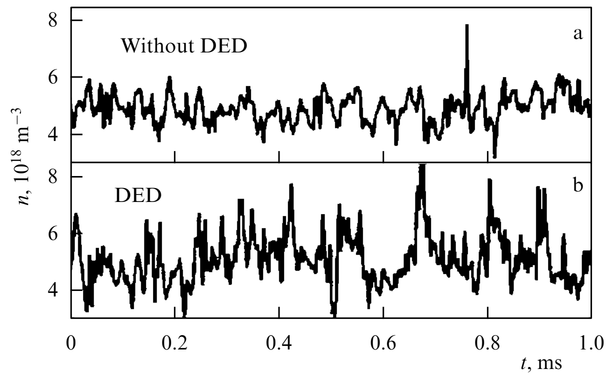

Figure 22. Space–time control of the edge plasma turbulence in the HYBTOK-II tokamak in experiments with an ergodic divertor. Plasma density oscillations (a) withot a DED, and (b) with a DED.

3.3 Structure functions and the singularity spectrum

The structure functions $S_q(\tau) = \langle|\delta_\tau X(t)|^q\rangle$, where $\delta_\tau X(t) = X(t+\tau) - X(t)$, are estimated from time signals $X(t)$: 1) the plasma density and particle flux across the magnetic field in fusion devices and 2) the magnetic fields and ion flux near Earth's magnetopause.

A power-law dependence like $S_q(\tau) \sim \tau^{\zeta(q)}$ (i.e., the simplest self-similarity) is observed only in limited time intervals spanning 1–1.5 orders of magnitude (Fig. 23). This interval corresponds to the inertial range considered in the classical models of isotropic developed turbulence (K41 and others). In the TBL near the magnetopause, this interval is observed for less than 1 s. In the laboratory edge plasma (in the T-10, HYBTOK-II, and JT-60U tokamaks, the LHD stellarator, and the NAGDIS-II device), it is observed on restricted time scales of the order of 10 μs [277].

In accordance with the moment hierarchy hypothesis in models of turbulence with intermittency (the extended self-similarity hypothesis, ESS), an analysis of the interdependence of the structure functions of different orders like $S_q \sim S_p^{\zeta(q)/\zeta(p)}$ reveals the property of generalized self-similarity (generalized scale invariance) [255, 277]. This property can be seen from the plot shown in the logarithmic scale in Fig. 24. The linear dependence of $S_q(\tau)$ on $S_3(\tau)$ is observed over almost three orders of magnitude of the scale change up to 300 s in the TBL magnetopause and 1 ms in all experimental data obtained in the T-10 and JT-60U tokamaks, the LHD stellarator, and the NAGDIS-II linear device. This dependence is observed in hydrodynamic turbulence [24] and MHD turbulence of the interplanetary plasma [86, 255, 278].

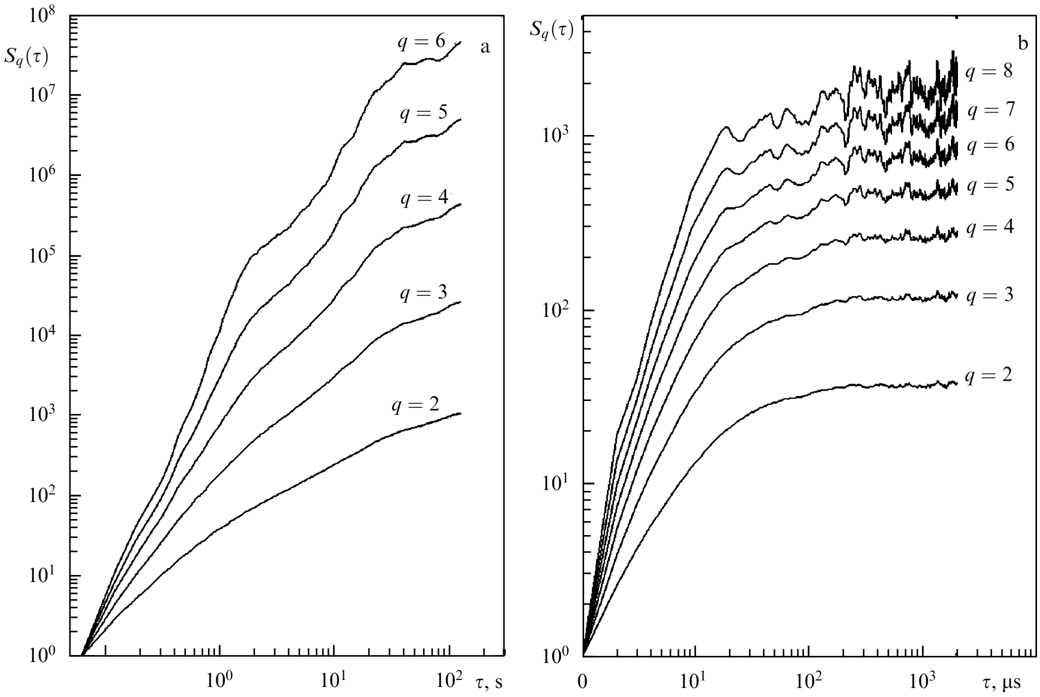

Figure 23. The plot of the structure function $S_q(\tau)$ moments of different orders vs the time scale τ. (a) Magnetic field B_x in the TBL in the magnetopause on 19.06.1998. (b) Plasma density in the SOL, T-10.

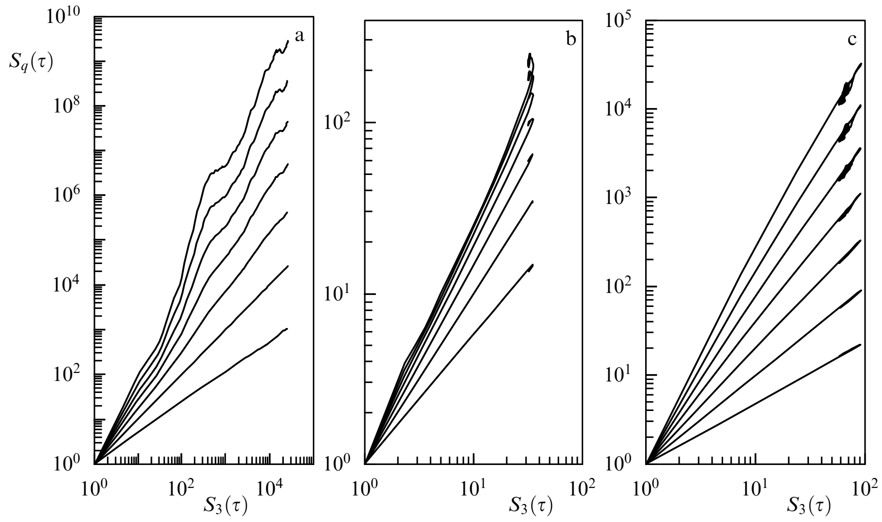

Figure 24. The plot of the structure function $S_q(\tau)$ moments of different orders ($q = 2, 3, 4, 5, 6, 7, 8$ from bottom up) vs the 3rd-order structure function $S_3(\tau)$ for the magnetic field B_x (a) in the TBL near the magnetopause and (b) for the plasma density in NAGDIS-II.

The generalized self-similarity indicates a statistical symmetry that provides the process invariance in a wide range of scales down to the dissipative one. In this process, the multifractal statistics and long-range correlations that provide enhanced turbulent transport are formed. In the edge plasma of an FD, this anomalous transport worsens the plasma confinement in the magnetic trap. In Earth's TBL magnetopause, this process largely determines the mechanism of plasma transport through the transport barrier of the TBL in the incoming flow.

In reality, the generalized self-similarity property allows increasing the accuracy of determining the structure function scaling in the experimental data analysis. The structure function scaling law $\zeta(q)/\zeta(3)$ normalized by the third-moment scaling law can be obtained from the slope of the logarithmic plot (Fig. 24).

Observations of the generalized self-similarity in intermittent turbulent plasma in space and laboratory conditions, where the boundary effects play a significant role, can be interpreted in terms of the log-Poisson model of turbulence (see below).

The property of generalized self-similarity and multifractality is characterized by a spectrum of singularities (multifractal spectrum). To estimate the singularity spectra $D(h)$ and the Hölder exponent h, wavelet methods are used (see [278–280]). In Fig. 28a, the range of the Hölder exponents is shown for different orders of the moment. In the statistical description of the process, similarly to the statistical thermodynamics [278–280], the variables h and q play the same roles as the energy and inverse temperature in thermodynamics.

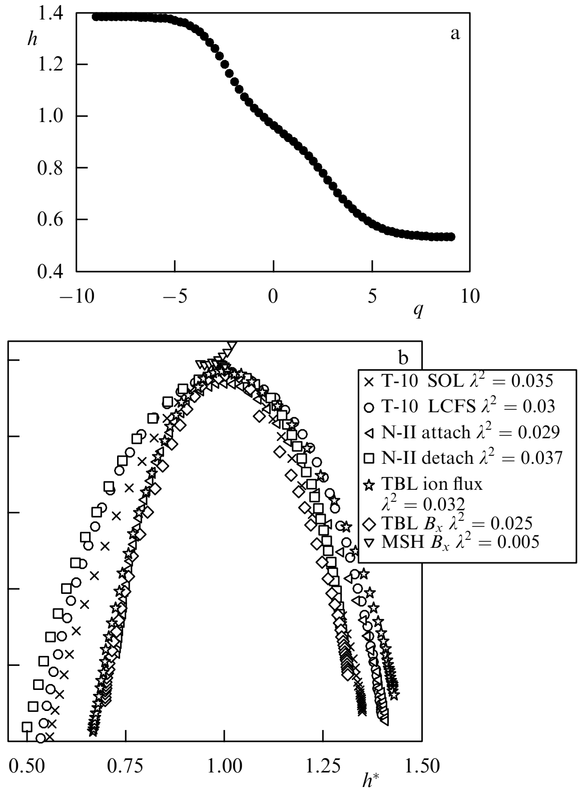

Figure 25. (a) The Hölder exponent h for different moment orders q. (b) The multifractal spectrum $D(h)$ as a function of the normalized Hölder exponent $h^* = 1 + (h - h_{D_{\max}})$ (centered at 1). Shown are turbulence in the edge plasma in the T-10 (T-10 SOL) tokamak, near the last closed field surface (T-10 LCFS), in NAGDIS-II for the low-confinement regime (N-II attach) and high-confinement regime (N-II detach); the ion flux in the TBL (TBL ion flux, 29.03.1996), the magnetic field in the TBL (TBL B_x, 19.06.1998) and the magnetic field in the MSH outside the TBL (MSH B_x). The multifractality exponents λ^2 for which $\zeta(q) = Hq - \lambda^2 q^2$ are also shown, demonstrating a deviation of $\zeta(q)$ from a linear dependence on q; the value of λ^2 for monofractal processes does not exceed 0.01 [256]

All signals detected in laboratory and cosmic plasma had a broadened spectrum $D(h)$, with a bell-like shape (Fig. 25b). The broadening and bell-like shape of the spectrum are the typical signatures of multifractal statistical processes. It is known from theory that for a Brownian process (Kolmogorov-like turbulence), $D(h)$ is a single point with the Hölder exponent $h = 1/3$, i.e., the process is characterized by one exponent. In our case, experimental values of the Hölder exponent exceed 1/3. The maximum value of $D(h)$ for all spectra almost attains unity. This implies that turbulent fluctuations are characterized by a rapid increase in amplitudes (the signal is almost singular everywhere). Hölder exponents $\gtrsim 2$ have never been observed. In the theoretical analysis of the statistical properties of turbulence, the Hölder exponent h characterizes the scaling law of the velocity fluctuations

$$\delta_l u \sim l^h . \tag{41}$$

Figure 25b plots the $D(h)$ spectrum as a function of the normalized Hölder exponent $h^* = 1 + (h - h_{D_{\max}})$ ($h_{D_{\max}}$ is the Hölder exponent at the maximum of $D(h)$). In this representation of the $h_{\max} - h_{\min}$ spectrum, we can compare the spectral broadening of different signals. The difference $h_{\max} - h_{\min}$ is the most important quantitative characteristic of the spectrum and can be used as an indicator of the degree of deviation from the isotropic Kolmogorov turbulence. Generally, the broadening of the spectrum $D(h)$ for detected signals falls within the range 0.4–1.3. Such values are observed in the edge plasma of laboratory devices: the T-10, HYBTOK-II, JT-60U, CASTOR tokamaks, the LHD stellarator, and the NAGDIS-II device [99, 281, 282]. The registered values of the spectral broadening $h_{\max} - h_{\min}$ are typical for strongly intermittent stochastic processes observed in numerical simulations of turbulence and in experiments with neutral fluids [24, 283]. In T-10 and TCABR tokamaks, the broadening $h_{\max} - h_{\min}$ is smaller in the velocity shear region [284].

In Fig. 25b, the multifractality index λ^2 (such that $\zeta(q) = Hq - \lambda^2 q^2$) characterizes the deviation of $\zeta(q)$ from the linear dependence on q. The value of λ^2 does not exceed 0.01 for mltifractal processes and $\lambda^2 \sim 0.02-0.04$ in plasma TBLs [255]. The close values of λ^2 stimulated a more profound comparison of the statistical properties of turbulence in boundary layers of FDs and the magnetosphere [20, 255].

3.4 Multifractal cascade process

As noted above, direct numerical solution of equations like (1) meets the fundamental problem of a significant increase in the number of degrees of the freedom when passing to smaller scales due to the cascade character of the process. The cascade models of turbulence are appropriate to describe turbulence with intermittency. The analysis of the stochastic cascade allows the description of many properties of turbulence with intermittency, including multiscaling and multifractality.

Experiments carried out in the T-10, HYBTOK-II, JT-60U, and TCBAR tokamaks, the LHD stellarator, and the NAGDIS-II linear plasma device revealed that the low-frequency near-wall turbulence demonstrates multifractality [90, 274, 281, 284, 285]. We recall that inhomogeneous fractal objects have the property of multifractality; in contrast to regular fractals, one fractal dimension is insufficient to describe them: a spectrum of fractal dimensions is needed. An inhomogeneous fractal object has geometric characteristics determined by its fractal dimension and statistical properties described by a distribution function with special characteristics (see [286]). The multifractal analysis concept is widely used in the physics of disordered media (for example, quantum phase transitions) and studies of the developed turbulence of hydrodynamic flows.

The multifractality property means that the distribution function of the increments of fluctuation amplitudes $\delta_l X = X(t + l) - X(t)$ changes from a quasi-Gaussian shape at large l to a non-Gaussian shape with 'thick tails' at small scales (lags) l. For the edge plasma in T-10 and the LHD stellarator, this transformation is illustrated by Fig. 26 for lags $l \sim 1-1000$ μs. This property was observed in the turbulent edge plasma of the tokamaks HYBTOK-II, JT-60U, CASTOR, TCABR, Tore Supra, and the NAGDIS-II device [225, 284, 285, 287]. The evolution of the distribution function from significantly non-Gaussian at small lags to quasi-Gaussian at large lags (more than 200–500 μs) evidences the multifractal character of the process. We recall that for a monofractal process (for example, the Brownian process), the distribution function of the increments is independent of the lag and is always Gaussian.

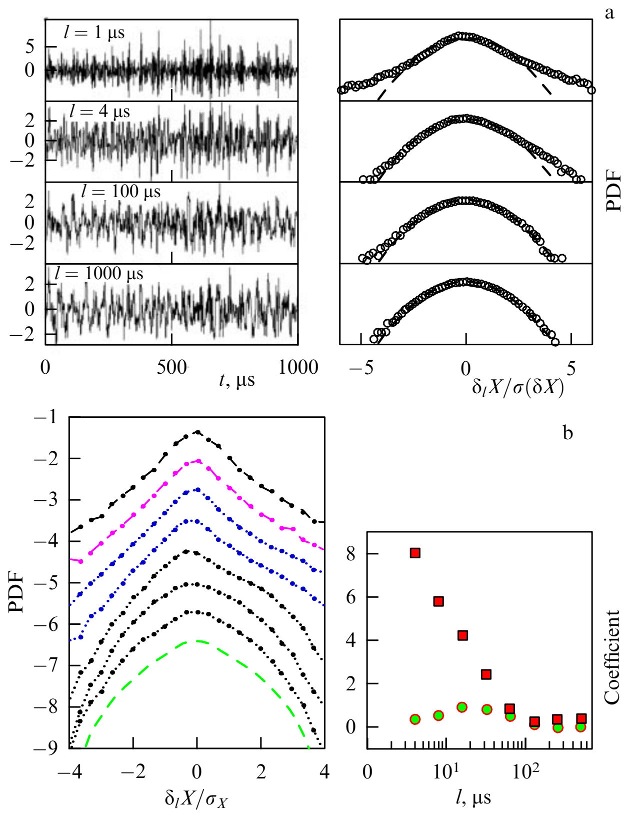

Figure 26. (a) Records of the differences $\delta_l X = X(t+l) - X(t)$ on the scales $l = 1-1000$ μs (left) and the distribution function $P_l(\delta X)$ (in semi-logarithmic scale) (right). There is the time scale $T \sim 100$ μs on which the Gaussianity property is violated. (b) The distribution function $P_l(\delta X)$ for the signal increments $\delta_l X = X(t+l) - X(t)$ on the time scales $l = 1, 2, 4, 8, 16, 32, 64, 128, 256$ μs (from top down, with the curves shifted arbitrarily) in semi-logarithmic scale for the probe signal in the edge plasma of the T-10 tokamak, $r = 32$ cm. Abscissa: $\delta_l X$ normalized to the standard deviation value. Right: coefficients of the asymmetry (circles) and excess (squares) of the corresponding PDF in the left plot as a function of lag l of $\delta_l X$ increments.

The multifractatilty property means a multiscale character of the process. This shows up in special correlation properties: the process is characterized not by a single time or space scale at which correlations decay exponentially (as in the simplest Brownian process) but by a range of scales at which correlations have a power-law dependence on the scale, i.e., long-range correlations exist.

From the dependence of the PDF on the differences of signals, the characteristic time scale — the boundary scale of multifractality — can be found. It is determined by the lag at which the PDF of the signal differences ceases to be Gaussian; on the asymmetry and excess plot, this value corresponds to the lag at which the differences vanish. In Fig. 26, these time scales for different cases are $\sim 50-500$ μs. This is the typical time that was registered in experiments in the T-10, HYBTOK-II, and CASTOR tokamaks and the LHD and NAGDIS-II stellarator.

To describe turbulence with intermittency, we can use the model of anisotropic multiplicative random processes (see review [90]). The multifractal model deals with a boundary scale in the process (for example, the maximum scale) and is based on the assumption that consecutive cascade steps determine the flux distribution between cells of a smaller scale and that the cascade between any scales l_1 and l_2 ($l_1 < l_2$, $l_1 = \lambda l_2$, $l_2 = \lambda' L$) is equivalent to the cascade from the maximum scale L to l_2 with the scale factor $\lambda\lambda'$.

The multifractality can be described in terms of the multiplicative cascade

$$\delta u(l) = W(l, L)\,\delta u(L)\,, \quad \delta u(l) = u(x+l) - u(x)\,. \qquad (42)$$

For $l < L$, the generator $W(l, L)$ is a random scalar proportional to $(l/L)^h$. For $l_1 < l_2 < l_3$, we then find

$$W(l_1, l_3) = W(l_1, l_2) \bullet W(l_2, l_3)\,. \qquad (43)$$

Properties of the generator W determine the statistics of the process and the self-similarity properties. The scaling function $\zeta(q)$ is the characteristic function of W. The scaling law $\zeta(q)$ determined from experiment can be used in choosing the cascade model parameters.

In discrete cascades, a finite cascade step is assumed: the ratio of scales is $1/2 \leqslant \lambda < 1$. Continuous cascade scales (so-called continuous cascades) are also used. For this, it is necessary to decrease the step value between consecutive steps of a discrete cascade. Such a cascade can be formally (mathematically) considered (see [87]) for any $\lambda < 1$ and even $\lambda < 1/2$, but statistical relations between different structures depend not on the metric of the ordinary space but on a metric associated with the parameterization. The distance between structures on a given scale is determined by the hierarchy level in the cascade. That is, the distance between centers of adjacent cells is not homogeneous any more. The hypothesis of the universal multifractal process [87] assumes the renormalization of nonlinear mixing in a finite range of scales. This enables overcoming difficulties due to discretization.

Stochastic multifractal cascade models have symmetries similar to those of deterministic equations, for example, scaling laws and the energy flux conservation. Still, there is a significant difference between equations for vector fields (MHD and Navier–Stokes equations) and cascade models for the scalar energy flux. To overcome this difference, vector cascade models [87], so-called Li cascades, were developed, whose properties are similar to those of deterministic multidimensional models. In the Li cascades, new symmetries emerge that have not been studied to date. Strictly speaking, in three-dimensional space, the scalar approach is already insufficient, and turbulence should be studied using Li cascades; however, the main properties of cascades can be determined using the scalar approach.

4. Comparison of experimental data with models of turbulence

4.1 Standard cascade models

To develop an adequate model of a turbulent process such that properties observed in experiments be described, scaling laws for experimental structure functions should be compared with different cascade models. A scaling law contains integral information on the statistical properties of turbulence. In a statistically inhomogeneous process, $\zeta(q)$ is a nonlinear function of q.

To calculate the scaling law $\zeta(q)$ of a structure function $S_q(\tau) \sim \tau^{\zeta(q)}$ of experimental signals, the structure functions for integer q have been traditionally calculated. In this way, it is impossible to determine nonlinear characteristics of $\zeta(q)$

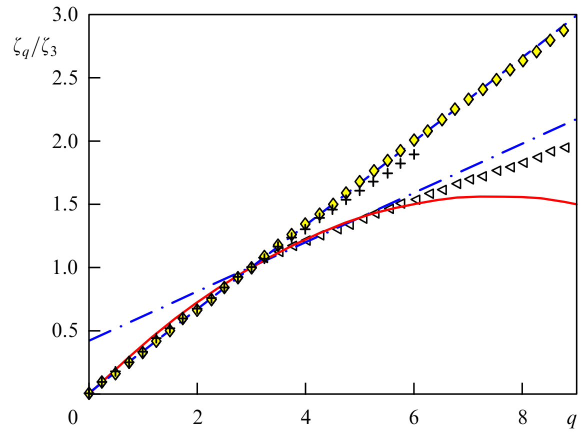

Figure 27. The scaling law of the structure function of turbulence in the outer cusp of Earth's magnetosphere (diamonds), the magnetic field component B_y (directed approximately along Earth's orbit) from the Interball-1 data of 23.06.1998, the plasma density in the shear layer near the last closed field surface in the T-10 tokamak (crosses) and in the far SOL of the LHD stellarator (triangles). For comparison, scaling laws of the K41 (dashed curve), log-normal (solid curve), and β-models (dashed-dotted curve) of turbulence are shown.

with high accuracy. To accurately determine the scaling law $\zeta(q)$, the wavelet transform modulus maxima method (WTMM) has been developed recently [278–280]. This method takes the scale invariance of turbulence into account. The WTMM method deals with the analysis of the partition function

$$Z(q,l) = \sum_{\{t_i(l)\}_i} \left| T_\psi\{t_i(l),l\} \right|^q \sim l^{\zeta(q)} , \tag{44}$$

where $\{t_i(l)\}_i$ corresponds to maxima of the modulus of the wavelet transform T_ψ and $q \in R$. The method is more precise in analyzing experimental data than the traditional structure function method (see [278–280]). It allows calculating the scaling law $\zeta(q)$ for large negative and positive q, and the acceptable accuracy of the analysis of modern experimental data is reached for the interval $q \in \{-4, 9\}$ with a step up to 0.05.

As we show below, most data obtained in Earth's TBL magnetosphere and in the near-wall zone of FDs are not described by the standard cascade models of developed isotropic turbulence (K41, log-normal, and so on). Only restricted zones where turbulence can be described by the K41 model have been observed in experiments. These regions are typically characterized by a strong shear flow, which can effectively destroy and mix turbulent structures. Scaling laws of the structure functions $\zeta(q)$ in these regions of the laboratory plasma (the shear zone in the T-10 tokamak) and in cosmic plasma (the outer cusp of the magnetosphere) are shown in Fig. 27. In the same figure, the scaling laws for the K41, log-normal (with the intermittency parameter 0.5) and β-models (with the standard parameter $\beta = 3/4$) are shown. The log-normal and β-models of turbulence do not describe experimental data either in shear flows or in turbulent regions with strong intermittency (see, e.g., the data in Fig. 27 on the near-wall turbulence with strong intermittency observed in the LHD stellarator).

4.2 Applicability of the Iroshnikov–Kraichnan model

The Iroshnikov–Kraichnan (IK) model is actively discussed in application to observations in the interplanetary (see, e.g., [288]) and laboratory [289] plasmas. It is therefore useful to compare experimental data with this model. In the IK theory, $\zeta(4) = 1$ (in contrast to the Kolmogorov theory, in which $\zeta(3) = 1$). We compare experimental scaling laws $\zeta(q)/\zeta(4)$, normalized to the value $\zeta(4)$, with the prediction of the IK model $\zeta(q) = q/4$. Such a comparison for the data obtained by the Interball-1, Cluster-3, and Geotail SC is shown in Fig. 28. For comparison, also plotted is the log-Poisson scaling law, taking MHD effects (30) into account in the framework of the Politano–Pouquet model [86, 88]. The data from the TBL are not described by either the IK model ($\zeta(q) = q/4$) or the scaling law (30). The IK model well approximates B_x in the MSH (outside the TBL) and B_x in the solar wind (according to the Geotail satellite data). This suggests properties of turbulence close to the MHD turbulence with the strong anisotropy observed in the solar wind (see [290]).

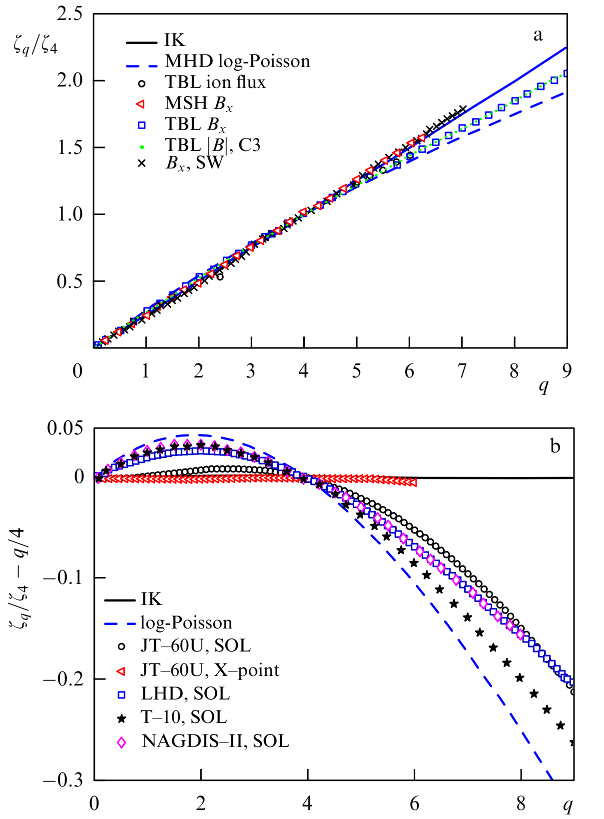

Figure 28. (a) The scaling laws $\zeta(q)/\zeta(4)$ for measurements by Interball-1 (MSH and TBL B_x), Cluster-3 (the vector **B** modulus in TBL), and Geotail (SW B_x). The solid line shows the Iroshnikov–Kraichnan scaling law $q/4$. The dotted line indicates the log-Poisson scaling law taking MHD effects (31) into account in the framework of the IK phenomenology. (b) Comparison of experimental scaling laws with the Iroshnikov–Kraichnan scaling law. The deviation of $\zeta(q)/\zeta(4)$ from the IK scaling law $q/4$ is shown. The data were obtained in the SOL plasma of the T-10 tokamak, at the outer edge of the SOL in JT-60U, at the divertor point in JT-60U, and in the edge plasma in LHD and NAGDIS-II. The dashed line shows the log-Poisson model taking two-dimensional dissipative structures (85) into account.

In the edge plasma in the T-10 and JT-60U tokamaks, the NAGDIS-II linear device, and the LHD stellarator [90, 277], a significant difference between experimental curves and the IK scaling law is observed (see Fig. 28b). The scaling law is close to that predicted by the IK model only in the vicinity of the X-point in the divertor zone of the JT-60U tokamak. This can be explained by a significant decorrelation and stochastization of the magnetic structure (as follows from theoretical descriptions) near the X-point. Close to the X-point, stochastization is likely to affect the plasma dynamics much more strongly, and methods developed for strong MHD-turbulence should be used there. Except for this unique case, all observed scaling laws have been observed to differ from the IK model predictions.

The results of experimental studies imply that the Iroshnikov–Kraichnan model is inapplicable to the low-frequency plasma turbulence in turbulent boundary layers [90, 277].

Kadomtsev [12] explained the invalidity of the 'weak coupling approximation' used in the IK model to describe small-scale fluctuations of the developed turbulence. In the Kraichnan scheme, the effect of large-scale fluctuations on the evolution of small-scale inhomogeneities is overestimated: this effect is reduced to the transfer of small-scale fluctuations with a small deformation (the adiabatic approximation). In the case of strong plasma turbulence in TBLs, this approximation is invalid.

Most generally, plasma turbulence should be treated in three-dimensional (3D) geometry. Three-dimensional turbulence is a dissipative system with a finite energy dissipation rate, even for very small viscosity. All aspects of the applicability of the two-dimensional turbulence model in the analysis of turbulent flows are relevant to the treatment of low-frequency turbulence in the edge plasma. The justification of the two-dimensional approach depends on the required level of detailed description and the characteristics of turbulence to be determined. Although 2D models of plasma turbulence describe many typical properties observed in experiments (broadened spectra, frequency band, and so on), many models cannot describe such important properties as intermittency, multiscale invariance, and cascade processes in detail. This limitation of 2D models of the magnetized plasma is due to the loss of symmetries related to the true 3D scale invariance, which is frequently changed (or broken) in deriving 2D equations of motion. As noted above, in hydrodynamics, the properties of 2D and 3D flows are fundamentally different (see [24, 32]). The two-dimensional and three-dimensional ideal (nondissipative) MHD equations give rise to three invariants [288, 291, 292]. In both 2D and 3D models, the energy $E = 1/2\int(u^2 + B^2)\,\mathrm{d}\mathbf{r}$ and cross helicity $H_{\mathrm{v}} = \int \mathbf{uB}\,\mathrm{d}\mathbf{r}$ are conserved. The spectral density $E(k)$ characterizes the direct cascade, although $H_{\mathrm{v}}(k)$ is possibly a mixed-type cascade. The third invariant is the magnetic helicity $H = \int \mathbf{A}\,\mathbf{B}\,\mathrm{d}\mathbf{r}$ in 3D and the rms potential $H_{\mathrm{A}} = \int \mathbf{A}^2\mathrm{d}\mathbf{r}$ in 2D; both $H(k)$ and $H_{\mathrm{A}}(k)$ are responsible for the inverse cascade formation. Because of this similarity, many theoretical models do not distinguish between the 2D and 3D approaches in considering the energy spectrum and the velocity component along the magnetic field. Despite this formal similarity, there is a significant difference: while there are always two ideal invariants in 2D MHD, only energy is conserved in 3D for $H = H_{\mathrm{v}} = 0$. Therefore, in considering the properties of the turbulent cascade and analyzing the role of structures of different dimensions (especially one-dimensional), the 3D description of the magnetized plasma is closer to the hydrodynamic one than the 2D description. That is, the use of cascade models (including the log-Poisson one), which were developed for hydrodynamic turbulence to describe the turbulent cascade of the near-wall turbulence in a tokamak, does not contradict analytic theories that consider strong anisotropy in the magnetic field.

We note that this does not restrict the possibility of comparing the results of turbulent cascade studies with theoretical and numerical models of the near-wall turbulence using the two-dimensional approach. We recall that in the interplanetary plasma, the GS95 model of moderate turbulence superseded the IK model (see Section 1.3.4). The validity of the assumptions of the GS95 model to describe plasma in a TBL remains an open issue that requires experimental testing.

4.3 The log-Poisson model

The scaling laws $\zeta(q)$ of the structure functions for laboratory and space plasma are presented in Fig. 29. We note the significant deviation of experimental spectra in the TBL from the Kolmogorov law. This discrepancy is most pronounced in Fig. 29b, where the difference between the experimental data and the K41 model is plotted. The

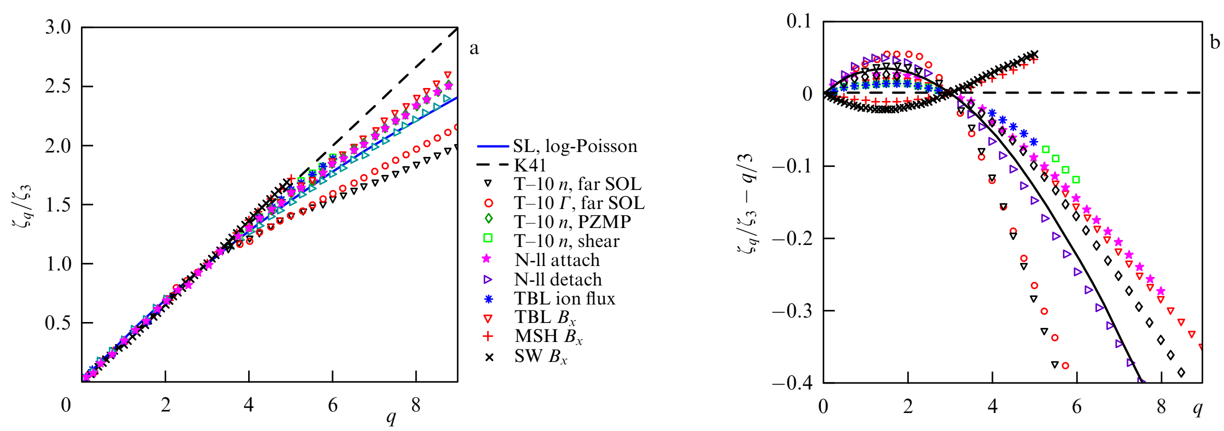

Figure 29. (a) The scaling law of the near-wall turbulence structure function in fusion plasmas and the geomagnetic trap of Earth. The K41 spectrum (dashed curve) and the scaling law of the log-Poisson model (solid line) with the parameters $\beta = \Delta = 2/3$ are shown for comparison. (b) The deviation of the scaling laws of the structure function from the K41 spectrum. The line marks the log-Poisson model for the parameters $\beta = \Delta = 2/3$. The edge plasma turbulence in the T-10 tokamak (T-10 n far SOL is the plasma density and T-10 Γ far SOL is the particle flux); in NAGDIS-II in the L-mode confinement (N-II attach) and H-mode confinement (N-II detach); the ion flux in the TBL (TBL ion flux, 29.03.1996), the magnetic field in the TBL (TBL B_x, 19.06.1998), and the magnetic field in the MSH outside the TBL (MSH B_x), and in the solar wind from the Geotail data (SW B_x).

Table 3.

Experimental data	Δ	β
T-10, n_e, $r = 34$ cm	0.43	0.33
T-10, n_e, $r = 36$ cm	0.68	0.35
T-10 flux, $r = 36$ cm	0.53	0.25
T-10 LCFS, n_e, $r = 30$ cm	0.23	0.25
T-10 shear layer, n_e, $r = 29$ cm	0.9	0.91
NAGDIS-II attach, n_e, $r = 18$ cm	0.23	0.36
NAGDIS-II detach, n_e, $r = 18$ cm	0.35	0.3
TBL near Earth's magnetopause, B_x	0.24	0.38
MSH outside the TBL, B_x	≈ 0	1
MPL near Earth's magnetopause, ion flux	0.2	0.36
Cluster 1, 2.02.2003, MP, B_x	0.38	0.56
Cluster 1, 2.02.2003, barrier near the Earth TBL B_x	0.12	0.45
Interball-1, 22.12.1996, B_z in geomagnetic tail	0.15	0.26

experimental scaling laws $\zeta(q)$ can be described by log-Poisson model spectrum (23) upon adjusting the parameters β and Δ. These parameters, determined by a nonlinear fit to scaling law (23), are listed in Table 3. They can vary, but their variations are small, except for turbulence in the MSH far from the TBL (where the scaling law is close to the Kolmogorov one) and in the velocity shear layer (where the destruction of turbulent eddies is assumed) in tokamaks [293].

The data also deviate from the values $\beta = \Delta = 2/3$ that characterize the isotropic three-dimensional turbulence in the ShL model (24) [69, 70]. The observation of Δ in the range from 0.2 to 0.43 (Table 3) can be interpreted as evidence for the dominating contribution of quasi-one-dimensional structures to turbulence with intermittency [70]. The anisotropic cascade consideration allows studying this question in detail (see below).

To verify the log-Poisson hypothesis on power-law scaling (16), scaling laws for the moments $\Pi_q(\tau) = S_{q+1}(\tau)/S_q(\tau)$ were studied. The dependences in the form (see [32])

$$\Pi_{q+1} = (\Pi_q)^{\delta_q}$$

were analyzed. Figure 30 shows the typical hierarchical dependence of Π_{q+1} on Π_q in the range of q from 1 to 8 on the logarithmic scale. All data are arranged along a straight line, which is an evidence in favor of the hierarchy of moments predicted by the log-Poisson model with constant parameters A_q in (16). If there were no such law, groups of points would lie along nonparallel segments or not lie along one line at all.

The exponent δ_q ranges from δ_0, corresponding to the mean flux $\Pi_0(l) \sim l^{\delta_0}$, to δ_∞, corresponding to the limit case $\Pi_\infty(l) \sim l^{\delta_\infty}$. For different types of turbulence, the dependence δ_q on q is different (see [32]):

1) $\delta_q = 0$ is the K41 model, a monofractal model;

2) $\delta_q \equiv$ const signifies that the degree of inhomogeneity does not increase as the order increases, but even the first-order moment depends on the scale of averaging (for example, strong isolated eddies in turbulence);

3) $\delta_0 = 0$ and $\delta_\infty = 2/3$ pertain to the She–Leveque model, where the mean (first moment) is independent of scale and there is a limit value of δ_q for large moments;

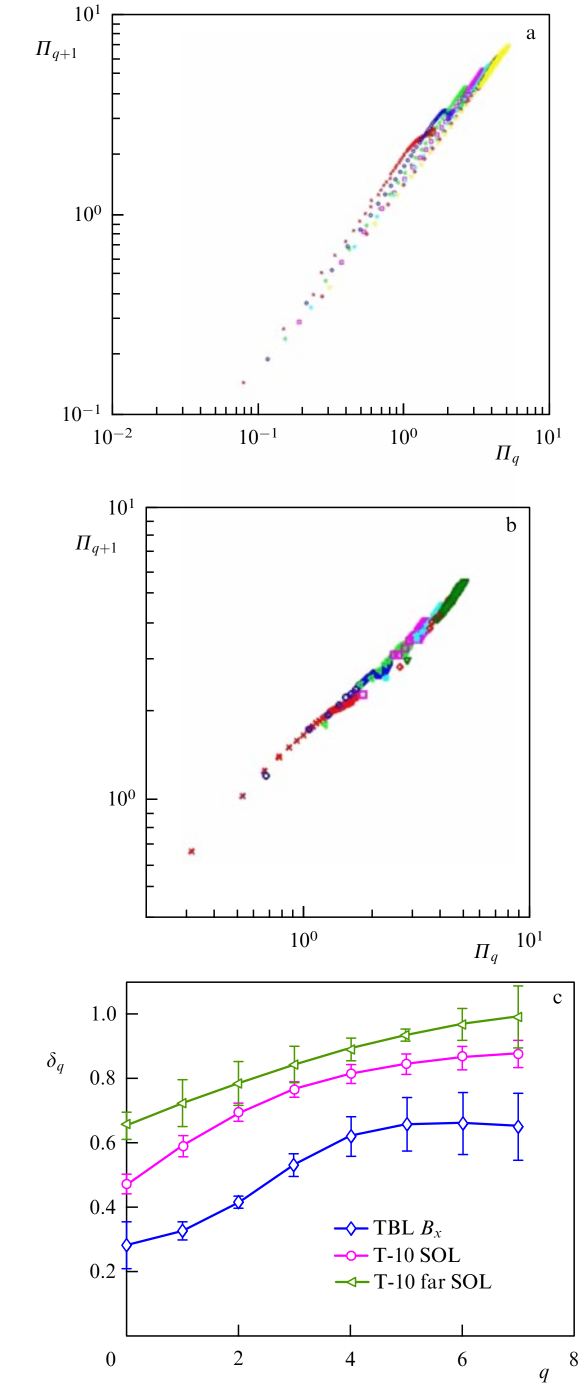

Figure 30. The relative moments Π_{q+1} as functions of Π_q. Each group of points corresponds to a certain q from the interval $\{1, 8\}$; (a) B_x in TBL (Interball-1). (b) The plasma density at $r = 32$ cm in SOL of T-10. (c) The dependence of the exponent δ_q on the moment order q. Plotted are the magnetic field in the magnetosphere TBL (TBL B_x), plasma density in the SOL plasma of the T-10 tokamak (T-10 SOL) at $r = 31$ cm, and in the far SOL (T-10 far SOL) at $r = 36$ cm.

4) $\delta_0 =$ const with δ_∞ being bounded indicates that the mean value depends on the scale and the exponent increases with q. In this case, we find $\Delta = (d_\infty - d_0)/\zeta_3$ from the moment hierarchy in the ShLD model. Then δ_q can be written in the form

$$\delta_q = \delta_\infty + \zeta_3 \Delta H(q)\,, \tag{45}$$

where $H(q)$ is a monotonically decreasing function with $H(0) = 1$ and $H(\infty) = 0$. In the simplest case, this is the exponential $H(q) = \exp(-aq)$ (see [20]). It can be shown by substituting in the original definitions of the moment hierarchy that the ShL model implies such an exponential with the dependence of the exponent $\beta = \exp(-a)$ [32].

The dependence δ_q is plotted in Fig. 30c. For both for laboratory and TBL plasma, this dependence suggests the moment hierarchy predicted by the ShLD hypothesis: the mean value depends on the scale and the exponent increases with q. This also means that isolated eddies do not dominate in the considered data.

A note should be made regarding the spectrum of moments of the direct and inverse cascades. It follows from the definition of $\langle \varepsilon_l \rangle$ that the quantities Π_1 and δ_q characterize the intensity of the energy transfer processes, irrespective of their direction. Therefore, the inverse cascade can also be characterized by δ_q. This note also pertains to the spectrum of $\zeta(q)$.

To conclude this section, we note that in the turbulent flow of neutral fluids, spectra close to those in the log-Poisson model have also been observed (see Section 2.1). The similarity of scaling laws in different turbulent media points to the universal character of the structure of developed turbulence with intermittency.

5. Anisotropic turbulence cascade and dimension of dissipative structures

To study the properties of dissipative structures, scaling laws of the dissipation energy $\varepsilon_l^\infty \sim l^{-\Delta}$ and the velocity difference $\delta_l u \sim l^{1/g}$ should be considered [291] (the parameter is $g = 3$ in the K41 model and $g = 4$ in the IK model). In the log-Poisson model, the exponent β is related to Δ and the codimension C_0 of dissipative structures as $\beta = 1 - \Delta/C_0$ (see [86]), with $C_0 = 3 - D$, where D is the dissipative structure dimension. In three-dimensional space, $C_0 = 2$ for one-dimensional filaments ($D = 1$) and $C_0 = 1$ for sheet-like structures ($D_0 = 2$). The scaling law in the log-Poisson model (28) can be written as

$$\zeta(q) = (1 - D)\,\frac{q}{g} + C_0\left(1 - \left[1 - \frac{D}{C_0}\right]^{q/g}\right). \tag{46}$$

Usually, the relation between Δ and g is found by assuming the same scaling law $\varepsilon_l^\infty \sim E^\infty/t_l^\infty$ for the time scales t_l^∞ of dissipation (E^∞ is the amount of energy dissipated by singular structures) and the time of nonlinear energy transfer t_l^{NL} down the cascade $\varepsilon \sim \delta_l u^2/t_l^{\mathrm{NL}}$. Assuming $\varepsilon_l^\infty \sim l^{-\Delta}$ and $\delta_l u \sim l^{1/g}$, we obtain the relation $\Delta = 2/g$ between the parameters. In the ShL model, these parameters are $C_0 = 2$, $g = 3$, and $\Delta = 2/3$. In the model of turbulence taking the MHD effects into account, $g = 4$, $\Delta = 1/2$, and $C_0 = 1$ under the assumption that two-dimensional current sheets are dissipative structures. Computer simulations of three-dimensional MHD turbulence (the Biskamp–Mueller model, BM [291]) showed that scaling laws (47) are well reproduced for the combination $g = 3$, $\Delta = 2/3$, and $C_0 = 1$ by assuming the hydrodynamic scaling law in sheet-like two-dimensional dissipative structures. The dimension of dissipative structures D (see Fig. 31a) determines the probability density distribution of active turbulent zones in a turbulent medium with intermittency, and it is therefore important to know which dissipative structures determine the scaling properties essentially (or preferentially, if structures with different dimensions can exist).

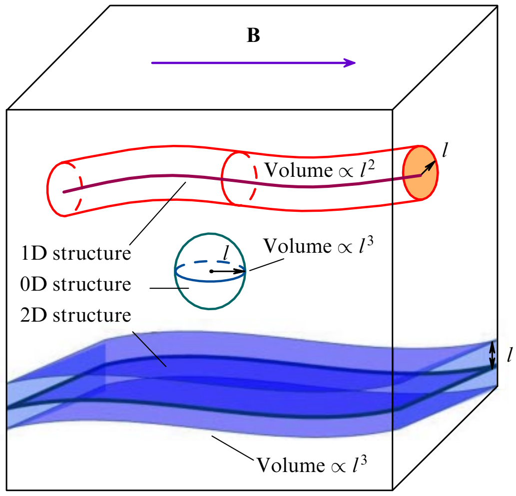

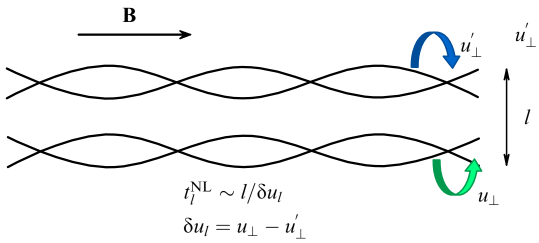

Figure 31. (a) Diagram of objects with different dimensions. The probability that a sphere of radius l is filled with objects of dimension D is $P \sim l^{3-D}$ as $l \to 0$. (b) Diagram of the nonlinear interaction of filamentary dissipative structures ($D = 1$) in the direction across the field. This is the general case of anisotropy in the cascade intensity where the cross energy cascade is characterized by a Kolmogorov-type locality.

We consider a more general case of anisotropy in the cascade intensity. Following [291], it is possible to relax the assumption of equal scaling for t_l^{NL} and t_l^∞. Instead, we assume that t_l^∞ satisfies the K41 scaling law $t_l^\infty \sim l/\delta_l u \sim l^{1-1/g}$ with $\Delta = 1 - 1/g$. For $C_0 = 1$, this leads to the BM scaling law [291]

$$\zeta(q) = \frac{q}{g^2} + 1 - (g)^{-q/g}. \tag{47}$$

Another scaling law $\zeta(q)$ of structure functions is proposed in [277, 278]. As in the above case, using the estimate $t_l^\infty \sim l/\delta_l u \sim l^{1-1/g_f}$ for one-dimensional filamentary dissipative structures with $C_0 = 2$, we obtain the scaling law [277, 278]

$$\zeta_f(q) = \frac{q}{g_f^2} + 2\left[1 - \left(\frac{1 + g_f}{2g_f}\right)^{q/g_f}\right]. \tag{48}$$

In this approach, the value $g_f/3$ is the ratio of the cascade intensity to its intensity in the K41 model. In [291], a modified time of the energy transfer was proposed:

$$t_l^{\mathrm{NL}} \sim \left(\frac{l}{l_0}\right)^{\theta}\left(\frac{l}{\delta_l u}\right), \tag{49}$$

which allows distinguishing between t_l^{NL} and t_l^∞ and characterizing the cascade intensity separately for fluctuations with polarization perpendicular and parallel to the field. Here, l_0 is an arbitrary length scale and θ is a dimensionless parameter. A diagram of the process when the nonlinear interaction in the perpendicular direction is characterized by a Kolmogorov-type locality, i.e., only eddies with close $k_\perp$ interact nonlinearly, is presented in Fig. 31b. This diagram shows the conditions in the SOL in tokamaks and other FDs: the magnetic lines are open, and turbulence appears preferentially in the flute structures along the magnetic field. In Earth's MSH TBL, there are also perturbations extended along the field. Assuming the persistent energy transfer down cascade $\varepsilon \sim \delta_l u^2 / t_l^{\mathrm{NL}} = \mathrm{const}$, we obtain

$$t_l^{\mathrm{NL}} \sim l^{(1+q)\,2/3} . \qquad (50)$$

We recall that in the standard phenomenology, $t_l^{\mathrm{NL}} \sim l^{2/g}$. In the modified approach, the cascade intensity depends on the factor $(l/l_0)^{\theta}$:

1) $\theta = 0$ $(g = 3)$ for the isotropic K41 cascade,

2) $\theta < 0$ $(g > 3)$ corresponds to cascade enhancement compared to K41,

3) $\theta > 0$ $(g < 3)$ corresponds to cascade weakening compared to K41.

Scaling law (49) can be used in studies of turbulent media with intermittency and strong anisotropy, where one-dimensional filamentary structures are likely to dominate. Such conditions are realized in turbulent plasma boundary layers of Earth's magnetosphere [20]. Outside the TBL, fluctuations of B_x are characterized by an enhanced cascade process with $\theta > 0$ $(g < 3)$.

Figure 32 shows the comparison of experimental scaling laws with model laws (48) and (49). In the main SOL, the scaling law $\zeta(q)$ is described by the model with one-dimensional dissipative structures (49); in the far SOL, the scaling law for higher-order moments q is close to that in the model with two-dimensional dissipative structures (48).

The radial dependence of the parameters g and g_f in the near-wall turbulence in the T-10 tokamak is presented in Fig. 32c. The uniform norm of difference (the relative error in determining the fitting parameters) ranges from 5×10^{-2} to 5×10^{-5}, which evidences a good approximation. In almost all of the SOL and inside the poloidal rotation shear region $(28 < r < 29.5$ cm), the parameter g_f is close to 3. As noted above, this can signal the presence of one-dimensional singular dissipative structures, because the experimental scaling law is closer to (49). In the far SOL in the T-10 tokamak, the cascade properties at the small radius $r = 36$ cm are closer to those in the model with two-dimensional dissipative structures $(g \approx 3)$ with scaling law (48). In this case, two-dimensional vortex structures are likely to contribute most. A similar process with vortex structures was observed in numerical models with different complexity levels developed for the edge plasma in FDs (see, e.g., [27]).

Table 4 lists values of g and g_f in FDs and the TBL of Earth's magnetosphere. In most experiments, the parameter g_f in the main SOL is close to 3, i.e., filamentary dissipative structures (with quasi-one-dimensional topology) described by scaling law (49) dominate in boundary layers.

In experiments performed in the T-10 tokamak [90] and other tokamaks (see, e.g., [260]) and stellarators (LHD [294] and others), large-scale structures are observed in the edge plasma, which are called 'blobs' in the literature. The radial motion of these structures shows up in the signals of probing devices in the form of large-amplitude bursts of an irregular shape. Other structures, eddies, and space–time modes have also been registered. All these structures result from low-frequency plasma turbulence. The spectral characteristics of such structures do not allow concluding that they exist independently of the entire turbulent motion. For example, blobs contribute to the low-frequency part of the Fourier spectrum at frequencies $\sim 1-30$ kHz and to the structure functions at times $\sim 40-1000$ μs. However, there are no monochromatic peaks in the spectra and spectral functions, and the spectra are broadened. It is incorrect to regard them as evidence of isolated structures. Taking numerous experimental studies performed in the T-10 tokamak and other

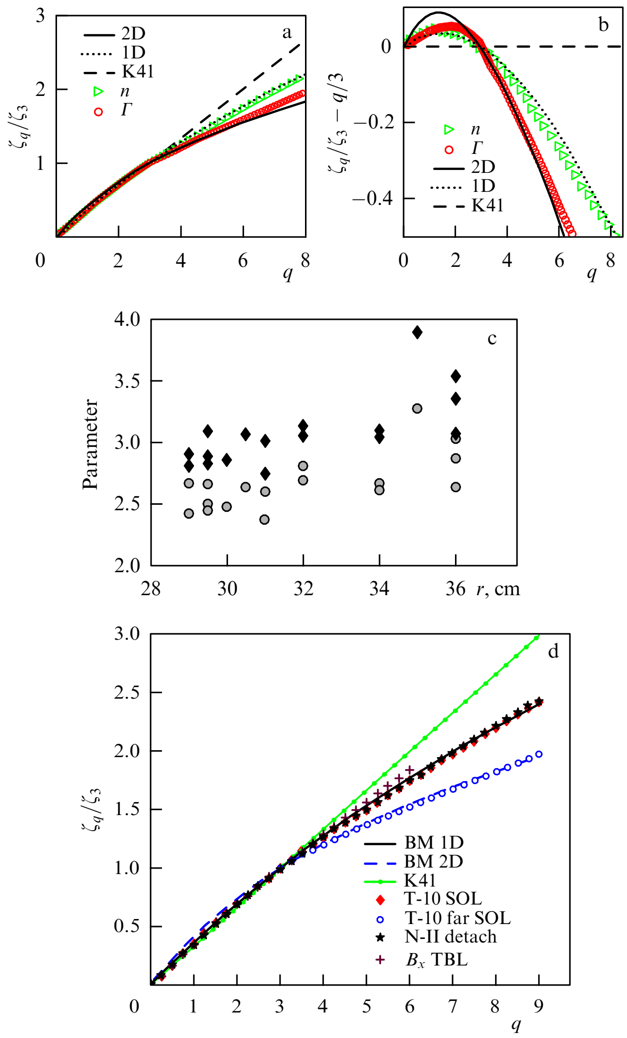

Figure 32. (a) The experimental scaling law of the structure function and (b) its deviation from the Kolmogorov spectrum. The SOL plasma density at $r = 34$ cm (triangles) and the cross-field particle flux Γ in the far SOL at $r = 36$ cm (circles). The K41 model (dashed line), modified scaling law (49) for 1D dissipative structures (dashed-dotted line), Biskamp–Mueller (BM) structures (48), and 2D dissipative structures (solid line) for the T-10 tokamak plasma. (c) The near-wall turbulence characteristics in the T-10 tokamak plasma. The parameter of scaling (48) is g (circles) and that of (49) is g_f (diamonds). The parameter g_f is close to 3 almost everywhere in the SOL. (d) The scaling law of the near-wall turbulence in the T-10 tokamak plasma and the magnetic field in the TBL. In the TBL, the main SOL of the T-10 tokamak and in NAGDIS-II (N-II detach, $r = 18$ mm), the scaling law is described by (49) in the model with one-dimensional dissipative structures (1D BM, shown with the solid line); in the far SOL, the scaling at high q is close to (48) in the model with two-dimensional dissipative structures (2D BM, shown with the dashed line).

Table 4. Paremeters g and g_f obtained by fitting the experimental scaling laws by scaling laws (48) and (49).

Experiment	g	g_f
T-10 SOL, n_e, $r = 34$ cm	2.61	3.03
T-10 SOL, n_e, $r = 36$ cm	3.02	3.53
T-10 SOL, flux, Γ, $r = 36$ cm	2.9	3.4
T-10 LCFS, n_e, $r = 30$ cm	2.5	2.87
T-10 shear layer, n_e, $r = 29$ cm	2.35	2.73
NAGDIS-II attach, n_e, $r = 18$ mm	2.65	3.05
NAGDIS-II detach, n_e, $r = 18$ mm	2.59	3.0
LHD, SOL n_e, long magnetic field line	2.3 – 2.6	2.8 – 3.1
LHD, SOL n_e, short magnetic field line	2.5 – 2.8	3.1 – 3.3
JT-60U, SOL n_e, $r = 400$ mm from separatrix	2.63	3.06
Cluster 4, 02.02.2003, V_z, MSH barrier of Earth	2.58	3.03
Cluster 4, 02.02.2003, V_z, TBL of MSH of Earth	2.48	2.9
Interball-1, 22.12.1996, B_z in the geomagnetic tail	2.4	2.76

tokamaks into account, we can conclude that there is a strong nonlinear mutual dependence of all structures and modes of the edge plasma; this interdependence is considered in modern theoretical models (see [27, 43, 44, 97]). The results of the above analysis in the framework of the log-Poisson model suggest the topology of structures responsible for dissipation in the edge turbulence. These structures can be associated both with the coherent phenomena discussed above, which were frequently observed in experiments, and with structures that are not pronounced on the background of strong turbulence in the edge plasma. We note that dissipative structures with different geometries (topologies) can coexist, as is discussed in the log-Poisson model [295]. Theoretical considerations [295] of a random multiplicative process (such as the log-Poisson cascade) allow the process to include dissipative structures with different geometries, including fractal ones. Properties of the experimental scaling laws discussed above are satisfactorily described by the log-Poisson model by assuming one-dimensional dissipative structures. Our method does not allow obtaining information on the specific spatial shape of quasi-one-dimensional dissipative structures. From the symmetry properties of MHD flows (for example, the treatment of helicity), it is possible to assume that they have a spiral-like complex shape, predominantly stretched along the magnetic field. In the case of the TBL above the polar cusps of Earth's magnetosphere, the one-dimensionality can be due to the symmetry of plasma streams (flows that are parallel to the magnetopause) [18–20, 28]. The effect of boundaries is in the interaction of fluctuations in the incident flow with waves reflected from the magnetopause [20]. For a detailed study of the dissipative structure geometry and confirmation of the obtained results using the log-Poisson model phenomenology, dedicated experiments should be carried out.

The scaling properties of turbulence generally depend on the dissipation scale properties, where viscous effects are important and the time of nonlinear interaction is of the order of the diffusion time. It is therefore useful to compare dissipative scales λ_v in turbulence for an ordinary liquid and for plasma described by the MHD equations. In an ordinary fluid [6],

$$\lambda_v \sim L\,\mathrm{Re}^{-3/4}, \tag{51}$$

where L is the macro scale of motion characterized by the velocity U. In the plasma in a strong magnetic field, the cascade anisotropy produces a wider dissipative scale, which can be estimated as [296]

$$\lambda_B \sim L\,\mathrm{Re}^{-2/3}. \tag{52}$$

Appreciable differences between the dissipative scales in plasma and those in hydrodynamic turbulence become important for very large Reynolds numbers only (for example, in the central zone of a hot plasma in big tokamaks or in the interplanetary plasma, where $\mathrm{Re} \sim 10^5 - 10^{10}$). It is difficult to estimate the Reynolds number in the edge plasma of a tokamak because the viscosity can vary in a very broad range. The value of Re derived from approximate estimates in the edge plasma of a tokamak and other FDs is relatively small (possibly from ~ 10 [260] to ~ 1000). In Earth's magnetosphere, the TBL Re is also estimated in the range from ~ 30 to ~ 600 [29]. This means that for relatively small Reynolds numbers, the magnetic field effects are not very important: at $\mathrm{Re} \sim 1000$, the dissipative scale λ_B is only doubled in comparison with λ_v. This is possibly one of the reasons for the similarity between the energy cascade properties in hydrodynamic turbulence with intermittency and low-frequency turbulence in the edge plasma in a tokamak [116].

6. Transport characteristics in an intermittent turbulent medium

The log-Poisson scaling exponents β, Δ, and g_f obtained in experiments (Table 3 and 4) can be used to determine the scaling law of turbulent plasma transport. Here, approaches developed in statistical physics are applied, which take the scaling properties of multifractal cascades and generalized self-similarity into account [20]. As discussed above, diffusion is determined in such processes by fractal dimensions and can be described by the diffusion equation with noninteger derivatives (see, e.g., [59–61]).

The diffusion properties should be considered using the concept of a multifractal multiplicative cascade (see, e.g., [297]). In this approach, the scaling law of generalized diffusion depends on that of the structure function $\zeta(q)$ as [243]

$$D \propto \tau^{K(-1)}, \quad K(q) = q - \zeta(3q). \tag{53}$$

This scaling law is used to estimate the transport in a statistically inhomogeneous medium with percolation properties. The exponent $K(-1)$ in (53) is determined by the fractal properties of the medium and is characterized (on average) by the topological properties (connectedness properties that determine the transport) of the stochastic structure of the near-wall turbulence.

From Table 3 for experimentally determined exponents in different devices and formulas for the log-Poisson model (23) and (49), we have $K(-1) \approx 0.1 - 0.7$. The displacement of a particle with time is given by

$$\langle \delta x^2 \rangle \propto D\tau \propto \tau^{\alpha} \tag{54}$$

Table 5. The scaling exponent of transport in Earth's magnetosphere TBL and in the edge plasma of fusion reactors

Experimental data	α
Cluster 3, 1; Barrier: 02.02.2003, B_z	1.1 – 1.15
Cluster 3, 1; MP: 02.02.2003, B_z	1.3
Cluster 1, MSH: 03.02.2003, B_z	≈ 1
Interball-1, 22.12.1996, B_z in the geomagnetic tail	1.42
Tokamak T-10, n_e	1.33
Tokamak JT-60U, n_e	1.33
Tokamak JT-60U, n_e, X-point of divertor	≈ 1
Stellarator LHD, n_e	1.4
Linear device NAGDIS-II, n_e	1.41

with $\alpha \propto 1 + K(-1) \approx 1.1 - 1.7 > 1$. This scaling law implies superdiffusion. We recall that $\alpha = 1$ for the normal (Brownian) diffusion and the convective (ballistic) motion is characterized by the value $\alpha = 2$.

The edge plasma in T-10 and JT-60U tokamaks, the LHD stellarator, and the NAGDIS-II linear plasma device, where $\alpha \approx 1.2 - 1.4$ (Table 5) [281, 282], remains 'superdiffusional' in a wide range of plasma parameters. Only at the X-point of the divertor and near the last closed magnetic surface in the JT-60U tokamak do we have $\alpha \approx 1$. This is related to a decrease in correlations in this region and the turbulence statistics approaching Gaussian.

We note that the superdiffusion scaling law of B_z is observed in Earth's geomagnetic tail (Table 5). The data on B_z were obtained in the zone of the geomagnetic tail where the mean magnetic field components are $B_y = -2.7$ nT and $B_z = 2.4$ nT, and the rms amplitude fluctuations are $\delta B_y = 3.3$ nT and $\delta B_z = 2.4$ nT (the data were obtained in the region where the process develops on closed field lines, because the mean vertical component of the field is $B_z > 0$). The mean and the variance of fluctuations of B_y slightly exceed these parameters for B_z; this implies that turbulence is one-dimensional (in the sense of Fig. 31, although such structures are also called two-dimensional in geophysics), as near Earth's magnetopause. The superdiffusion scaling law of B_z with $\alpha = 1.2$ can signal the presence of long-range correlations in Earth's magnetosphere tail, i.e., the character of transport processes is determined not only by local properties of fluctuations but also by long-range correlations along the tail (see also [298, 299]).

It is useful to independently estimate the scaling law of particle displacement [17]. For this, we use Eqn (9) for superdiffusion in a turbulent medium with 'Lévy flights' taken from [300]: $\langle \delta x^2 \rangle \propto \tau^{2/\gamma}$, where γ is the Lévy function exponent [17]. It was shown in [18] that in the TBL of 19 June 1998, the probability distribution of the magnetic field vector turning angle is approximated by the Lévy function with the exponent $\gamma = 1.17$. This yields the scaling law $\langle \delta x^2 \rangle \propto \tau^{1.7}$, where the exponent falls within the interval obtained from the log-Poisson model, which independently confirms the superdiffusion property.

To describe the transport properties, the fractional Fokker–Planck–Kolmogorov equation should be used; noninteger exponents are related to the fractal dimension (or the spectrum of fractal dimensions) of the process (see [61]). The parameters of scaling laws and multifractal spectra determined from experiment can be used to construct models of turbulence in TBL based on the noninteger Fokker–Planck–Kolmogorov equation.

7. Conclusions

We can conclude that plasma turbulence in the TBL near the magnetosphere and in the edge plasma in fusion devices is characterized by intermittency, generalized self-similarity, multifractality, and anisotropic cascade processes. The scaling laws of statistical moments are well described by the log-Poisson model of turbulence with a random anisotropic cascade under the assumption of one-dimensional dissipative structures. These properties are also observed in the turbulence of a neutral fluid, which can suggest the universality of statistical properties of turbulence with intermittency.

In magnetospheric TBLs and the edge plasma of FDs, the transport has a superdiffusion character, which should be taken into account in constructing quantitative transport models [cf. (39) for the classical diffusion].

The data obtained here improve the understanding of the properties of intermittent turbulence under the dominance of boundary effects. To verify the assumption on the universal character of the turbulence intermittency in boundary plasma layers, an analysis of large experimental databases is needed. The confirmation of the applicability of the log-Poisson model to a large volume of statistical data would open the prospect of a quantitative description of turbulent transport processes in a multifractal medium using the scaling laws of statistical moments.

The authors acknowledge the support through the grants of RF Rosatom, RFBR 06-02-17256 and 06-02-72561, the State Contract of RF 02.740.11.5064, the Japanese Scientific Society JSPS and the LAIM project (Japan), ISSI (Team132), INTAS-03-50-4872, and INTAS 05-1000008-8050. We also thank V A Vershkov, C A Grashin, and the research group at the T-10 tokamak for help in obtaining the experimental data, G N Zastenker for providing us with the data from the Interball-1 satellite, and Sh Takamura, N Ono, S Masuzaki, and N Asakura for the possibility of using the experimental data from the LHD, JT-60U, HYBTOK-II, and NAGDIS-II fusion devices.

References

1. Kolmogorov A N *Dokl. Akad. Nauk SSSR* **30** 299 (1941) [*C.R. (Dokl.) Acad. Sci. USSR* **30** 299 (1941)]
2. Kolmogorov A N *Dokl. Akad. Nauk SSSR* **32** 19 (1941) [*C.R. (Dokl.) Acad. Sci. USSR* **32** 19 (1941)]
3. Monin A S, Yaglom A M *Statisticheskaya Gidromekhanika* (Statistical Fluid Mechanics) Vols 1, 2 (Moscow.: Nauka, 1965, 1967) [Translated into English (Cambridge, Mass.: MIT Press, 1971, 1975)]
4. Lathrop D P, Fineberg J, Swinney H L *Phys. Rev. Lett.* **68** 1515 (1992)
5. Cadot O et al. *Phys. Rev. E* **56** 427 (1997)
6. Landau L D, Lifshitz E M *Gidrodinamika* (Fluid Mechanics) (Moscow: Nauka, 1986) [Translated into English (Oxford: Pergamon Press, 1987)]
7. Sreenivasan K R, in *Frontiers in Experimental Fluid Mechanics* (Ed. M Gad-el-Hak) (Berlin: Springer-Verlag, 1989) p. 159
8. Barenblatt G I *Usp. Mat. Nauk* **59** (1) 45 (2004) [*Russ. Math. Surv.* **59** 47 (2004)]
9. Barenblatt G I, Prostokishin V M *J. Fluid Mech.* **248** 521 (1993)
10. Zagarola M V, Perry A E, Smits A J *Phys. Fluids* **9** 2094 (1997)
11. Barenblatt G I, Chorin A J *Phys. Fluids* **10** 1043 (1998)

12. Kadomtsev B B, in *Voprosy Teorii Plazmy* (Reviews in Plasma Physics) Vol. 4 (Ed. M A Leontovich) (Moscow: Atomizdat, 1964) p. 188 [Translated into English: Vol. 4 (Ed. M A Leontovich) (New York: Consultants Bureau, 1971)]
13. Kadomtsev B B *Kollektivnye Yavleniya v Plazme* (Cooperative Effects in Plasmas) (Moscow: Nauka, 1988) [Translated into English: in *Reviews of Plasma Physics* Vol. 22 (Ed. V D Shafranov) (New York: Kluwer Acad./Plenum Publ., 2001) p. 1]
14. Zweben S J et al. *Plasma Phys. Control. Fusion* **49** S1 (2007)
15. Carreras B A, Lynch V E, LaBombard B *Phys. Plasmas* **8** 3702 (2001)
16. Kadomtsev B B *Tokamak Plasma*: *a Complex Physical System* (Bristol: IOP Publ., 1992)
17. Savin S P et al. *Pis'ma Zh. Ekp. Teor. Fiz.* **74** 620 (2001) [*JETP Lett.* **74** 547 (2001)]
18. Savin S et al. *Nonlin. Proces. Geophys.* **9** 443 (2002)
19. Savin S et al. *Surv. Geophys.* **26** 95 (2005)
20. Savin S et al. *Pis'ma Zh. Ekp. Teor. Fiz.* **87** 691 (2008) [*JETP Lett.* **87** 593 (2008)]
21. Savin S P et al. *Pis'ma Zh. Ekp. Teor. Fiz.* **79** 452 (2004) [*JETP Lett.* **79** 368 (2004)]
22. Savin S et al. *Planet. Space Sci.* **53** 133 (2005)
23. Novikov E A, Stewart R U *Izv. Akad. Nauk SSSR. Ser. Geofiz.* (3) 408 (1964)
24. Frisch U *Turbulence. The Legacy of A.N. Kolmogorov* (Cambridge: Cambridge Univ. Press, 1995) [Translated into Russian (Moscow: Fazis, 1998)]
25. Budaev V P et al. *Nucl. Fusion* **48** 024014 (2008)
26. Scott B D *Phys. Plasmas* **12** 062314 (2005)
27. Pastukhov V P *Fiz. Plazmy* **31** 628 (2005) [*Plasma Phys. Rep.* **31** 577 (2005)]
28. Zelenyi L M, Milovanov A V *Usp. Fiz. Nauk* **174** 809 (2004) [*Phys. Usp.* **47** 749 (2004)]
29. Zelenyi L M, Veselovskii I S (Eds) *Plazmennaya Geliogeofizika* (Plasma Heliogeophysics) (Moscow: Fizmatlit, 2008)
30. Biskamp D, Schwarz E *Phys. Plasmas* **8** 3282 (2001)
31. Biskamp D, Müller W-C *Phys. Plasmas* **7** 4889 (2000)
32. Frik P G *Turbulentnost'*: *Podkhody i Modeli* (Turbulence: Approaches and Models) (Moscow–Izhevsk: Inst. Komp. Issled., 2003)
33. Landau L D, Lifshitz E M *Teoriya Polya* (The Classical Theory of Fields) (Moscow: Fizmatlit, 2001) [Translated into English (Oxford: Pergamon Press, 1980)]
34. Prigogine I *Introduction to Thermodynamics of Irreversible Processes* (Springfield, Ill.: Thomas, 1955) [Translated into Russian (Moscow – Izhevsk: RKhD, 2001)]
35. Parisi G, Frish U, in *Turbulence and Predictability in Geophysical Fluid Dynamics and Climate Dynamics* (Eds M Ghil, R Benzi, G Parisi) (Amsterdam: North-Holland, 1985) p. 71
36. Gogoberidze G *Phys. Plasmas* **14** 022304 (2007)
37. Milliontchikov M D *Dokl. Akad. Nauk SSSR* **32** 611 (1941) [*C.R.* (*Dokl.*) *Acad. Sci. USSR* **32** 611 (1941)]
38. Kraichnan R H *J. Fluid Mech.* **5** 497 (1959)
39. Kadomtsev B B *Plasma Turbulence* (London: Academic Press, 1965)
40. Bykov A M, Toptygin I N *Usp. Fiz. Nauk* **163** (11) 19 (1993) [*Phys. Usp.* **36** 1020 (1993)]
41. Braginskii S I, in *Voprosy Teorii Plazmy* (Reviews in Plasma Physics) Iss. 1 (Ed. M A Leontovich) (Moscow: Gosatomizdat, 1963) p. 183 [Translated into English: Vol. 1 (Ed. M A Leontovich) (New York: Consultants Bureau, 1965) p. 205]
42. Zeiler A, Drake J F, Rogers B *Phys. Plasmas* **4** 2134 (1997)
43. Horton W *Phys. Rep.* **192** 1 (1990)
44. Scott B *Plasma Phys. Control. Fusion* **39** 471 (1997)
45. Shurygin R V *Fiz. Plazmy* **30** 387 (2004) [*Plasma Phys. Rep.* **30** 353 (2004)]
46. Ovsyannikov L V *Gruppovye Svoistva Differentsial'nykh Uravnenii* (Group Properties of Differential Equations) (Novosibirsk: Izd. SO AN SSSR, 1962)
47. Olver P J *Applications of Lie Groups to Differential Equations* (New York: Springer-Verlag, 1993)
48. Gusyatnikova V N et al. *Acta Appl. Math.* **15** 23 (1989)
49. Samokhin A V *Dokl. Akad. Nauk SSSR* **285** 1101 (1985) [*Sov. Phys. Dokl.* **30** 1020 (1985)]
50. Gridnev I P *Zh. Priklad. Mekh. Tekh. Fiz.* **9** (6) 103 (1968) [*J. Appl. Mech. Tech. Phys.* **9** 718 (1968)]
51. Ibragimov N H (Ed.) *CRC Handbook of Lie Group Analysis of Differential Equations* Vols 1 – 3 (Boca Raton: CRC Press, 1994 – 1996)
52. Nucci M C *Atti Semin. Mat. Fis. Univ. Modena* **33** 21 (1984)
53. Biferale L, Procaccia I *Phys. Rep.* **414** 43 (2005)
54. Cartes C et al. *Fluid Dyn. Res.* **41** 011404 (2009)
55. Kolmogorov A N *J. Fluid Mech.* **13** 82 (1962)
56. Pukhnachev V V *Usp. Mekh.* **4** (1) 1 (2006)
57. Akhiezer A I, Berestetskii V B *Kvantovaya Elektrodinamika* (Quantum Electrodynamics) (Moscow: Nauka, 1981) [Translated into English (New York: Interscience Publ., 1965)]
58. Adzhemyan L Ts, Antonov N V, Vasil'ev A N *Usp. Fiz. Nauk* **166** 1257 (1996) [*Phys. Usp.* **39** 1193 (1996)]
59. Chukbar K V *Zh. Eksp. Teor. Fiz.* **108** 1875 (1995) [*JETP* **81** 1025 (1995)]
60. Chechkin A V, Gorenflo R, Sokolov I M *Phys. Rev. E* **66** 046129 (2002)
61. Uchaikin V V *Metod Drobnykh Proizvodnykh* (Method of Non-Integer Derivatives) (Ulyanovsk: Artishok, 2008)
62. Liapounoff A *Obshchaya Zadacha ob Ustoichivosti Dvizheniya* (Kharkov: Khar'kovsk. Mat. Obshchestvo, 1892); (Moscow – Leningrad: GITTL, 1950) [Translated into French: 'Problème général de la stabilité du mouvement' *Ann. Fac. Sci. Toulouse* **9** 203 (1907); *Annals of Mathematics Studies* Vol. 17 (Princeton, N.J.: Princeton Univ. Press, 1947); translated into English: Lyapunov A M *The General Problem of the Stability of Motion* (London: Taylor & Francis, 1992)]
63. Oseledets V I *Tr. Moskovskogo Mat. Obshchestva* **19** 179 (1968) [*Trans. Moscow Math. Soc.* **19** 197 (1968)]
64. Zaslavsky G M, Sagdeev R Z *Vvedenie v Nelineinuyu Fiziku. Ot Mayatnika do Turbulentnosti i Khaosa* (Introduction to Nonlinear Physics: from the Pendulum to Turbulence and Chaos) (Moscow: Nauka, 1988); Sagdeev R Z, Usikov D A, Zaslavsky G M *Nonlinear Physics*: *from the Pendulum to Turbulence and Chaos* (Chur: Harwood Acad. Publ., 1988)
65. Landau L D, Lifshitz E M *Statisticheskaya Fizika* (Statistical Physics) Vol. 1 (Moscow: Fizmatlit, 2001) [Translated into English: Vol. 1 (Oxford: Pergamon Press, 1980)]
66. Gnedenko B V *Kurs Teorii Veroyatnostei* (Course in Theory of Probability) (Moscow: URSS, 2001) [Translated into English: *Theory of Probability* (Amsterdam: Gordon and Breach Sci. Publ., 1980)]
67. Batanov G M et al. *Pis'ma Zh. Eksp. Teor. Fiz.* **78** 974 (2003) [*JETP Lett.* **78** 502 (2003)]
68. Skvortsova N N et al. *Plasma Phys. Control. Fusion* **48** A393 (2006)
69. She Z-S, Leveque E *Phys. Rev. Lett.* **72** 336 (1994)
70. Dubrulle B *Phys. Rev. Lett.* **73** 959 (1994)
71. Schertzer D, Lovejoy S, Hubert P, in *Mathematical Problems in Environmental Science and Engineering* (Ser. in Contemporary Applied Mathematics, Vol. 4, Eds A Ern, L Weiping) (Beijing: Higher Education Press, 2002) p. 106
72. Isichenko M B *Rev. Mod. Phys.* **64** 961 (1992)
73. Kraichnan R H *J. Fluid Mech.* **41** 189 (1970)
74. Kraichnan R H *J. Fluid Mech.* **5** 497 (1959)
75. Iroshnikov P S *Astron. Zh.* **40** 742 (1963) [*Sov. Astron.* **7** 566 (1964)]
76. Kraichnan R H *Phys. Fluids* **85** 575 (1965)
77. Goldreich P, Sridhar S *Astrophys. J.* **438** 763 (1995)
78. Schekochihin A A, Cowley S C, in *Magnetohydrodynamics*: *Historical Evolution and Trends* (Eds S Molokov, R Moreau, H K Moffatt) (Berlin: Springer, 2007) p. 85
79. Boldyrev S *Phys. Rev. Lett.* **96** 115002 (2006)
80. Biskamp D, Müller W-C *Phys. Plasmas* **7** 4889 (2000)
81. Benzi R et al. *Phys. Rev. E* **48** R29 (1993)
82. Schertzer D et al. *Fractals* **5** 427 (1997)
83. Schertzer D, Lovejoy S *Physica A* **338** 173 (2004)
84. Arneodo A, Bacry E, Muzy J F *J. Math. Phys.* **39** 4142 (1998)
85. She Z-S, Waymire E C *Phys. Rev. Lett.* **74** 262 (1995)
86. Politano H, Pouquet A, Carbone V *Europhys. Lett.* **43** 516 (1998)
87. Schertzer D, Lovejoy S, Hubert P "An introduction to stochastic multifractal fields", http://www.enpc.fr/multifractal/online/DS_course_0801.pdf
88. Politano H, Pouquet A *Geophys. Res. Lett.* **25** 273 (1998)

89. Chen F F *Introduction to Plasma Physics and Controlled Fusion* (Berlin: Springer, 1984) [Translated into Russian (Moscow: Mir, 1987)]
90. Budaev V P, in *Stokhasticheskie Modeli Strukturnoi Plazmennoi Turbulentnosti* (Stochastic Models of Structured Plasma Turbulence) (Eds V Yu Korolev, N N Skvortsova) (Moscow: MAKS Press, 2003) p. 125
91. Budaev V P *Czech. J. Phys.* **48** (S3) 121 (1998)
92. Boedo J A et al. *Phys. Plasmas* **8** 4826 (2001)
93. Budaev V P et al. *J. Nucl. Mater.* **176 – 177** 705 (1990)
94. Wagner F et al. *Phys. Rev. Lett.* **49** 1408 (1982)
95. Kuznetsov E A et al. *Pis'ma Zh. Eksp. Teor. Fiz.* **85** 288 (2007) [*JETP Lett.* **85** 236 (2007)]
96. Savin S et al. *Planet. Space Sci.* **59** 606 (2011)
97. Pastukhov V P, Chudin N V *Pis'ma Zh. Eksp. Teor. Fiz.* **82** 395 (2005) [Pastukhov V P, Chudin N V *JETP Lett.* **82** 356 (2005)]
98. Bak P, Tang C, Wiesenfeld K *Phys. Rev. A* **38** 364 (1988)
99. Budaev V P et al. *Nucl. Fusion* **46** S181 (2006)
100. Clauser F H *Adv. Appl. Mech.* **56** 1 (1956)
101. Townsend A A *The Structure of Turbulent Shear Flow* (Cambridge: Cambridge Univ. Press, 1956)
102. Panton R (Ed.) *Self-Sustaining Mechanisms of Wall Turbulence* (Southampton: Computational Mechanics Publ., 1997)
103. Marusic I et al. *Phys. Fluids* **22** 065103 (2010)
104. Zagarola M V "Mean flow scaling in turbulent pipe flow", Ph.D. Thesis (Princeton: Princeton Univ. Press, 1996)
105. Tsuji Y, Nakamura I *Phys. Fluids* **11** 647 (1999)
106. Monkewitz P A, Chauhan K A, Nagib H M *Phys. Fluids* **19** 115101 (2007)
107. Barenblatt G I et al. *Proc. Natl. Acad. Sci. USA* **94** 7817 (1997)
108. George W K, Castillo L *Appl. Mech. Rev.* **50** 689 (1997)
109. Klewicki J et al. *Philos. Trans. R. Soc. London A* **365** 823 (2007)
110. L'vov V S, Procaccia I, Rudenko O *Phys. Rev. Lett.* **100** 054504 (2008)
111. Zagarola M V, Smits A J *J. Fluid Mech.* **373** 33 (1998)
112. McKeon B J, Sreenivasan K R *Philos. Trans. R. Soc. London A* **365** 635 (2007)
113. Panton R L *Prog. Aerospace Sci.* **37** 341 (2001)
114. Adrian R J *Phys. Fluids* **19** 041301 (2007)
115. Grek G R, Kozlov V V, Chernorai V G *Usp. Mekh.* **4** (1) 52 (2006)
116. Zybin K P et al. *Zh. Eksp. Teor. Fiz.* **132** 510 (2007) [*JETP* **105** 455 (2007)]
117. Zybin K P et al. *Phys. Rev. Lett.* **100** 174504 (2008)
118. Zybin K P et al. *Zh. Eksp. Teor. Fiz.* **134** 1024 (2008) [*JETP* **107** 879 (2008)]
119. Zybin K P, Sirota V A, Ilyin A S *Phys. Rev. E* **82** 056324 (2010)
120. Zybin K P, Sirota V A *Phys. Rev. Lett.* **104** 154501 (2010)
121. Xu H et al. *Phys. Rev. Lett.* **96** 024503 (2006)
122. Sreenivasan K R *Rev. Mod. Phys.* **71** S383 (1999)
123. Arneodo A et al. *Europhys. Lett.* **34** 411 (1996)
124. Klewicki J C, Foss J F, Wallace J M, in *Flow at Ultra-High Reynolds and Rayleigh Numbers* (Eds R J Donnelly, K R Sreenivasan) (New York: Springer, 1998) p. 450
125. Nagib H M, Chauhan K A, Monkewitz P A *Philos. Trans. R. Soc. London A* **365** 755 (2007)
126. Carlier J, Stanislas M *J. Fluid Mech.* **535** 143 (2005)
127. Nickels T B et al. *Phys. Rev. Lett.* **95** 074501 (2005)
128. Maurer J, Tabeling P, Zocchi G *Europhys. Lett.* **26** 31 (1994); Zocchi G et al. *Phys. Rev. E* **50** 3693 (1994); Belin F, Tabeling P, Willaime H *Physica D* **93** 52 (1996)
129. Anselmet F et al. *J. Fluid Mech.* **140** 63 (1984); Marchand M, These INPG (Grenoble: National Polytechnical Inst. of Grenoble, 1993)
130. Chabaud B et al. *Phys. Rev. Lett.* **73** 3227 (1994)
131. Baudet C, Ciliberto S, Phan N T *J. Physique II* **3** 293 (1993)
132. Van de Water W, Van der Vorst B, Van de Wetering E *Europhys. Lett.* **16** 443 (1991)
133. Camussi R et al. *Phys. Fluids* **8** 1181 (1996)
134. Lumley J L *Phys. Fluids* **8** 1056 (1965)
135. Dahm W J A, Southerland K B, Buch K A *Phys. Fluids A* **3** 1115 (1991)
136. Adrian R J *Annu. Rev. Fluid Mech.* **23** 261 (1991)
137. Batchelor G K, Townsend A A *Proc. R. Soc. London A* **199** 238 (1949)
138. Cadot O, Douady S, Couder Y *Phys. Fluids* **7** 630 (1995)
139. Camussi R et al. *Phys. Fluids* **8** 1181 (1996)
140. Camussi R et al. *Phys. Fluids* **20** 075113 (2008)
141. Borodulin V I, Abstract of Doct. Phys. Math. Sci. Thesis (Novosibirsk: Institute of Theoretical and Applied Mechanics, 2009)
142. Meneveau C, Sreenivasan K R *J. Fluid Mech.* **224** 429 (1991)
143. Rosales C, Meneveau C *Phys. Rev. E* **78** 016313 (2008)
144. Lovejoy S, Schertzer D, Tuck A F *Phys. Rev. E* **70** 036306 (2004)
145. Chigirinskaya Y et al. *Nonlin. Proces. Geophys.* **1** 105 (1994)
146. Finn D et al. *J. Appl. Meteor.* **40** 229 (2001)
147. Schmitt F et al. *C. R. Acad. Sci. Paris II* **314** 749 (1992)
148. Schmitt F et al. *Europhys. Lett.* **34** 195 (1996)
149. Pelletier J, in *Atmospheric and Oceanic Sciences* (Montreal: McGill, 1995)
150. Wang Y, in *Atmospheric and Oceanic Sciences* (Montreal: McGill, 1995)
151. Benzi R, Biferale L *J. Stat. Phys.* **135** 977 (2009)
152. Frisch U, Vergassola M *Europhys. Lett.* **14** 439 (1991)
153. Biferale L et al. *Phys. Rev. Lett.* **93** 064502 (2004)
154. Sreenivasan K, Schumacher J *Philos. Trans. R. Soc. London A* **368** 1561 (2010)
155. Villermaux E, Sixou B, Gagne Y *Phys. Fluids* **7** 2008 (1995)
156. Gledzer E B *Izv. Akad. Nauk SSSR. Fiz. Atmos. Okeana* **41** 733 (2005) [*Izv. Atmos. Ocean. Phys.* **41** 667 (2005)]
157. Lee C B et al. *Experiments Fluids* **28** 243 (2000)
158. Balakumar B J, Adrian R J *Philos. Trans. R. Soc. London A* **365** 665 (2007)
159. Kim K C, Adrian R J *Phys. Fluids* **11** 417 (1999)
160. McKeon B J, Morrison J F *Philos. Trans. R. Soc. London A* **365** 771 (2007)
161. Toh S, Itano T *J. Fluid Mech.* **524** 249 (2005)
162. Rao K N, Narasimha R, Badri Narayanan M A *J. Fluid Mech.* **48** 339 (1971)
163. Hutchins N, Marusic I *Philos. Trans. R. Soc. London A* **365** 647 (2007)
164. Kachanov Yu S, Kozlov V V, Levchenko V Ya *Vozniknovenie Turbulentnosti v Pogranichnom Sloe* (Emergence of Turbulence in a Boundary Layer) (Novosibirsk: Nauka, 1982)
165. Klebanoff P S, Tidstrom K D, Sargent L M *J. Fluid Mech.* **12** 1 (1962)
166. Kachanov Y S, in *Recent Results in Laminar-Turbulent Transition* (Notes on Numerical Fluid Mechanics and Multidisciplinary Design, Vol. 86, Eds S Wagner, M Kloker, U Rist) (Berlin: Springer-Verlag, 2004) p. 1
167. Boiko A V et al. *The Origin of Turbulence in Near-Wall Flows* (Berlin: Springer-Verlag, 2002)
168. Litvinenko M V et al. *Zh. Priklad. Mekh. Tekh. Fiz.* **45** (3) 50 (2004) [*J. Appl. Mech. Tech. Phys.* **45** 349 (2004)]
169. Litvinenko Yu A et al. *Teplofiz. Aeromekh.* **11** 339 (2004) [*Thermophys. Aeromech.* **11** 329 (2004)]
170. Kozlov V V et al. *Zh. Priklad. Mekh. Tekh. Fiz.* **43** (2) 62 (2002) [*J. Appl. Mech. Tech. Phys.* **43** 224 (2002)]
171. Jiménez J *Annu. Rev. Fluid Mech.* **36** 173 (2004)
172. Kornilov V I *Teplofiz. Aeromekh.* **12** 183 (2005) [*Thermophys. Aeromech.* **12** 175 (2005)]
173. Chernyshov A A, Karelsky K V, Petrosyan A S *Phys. Plasmas* **17** 102307 (2010)
174. Chernyshov A A, Karelsky K V, Petrosyan A S *Phys. Fluids* **19** 055106 (2007)
175. Moin P, Mahesh K *Annu. Rev. Fluid Mech.* **30** 539 (1998)
176. Wu X, Moin P *J. Fluid Mech.* **630** 5 (2009)
177. Jiménez J, Moser R D *Philos. Trans. R. Soc. London A* **365** 715 (2007)
178. Schlatter P et al. *Phys. Fluids* **21** 051702 (2009)
179. Hu Z, Morfey C L, Sandham N D *AIAA J.* **44** 1541 (2006)
180. Abe H, Kawamura H, Choi H *J. Fluids Eng.* **126** 835 (2004)
181. Hutchins N, Marusic I *J. Fluid Mech.* **579** 1 (2007)
182. Marusic I, Heuer W D C *Phys. Rev. Lett.* **99** 114504 (2007)
183. Yakhot V, Sreenivasan K R *J. Stat. Phys.* **121** 823 (2005)
184. Toschi F, Bodenschatz E *Annu. Rev. Fluid Mech.* **41** 375 (2009)
185. Biferale L et al. *Phys. Fluids* **20** 065103 (2008)
186. Benzi R et al. *J. Fluid Mech.* **653** 221 (2010)
187. Voth G A et al. *J. Fluid Mech.* **469** 121 (2002)
188. Biferale L et al. *Phys. Fluids* **17** 021701 (2005)
189. Paschmann G et al. *J. Geophys. Res.* **81** 2883 (1976)

190. Haerendel G *J. Atmos. Terrestr. Phys.* **40** 343 (1978)
191. Antonova A E, Shabanskii V P *Geomagn. Aeron.* **15** 297 (1975) [*Geomagn. Aeron.* **15** 243 (1975)]
192. Spreiter J R, Briggs B R *J. Geophys. Res.* **67** 37 (1962)
193. Savin S P et al., in *Geospace Mass and Energy Flow: Results from the Intern. Solar-Terrestrial Physics Program* (Geophysical Monograph, Vol. 104, Eds J L Horwitz, D L Gallagh, W K Peterson) (Washington, DC: AGU, 1998) p. 25
194. Panov E V et al. *Kosmich. Issled.* **45** 285 (2007) [*Cosmic Res.* **45** 268 (2007)]
195. Savin S et al. *Nonlin. Proces. Geophys.* **13** 377 (2006)
196. Nedospasov A V *J. Nucl. Mater.* **196 – 198** 90 (1992)
197. Chen F F, in *Plasma Diagnostic Techniques* (Eds R H Huddlestone, S L Leonard) (New York: Academic Press, 1965) p. 113 [Translated into Russian (Moscow: Mir, 1967) p. 94]
198. Stangeby P C *The Plasma Boundary of Magnetic Fusion Devices* (London: Taylor & Francis, 2000)
199. Hutchinson I H *Principles of Plasma Diagnostics* (Cambridge: Cambridge Univ. Press, 2002)
200. Vershkov V A, Grashin S A, Chankin A V *J. Nucl. Mater.* **145 – 147** 611 (1987)
201. Budaev V P, Ivanov R S *J. Nucl. Mater.* **162 – 164** 322 (1989)
202. Shatalin S V et al. *Fiz. Plazmy* **33** 195 (2007) [*Plasma Phys. Rep.* **33** 169 (2007)]
203. Watkins J G et al. *Rev. Sci. Instrum.* **63** 4728 (1992)
204. Huber A et al. *Plasma Phys. Control. Fusion* **47** 409 (2005)
205. Gonçalves B et al. *J. Nucl. Mater.* **337 – 339** 376 (2005)
206. Antar G Y et al. *Phys. Plasmas* **10** 419 (2003)
207. Asakura N et al. *Phys. Rev. Lett.* **84** 3093 (2000)
208. Endler M et al. *Phys. Scripta* **51** 610 (1995)
209. Antar G Y, Counsell G, Ahn J-W *Phys. Plasmas* **12** 082503 (2005)
210. Skvortsova N N et al. *Plasma Phys. Control. Fusion* **48** A393 (2006)
211. Batanov G M et al. *Pis'ma Zh. Eksp. Teor. Fiz.* **73** 143 (2001) [*JETP Lett.* **73** 126 (2001)]
212. Tanaka K et al. *Nucl. Fusion* **46** 110 (2006)
213. Alonso J A et al. *Plasma Phys. Control. Fusion* **48** B465 (2006)
214. Carter T A *Phys. Plasmas* **13** 010701 (2006)
215. Chiu J S, Sen A K *Phys. Plasmas* **7** 4492 (2000)
216. Antoni V et al. *Phys. Rev. Lett.* **80** 4185 (1998)
217. Ohno N et al. *Contrib. Plasma Phys.* **44** 222 (2004)
218. Schmitz L et al. *J. Nucl. Mater.* **176 – 177** 522 (1990)
219. Boedo J A et al. *Rev. Sci. Instrum.* **70** 2997 (1999)
220. Biewer T M et al. *Rev. Sci. Instrum.* **75** 650 (2004)
221. Zweben S J, Taylor R J *Nucl. Fusion* **21** 193 (1981)
222. Graessle D E, Prager S C, Dexter R N *Phys. Fluids B* **3** 2626 (1991)
223. Stöckel J et al. *Plasma Phys. Control. Fusion* **41** A577 (1999)
224. Petrov A E, in *Stokhasticheskie Modeli Strukturnoi Plazmennoi Turbulentnosti* (Stochastic Models of Structured Plasma Turbulence) (Eds V Yu Korolev, N N Skvortsova) (Moscow: MAKS Press, 2003) p. 7
225. Budaev V P, in *Puti Uchenogo. E.P. Velikhov* (Ways of a Scientist. E.P. Velikhov) (Ed. V P Smirnov) (Moscow: RSC "Kurchatov Institute", 2007) p. 64
226. Budaev V P *Fiz. Plazmy* **25** 668 (1999) [*Plasma Phys. Rep.* **25** 610 (1999)]
227. Terry J L et al. *Phys. Plasmas* **10** 1739 (2003)
228. McKee G R et al. *Rev. Sci. Instrum.* **75** 3490 (2004)
229. Zweben S J et al. *Phys. Plasmas* **13** 056114 (2006)
230. Bleuel J et al. *New J. Phys.* **4** 38 (2002)
231. Huber A et al. *J. Nucl. Mater.* **266 – 269** 546 (1999)
232. Terry P W, Newman D E, Ware A S *Phys. Plasmas* **10** 1066 (2003)
233. McKee G R et al. *Nucl. Fusion* **41** 1235 (2001)
234. Zweben S J, Medley S S *Phys. Fluids B* **1** 2058 (1989)
235. Winslow D L et al. *Rev. Sci. Instrum.* **68** 396 (1997)
236. Thomsen H et al. *Phys. Plasmas* **9** 1233 (2002)
237. Zweben S J et al. *J. Nucl. Mater.* **145 – 147** 250 (1987)
238. Windisch T, Grulke O, Klinger T *J. Nucl. Mater.* **390 – 391** 395 (2009)
239. Surko C M, Slusher R E *Science* **221** 817 (1983)
240. Liewer P C *Nucl. Fusion* **25** 543 (1985)
241. Wootton A J et al. *Phys. Fluids B* **2** 2879 (1990)
242. Endler M *J. Nucl. Mater.* **266 – 269** 84 (1999)
243. Horton W *Rev. Mod. Phys.* **71** 735 (1999)
244. Endler M *Plasma Phys. Control. Fusion* **41** 1431 (1999)
245. Rhodes T L, Ritz C P, Bengtson R D *Nucl. Fusion* **33** 1147 (1993)
246. Ritz Ch P et al. *Phys. Rev. Lett.* **62** 1844 (1989)
247. Boedo J A et al. *Phys. Plasmas* **8** 4826 (2001)
248. Grulke O et al. *Phys. Plasmas* **13** 012306 (2006)
249. Kirnev G S et al. *J. Nucl. Mater.* **337 – 339** 352 (2005)
250. Budaev V P, Ivanov R S *J. Nucl. Mater.* **162 – 164** 322 (1989)
251. Budaev V et al. *Plasma Phys. Control. Fusion* **35** 429 (1993)
252. Heller M V A P et al. *Phys. Plasmas* **6** 846 (1999)
253. Sudo S et al. *Plasma Phys. Control. Fusion* **45** A425 (2003)
254. Masuzaki S et al. *Nucl. Fusion* **42** 750 (2002)
255. Budaev V P et al. *Plasma Phys. Control. Fusion* **50** 074014 (2008)
256. Budaev V P, Khimchenko L N *Zh. Eksp. Teor. Fiz.* **131** 711 (2007) [*JETP* **104** 629 (2007)]
257. Skvortsova N N et al. *Plasma Phys. Control. Fusion* **48** A393 (2006)
258. Budaev V P, Ivanov R S *Fiz. Plazmy* **17** 1332 (1991)
259. Carreras B A, Lynch V E, LaBombard B *Phys. Plasmas* **8** 3702 (2001)
260. Antar G Y et al. *Phys. Rev. Lett.* **87** 065001 (2001)
261. Budaev V P, Khimchenko L N *Vopr. Atom. Nauki Tekh. Termoyad. Sintez* (3) 34 (2008)
262. Ottino J M *The Kinematics of Mixing: Stretching, Chaos, and Transport* (Cambridge: Cambridge Univ. Press, 1989)
263. Arnold V I *Teoriya Katastrof* (Catastrophe Theory) (Moscow: Nauka, 1990) [Translated into English (Berlin: Springer-Verlag, 2004)]
264. Loskutov A Yu *Usp. Fiz. Nauk* **177** 989 (2007) [Loskutov A *Phys. Usp.* **50** 939 (2007)]
265. Jokipii J R *Astrophys. J.* **146** 480 (1966)
266. Schuster H G *Deterministic Chaos* (Weincheim: Physik-Verlag, 1984) [Translated into Russian (Moscow: Mir, 1988)]
267. Kuznetsov S P *Dinamicheskii Khaos* (Dynamical Chaos) (Moscow: Fizmatlit, 2001)
268. Budaev V P et al., in *Proc. 22nd European Physical Society Conf. on Controlled Fusion and Plasma Physics, Bornemouth, UK, 1995*, Pt. I, p. I-277
269. Loskutov A Yu *Vestnik Mosk. Gos. Univ. Ser 3. Fiz. Astron.* (2) 3 (2001)
270. Ott E, Grebogi C, Yorke J A *Phys. Rev. Lett.* **64** 1196 (1990)
271. Pyragas K *Phys. Lett. A* **170** 421 (1992)
272. Zajac J et al. *Czech. J. Phys.* **55** 1615 (2005)
273. Finken K H, Eich T, Kaleck A *Nucl. Fusion* **38** 515 (1998)
274. Budaev V P et al. *J. Nucl. Mater.* **313 – 316** 1309 (2003)
275. Budaev V P, in *Proc. 2nd Europhysics Workshop on the Role of Electric Fields in Plasma Confinement and Exhaust, Maastricht, The Netherlands, 19 – 20 June 1999*
276. Budaev V et al. *Nucl. Fusion* **44** S108 (2004)
277. Budaev V P *Fiz. Plazmy* **34** 867 (2008) [*Plasma Phys. Rep.* **34** 799 (2008)]
278. Muzy J F, Bacry E, Arneodo A *Phys. Rev. E* **47** 875 (1993)
279. Arneodo A, Muzy J F, Roux S G *J. Physique France II* **7** 363 (1997)
280. Bacry E, Muzy J F, Arnéodo A *J. Stat. Phys.* **70** 635 (1993)
281. Budaev V P et al. *Plasma Fusion Res.* **3** S1019 (2008)
282. Budaev V P *Contrib. Plasma Phys.* **50** 218 (2010)
283. Muzy J F, Bacry E, Arneodo A *Phys. Rev. Lett.* **67** 3515 (1991)
284. Budaev V P et al., in *Proc. 34th EPS Conf. on Plasma Physics Warsaw, 2 – 6 July 2007 ECA* Vol. 31F, p. 1.088
285. Budaev V P et al. *Contrib. Plasma Phys.* **48** 42 (2008)
286. Bozhokin S V, Parshin D A *Fraktaly i Mul'tifraktaly* (Fractals and Multifractals) (Moscow–Izhevsk: RKhD, 2001)
287. Budaev V P *Physica A* **344** 299 (2004)
288. Müller W-C, Biskamp D *Phys. Rev. Lett.* **84** 475 (2000)
289. Antar G Y *Phys. Rev. Lett.* **91** 055002 (2003)
290. Sorriso-Valvo L et al. *Europhys. Lett.* **75** 832 (2006)
291. Müller W-C, Biskamp D, Grappin R *Phys. Rev. E* **67** 066302 (2003)
292. Frisch U et al. *J. Fluid Mech.* **68** 769 (1975)
293. Budaev V P et al. *Nucl. Fusion* **46** S181 (2006)
294. Masuzaki S et al. *J. Nucl. Mater.* **313 – 316** 852 (2003)
295. She Z-S, Waymire E C *Phys. Rev. Lett.* **74** 262 (1995)
296. Mason J, Cattaneo F, Boldyrev S *Phys. Rev. Lett.* **97** 255002 (2006)
297. Lovejoy S, Schertzer D, Silas P *Water Resour. Res.* **34** 3283 (1998)
298. Petrukovich A A, in *Nonequilibrium Phenomena in Plasmas* (Eds A S Sharma, P K Kaw) (Dordrecht: Springer, 2005) p. 145
299. Vörös Z et al. *Nonlin. Proces. Geophys.* **14** 535 (2007)
300. Treumann R A *Geophys. Res. Lett.* **24** 1727 (1997)